# REPORT DOCUMENTATION PAGE

Form Approved OMB No. 0704-0188



| 1. REPORT DATE *(DD-MM-YYYY)* | 2. REPORT TYPE | 3. DATES COVERED *(From – To)* |
|---|---|---|
| 05-05-2008 | Final Report | 1 April 2007 - 18 August 09 |

**4. TITLE AND SUBTITLE**

Deflagration-To-Detonation Transition Control By Nanosecond Gas Discharges

**5a. CONTRACT NUMBER**
FA8655-03-D-0001, Delivery Order 0030

**5b. GRANT NUMBER**

**5c. PROGRAM ELEMENT NUMBER**

**6. AUTHOR(S)**

Professor Andrei Y Starikovskii

**5d. PROJECT NUMBER**

**5d. TASK NUMBER**

**5e. WORK UNIT NUMBER**

**7. PERFORMING ORGANIZATION NAME(S) AND ADDRESS(ES)**

Moscow Institute of Physics and Technology
9 Institutski Lane
Dolgoprudny 141700
Russia

**8. PERFORMING ORGANIZATION REPORT NUMBER**

N/A

**9. SPONSORING/MONITORING AGENCY NAME(S) AND ADDRESS(ES)**

EOARD
Unit 4515 BOX 14
APO AE 09421

**10. SPONSOR/MONITOR'S ACRONYM(S)**

**11. SPONSOR/MONITOR'S REPORT NUMBER(S)**
EOARD Task 06-9003

**12. DISTRIBUTION/AVAILABILITY STATEMENT**

Approved for public release; distribution is unlimited.

**13. SUPPLEMENTARY NOTES**

**14. ABSTRACT**

During the current project, an extensive experimental study of detonation initiation by high{voltage nanosecond gas discharges has been performed in a smooth detonation tube with different discharge chambers and various discharge cell numbers. The chambers were constructed on the basis of our previous studies and introduced analogous cell geometries. The discharge study performed in all the chamber has shown that three modes of discharge development are realized under the experimental conditions: a spark mode with high temperature channel formation, a streamer mode with non{uniform gas excitation, and a transient mode. The mechanisms of deflagration to detonation transition (DDT) under different discharge modes have been proposed and confirmed experimentally. Under spark and transient initiation, simultaneous ignition inside the discharge channel occurs, forming a shock wave and leading to a conventional deflagration to detonation transition (DDT) via an adiabatic explosion. Using a single{cell discharge chamber, the DDT length and time at 1 bar of initial pressure in the square smooth tube with a 20 mm transverse size amounts to 50 mm and 50 microseconds, respectively. The streamer mode of discharge development in the single{cell chamber at an initial pressure of 1 bar results in non{uniform mixture excitation and a successful DDT via a gradient mechanism, which has been confirmed by high-speed time-resolved ICCD imaging. The gradient mechanism implies a longer DDT time of 150 microseconds, though under significantly lower initiation energy of 1 J and a short DDT run-up distance of 50 mm. The gradient mechanism has been studied in more detail in a four{cell discharge chamber. The governing parameters have been established and a significantly higher efficiency in terms of detonation initiation has been achieved due to the enhanced geometry. Successful DDTs have been observed in a stoichiometric propane-oxygen mixture diluted with 40% of nitrogen under energy inputs as low as 200 mJ at initial pressures of 0.8 bar and higher. The run-up distance is within 80 mm, the DDT time is below 0.5 ms. A technique for detonation initiation in fuel-air mixtures in smooth detonation tubes can now be elaborated.

**15. SUBJECT TERMS**
EOARD, Combustion, Detonation, Plasma Combustion

| 16. SECURITY CLASSIFICATION OF: | | | 17. LIMITATION OF ABSTRACT | 18, NUMBER OF PAGES | 19a. NAME OF RESPONSIBLE PERSON |
|---|---|---|---|---|---|
| a. REPORT | b. ABSTRACT | c. THIS PAGE | | | SURYA SURAMPUDI |
| UNCLAS | UNCLAS | UNCLAS | UL | 78 | 19b. TELEPHONE NUMBER *(Include area code)* +44 (0)1895 616021 |

Moscow Institute of Physics and Technology
Physics of Nonequilibrium Systems Laboratory

# Deflagration-To-Detonation Transition Control By Nanosecond Gas Discharges

EOARD/CRDF Project # RUP2-1512-MO-06
Final Report, April 1, 2007 - April 1, 2008
Date Submitted: April 7, 2008

Edited by Dr. Andrei Yu. Starikovskii,
Moscow Institute of Physics and Technology
Physics of Nonequilibrium Systems Laboratory
Institutskii lane, 9, 141700,
Dolgoprudny, 141700, RUSSIA
Phone (+7 495) 408 6347
E-mail andreistarikovskii@gmail.com
URL http://neq.mipt.ru

# Declaration of Technical Data Conformity

The Contractor hereby declares that, to the best of its knowledge and belief, the technical data delivered herewith under this contract during the period 04/01/2007 through 03/31/2008 is complete, accurate, and complies with all material requirements of the Contract.

Date: 04/18/2008

Name and Title of Authorized Official: Prof. T.V. Kondranin, Vice-Rector, science, academic and innovations.

# Contents


Abstract . . . . . 1

**1 Previous Results: Multi–Cell Geometries** **1**
1.1 Detonation Initiation by Distributed Nanosecond Discharge . . 1
1.2 Detonation Initiation by Microsecond Spark Discharge . . . . 5
1.2.1 Experimental Setup . . . . . 5
1.2.2 Microsecond Discharge Development . . . . . 6

**2 Single–Cell Discharge Chamber** **12**
2.1 Experimental Setup . . . . . 12
2.2 Discharge Study: Development Modes . . . . . 15
2.2.1 Spatially Resolved Imaging . . . . . 15
2.2.2 Time–Resolved Imaging . . . . . 17
2.3 DDT Study Under Different Discharge Modes . . . . . 24
2.3.1 Initiation by Spark Discharge . . . . . 24
2.3.2 Initiation by Transient Plasma . . . . . 28
2.3.3 Initiation by Streamer Discharge: Gradient Mechanism 33
2.4 Discussion: Discharge Modes vs DDT Modes . . . . . 35

**3 Four–Cell Discharge Chamber** **42**
3.1 Experimental Setup . . . . . 42
3.2 Discharge Development: Gradient Shape . . . . . 44
3.3 Gradient Mechanism Study Under Different Conditions . . . . 47
3.3.1 Undiluted Propane–Oxygen Mixture . . . . . 47
3.3.2 Propane–Oxygen Mixture with 40% Nitrogen Dilution 60
3.3.3 Acetylene–Air Mixture . . . . . 68

**4 Discussion and Conclusions** **70**

**Abstract**

During the current project, an extensive experimental study of detonation initiation by high–voltage nanosecond gas discharges has been performed in a smooth detonation tube with different discharge chambers and various discharge cell numbers. The chambers were constructed on the basis of our previous studies and introduced analogous cell geometries. The discharge study performed in all the chamber has shown that three modes of discharge development are realized under the experimental conditions: a spark mode with high–temperature channel formation, a streamer mode with non–uniform gas excitation, and a transient mode. The mechanisms of deflagration to detonation transition (DDT) under different discharge modes have been proposed and confirmed experimentally. Under spark and transient initiation, simultaneous ignition inside the discharge channel occurs, forming a shock wave and leading to a conventional deflagration to detonation transition (DDT) via an adiabatic explosion. Using a single–cell discharge chamber, the DDT length and time at 1 bar of initial pressure in the square smooth tube with a 20 mm transverse size amounts to 50 mm and 50 $\mu$s, respectively. The streamer mode of discharge development in the single–cell chamber at an initial pressure of 1 bar results in non–uniform mixture excitation and a successful DDT via a gradient mechanism, which has been confirmed by high–speed time–resolved ICCD imaging. The gradient mechanism implies a longer DDT time of 150 $\mu$s, though under significantly lower initiation energy of 1 J and a short DDT run–up distance of 50 mm. The gradient mechanism has been studied in more detail in a four–cell discharge chamber. The governing parameters have been established and a significantly higher efficiency in terms of detonation initiation has been achieved due to the enhanced geometry. Successful DDTs have been observed in a stoichiometric propane–oxygen mixture diluted with 40% of nitrogen under energy inputs as low as 200 mJ at initial pressures of 0.8 bar and higher. The run–up distance is within 80 mm, the DDT time is below 0.5 ms. A technique for detonation initiation in fuel–air mixtures in smooth detonation tubes can now be elaborated.

# Chapter 1

# Previous Results: Multi–Cell Geometries

## 1.1 Detonation Initiation by Distributed Nanosecond Discharge

The experimental setup used for study of detonation initiation by a high-voltage nanosecond discharge is described in detail in our previous works [1, 2, 3]. The experiments were carried out in a detonation tube with inner diameter of 140 mm. The discharge was initiated by a 60 ns long high-voltage pulse with 12 ns rise time. Voltage amplitude ranged from 4 to 70 kV, the corresponding energy input range – from 70 mJ to 14 J. The discharge section was a distributed electrode system consisting of 131 discharge cell placed over the cross-section of the tube [4]. The pulse parameters were registered by a back-current shunt and a capacitive gauge. Flame propagation velocity was registered by 5 IR sensors installed along the detonation tube. Simultaneously, shock wave propagation velocity was measured by 2 schlieren sensors.

The discharge development was studied with an ICCD camera (LaVision Picostar 12HR) with nanosecond temporal resolution. The main contribution to the intensity of discharge radiation was made by $C^3\Pi_u,\ v' = 0 \rightarrow B^3\Pi_g,\ v'' = 0$ band of nitrogen at 337 nm. A series of images for the discharge development in air at 0.33 bar is presented in figure 1.1. Dark dots in the images correspond to the radiation of single discharge cells. The discharge had three temporal stages. During the first stage (0–15 ns), emission intensity rose steeply, reaching its maximum value. The emission at this stage was distributed quasihomogeneously over the discharge section. During the second stage (15–50 ns), the intensity decreased sharply. The third stage (t>200 ns) was the afterglow stage, when the emission was localized

within 1–2 discharge cells. Emission intensity of each subsequent stage decreased by about an order of magnitude comparing to the preceding one.

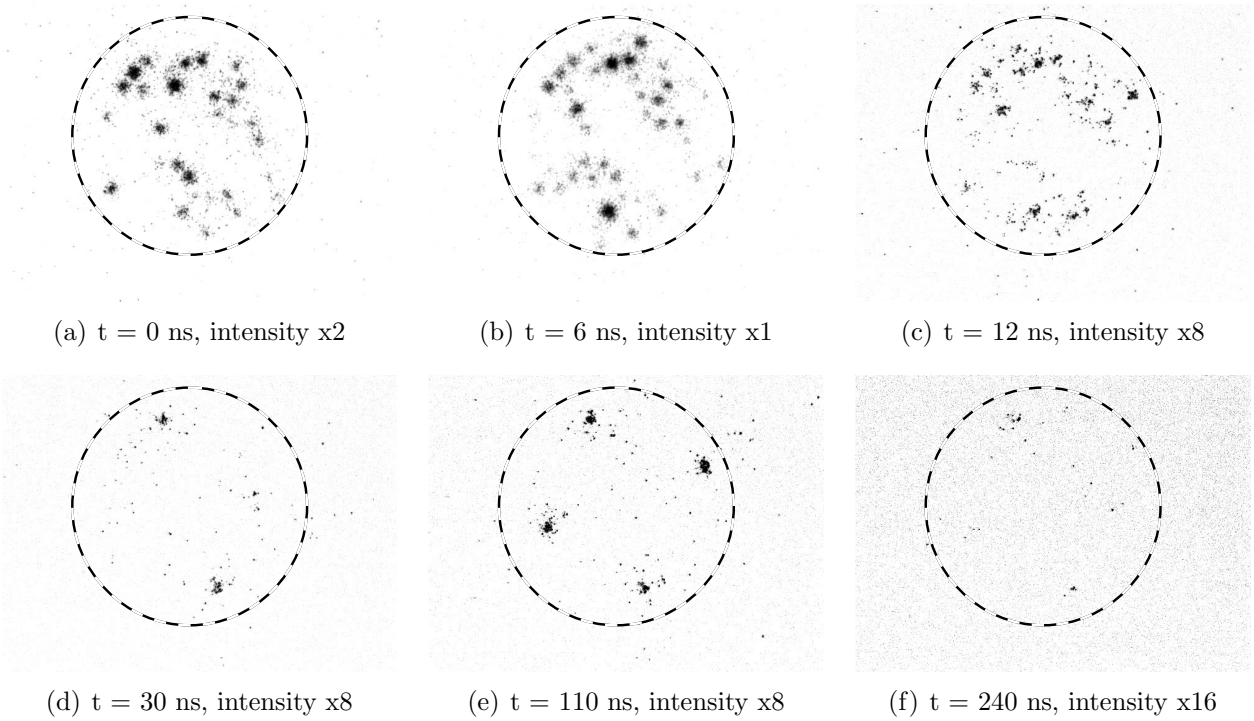

(a) t = 0 ns, intensity x2 (b) t = 6 ns, intensity x1 (c) t = 12 ns, intensity x8

(d) t = 30 ns, intensity x8 (e) t = 110 ns, intensity x8 (f) t = 240 ns, intensity x16

Fig. 1.1: Negative images of a nanosecond discharge development in air at 0.33 bar at different moments in time. Dashed line corresponds to the edge of the discharge chamber. Camera gate is 3 ns. Time was counted off from the moment when back-current shunt signal reached half of the maximum value.

The experiments in detonation initiation were carried out in different stoichiometric mixtures: $C_3H_8 + 5O_2 + xN_2$ ($0 \leq x \leq 4$), $C_3H_8/C_4H_{10} + 5O_2 + xN_2$ ($0 \leq x \leq 10$), $0.5C_6H_{14} + 4.5O_2 + xN_2$ ($0 \leq x \leq 3$), and $C_3H_8/C_4H_{10}$ + air. Initial pressure values varied from 0.15 to 1 bar. In the experiments, flame front velocity, shock wave velocity, and ignition delay times were measured simultaneously with initial mixture pressure, nitrogen dilution level, and nanosecond pulse parameters. The comparison of shock wave velocities obtained with schlieren sensors and flame front velocities obtained with IR sensors (see figure 1.2) showed that the velocities coincided in all supersonic propagation modes. This proved the possibility to use IR emission diagnostics for DDT study and allowed us to compare the velocity values obtained with the IR sensors with those obtained with the pressure transducers in the supersonic modes.

Under the current experimental conditions, three modes of flame propagation were observed: deflagration, with subsonic velocities of propagation, transient detonation, with supersonic velocities and high values of flame front

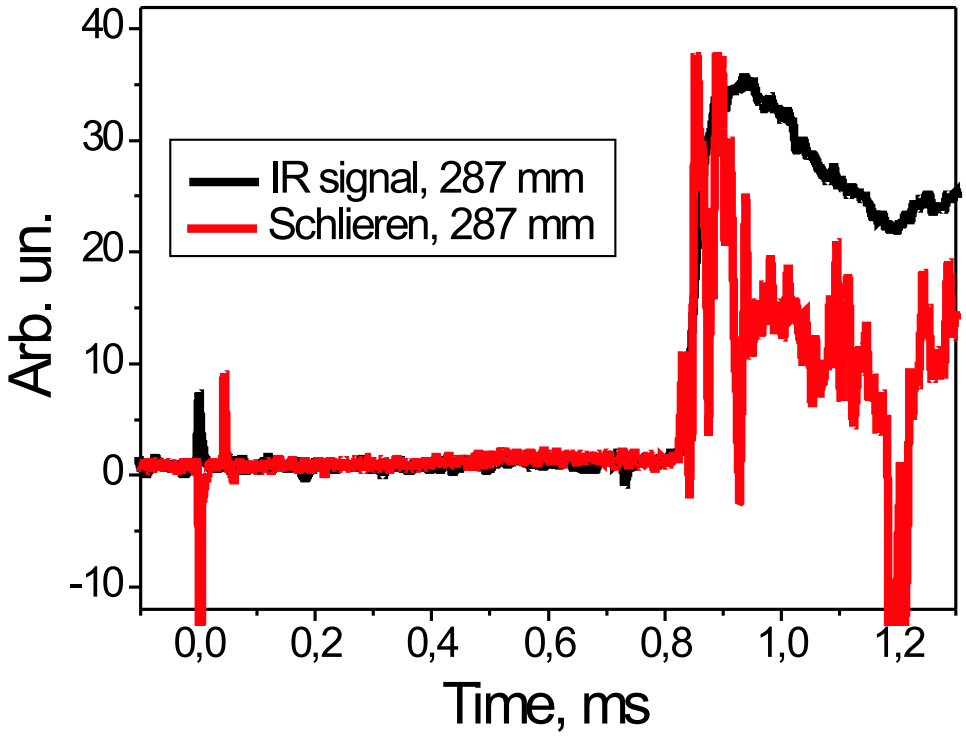


Fig. 1.2: Responses of IR sensor (black line) and Schlieren sensor (red line) in the same cross-section 287 mm away from the discharge chamber. $0.5C_6H_{14} + 4.5O_2 + 3N_2$ at 0.76 bar. Detonation.

acceleration along the tube, and Chapman-Jouguet (C-J) detonation. C-J velocity for all propane/butane mixtures under study was appr. 2400 m/s, whereas for all hexane mixtures it was appr. 2100 m/s. The results of these experiments are presented in figure 1.3 in terms of the dependences of flame front propagation velocity 400 mm (∼3 calibers) away from the discharge chamber upon initial mixture pressure, for different mixture compositions. Velocity values of ∼2400 m/s for propane/butane mixtures and ∼2100 m/s for hexane mixtures correspond to the experiments where C-J detonation were obtained. Relative velocity measurement error was the greatest for deflagration mode; nevertheless, its absolute value did not exceed 20 m/s.

At higher nitrogen dilution levels or at lower pressures, a deflagration mode was observed. In this mode, the flame front propagated with almost constant velocity of 50 to 300 m/s, gradually accelerating. Under lower nitrogen dilution levels or at higher pressures C-J detonation was observed. The measured velocity of flame front propagation corresponded to the calculated value.

In a small range of pressures between deflagration and C-J detonation, a nonstationary mode of transient detonation was observed. The velocities in this mode ranged from sonic speed in fresh mixture (∼300 m/s) to almost

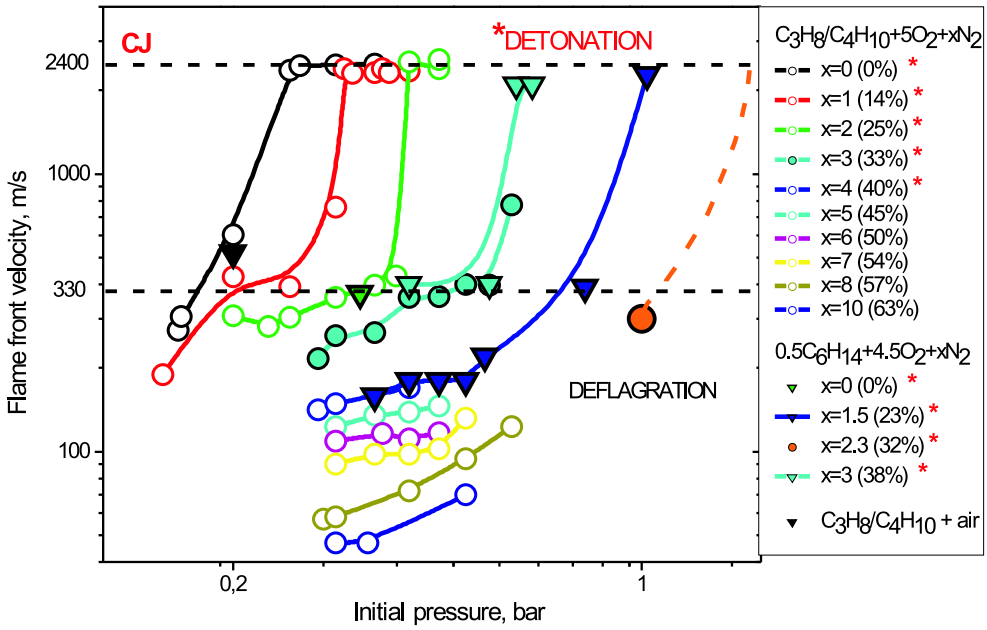


Fig. 1.3: Flame front velocity dependence upon initial mixture pressure for different mixture compositions under ignition by a nanosecond discharge. C-J velocity is 2400 m/s for propane/butane mixtures (circles) and 2100 m/s for hexane mixtures (triangles).

C-J velocity (∼2400 m/s). Transient detonation mode was characterized by strong flame front acceleration along the tube (∼$3{\cdot}10^6$ m/s$^2$) and strong dependence of velocity upon initial pressure.

The DDT was observed 400 mm away from the discharge chamber or closer in all mixtures with nitrogen dilution level up to 38%. The energy input in these cases did not exceed 3 J. For undiluted stoichiometric propane-oxygen mixture the DDT length and time amounted to, respectively, 130 mm and 0.6 ms, under energy input of 70 mJ. This value of energy input corresponded to 4 J/m$^2$ of energy per unit cross-section. In $0.5C_6H_{14} + 4.5O_2 + 3N_2$ mixture (38% $N_2$), the DDT length under energy input of 3 J at initial pressure of 1 bar was 300 mm, the DDT time was 0.6 ms. It is also seen from figure 1.3, that flame front velocities in propane/butane and hexane mixtures are the same for mixtures with the same values of nitrogen dilution, for which the combustion heat values are also close.

## 1.2 Detonation Initiation by Microsecond Spark Discharge

### 1.2.1 Experimental Setup

For comparison between detonation initiation and flame propagation modes under different initiation conditions a new setup has been assembled. The setup scheme is presented in figure 1.4a. The inner diameter and the length of the detonation tube (1) were 53 and 1000 mm, respectively. The discharge chamber (2) was mounted to one end of the tube. The geometry of the discharge chamber pictured in figure 1.4b was analogous to the one used for nanosecond detonation initiation and discussed in section 1.1 and Refs. [1, 2]. The high-voltage electrode was a distributed electrode system consisting of 28 pins separated from each other and from the ground electrode by a ceramic insulator. Each pin formed a discharge cell with interelectrode gap of 50 mm. The DC power supply (3) charged the feeding line (4) up to a voltage of 37 kV. A high-voltage pulse was formed on the electrode when the feeding line had been grounded by the thyratron (5). The pulse parameters were registered by the back-current shunt (6).

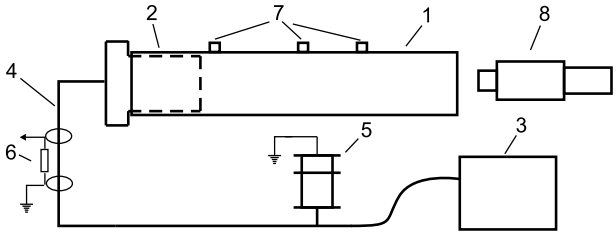


(a) Principal scheme of the setup: 1 – detonation tube, 2 – discharge chamber, 3 – DC power supply, 4 – high-voltage feeding line, $Z = 17$ Ohm, 5 – thyratron, 6 – back-current shunt, 7 – piezoelectric pressure transducers, 8 – ICCD camera with picosecond nanosecond resolution.

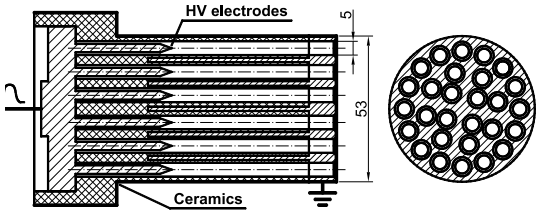


(b) Discharge chamber (2) consisting of 28 discharge cells: chamber diameter – 53 mm, discharge cell diameter – 5 mm, discharge cell length – 95 mm, interelectrode gap – 50 mm. [4]

Fig. 1.4: The setup for detonation initiation with microsecond spark discharge.

For shock and detonation waves velocity measurement piezoelectric pressure transducers (7) were used. The transducers were installed in the sidewalls of the tube at the distances of 3, 363, and 873 mm from the discharge chamber. A typical oscillogram of the pressure transducers signals is presented in figure 1.5. In this case the DDT took place between the 1st and the 2nd transducers. The error in pressure wave velocity measurement was determined mainly by the signal rise time. In detonation mode, the error value

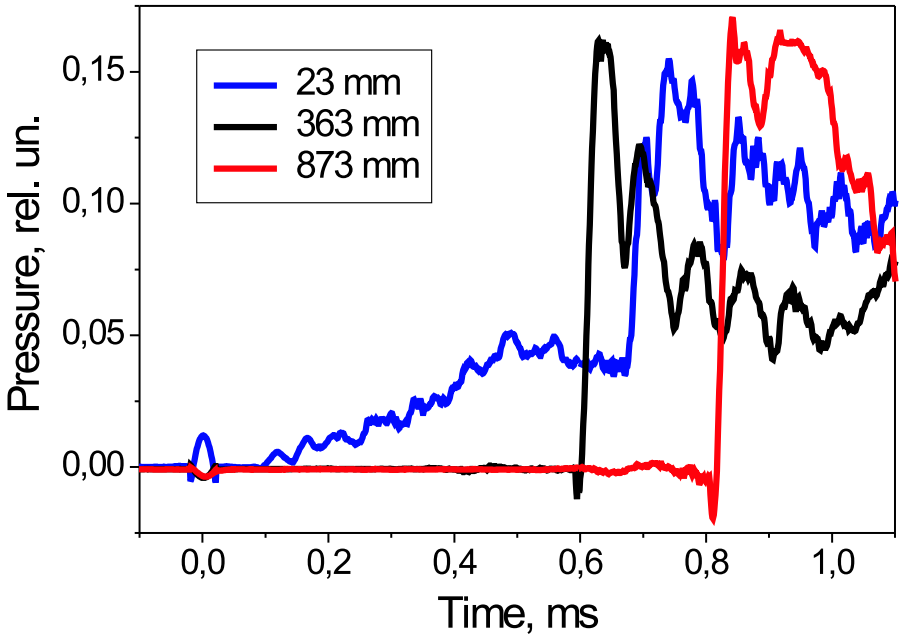


Fig. 1.5: A typical oscillogram of the pressure transducers signals. The distance from the discharge section is shown in the figure for every transducer. Initial mixture pressure 0.6 bar. Mixture: $C_3H_8/C_4H_{10} + 5O_2$. Detonation, shock wave velocity 2350 m/s measured between transducers 2 and 3. C-J velocity for the given mixture ~2400 m/s.

was insignificant due to the steepness of the shock wave front, whereas for deflagration modes the error could reach ~20 m/s.

Pulse parameters were the following: amplitude – 37 kV, width – 1–3 $\mu$s, rise time – ~100 ns. The rise time was determined by thyratron switching time. The energy input in this case was limited by the energy stored in the feeding line, which was equal to 14 J. The actual energy input value was not measured in the experiments. Images of discharge development were taken through the end of the detonation tube with an ICCD camera (8) with picosecond temporal resolution (LaVision Picostar 12HR). Radiation in the spectral range of 300–800 nm was registered in the experiments.

### 1.2.2 Microsecond Discharge Development

The discharge development was studied with the ICCD camera for this electrode configuration and pulse parameters. Temporal dependence of discharge emission integrated over the cross-section was registered under the same conditions by a photoelectric multiplier (PEM). This temporal dependence is presented in figure 1.6 for discharge development in air at 1 torr. The cor-

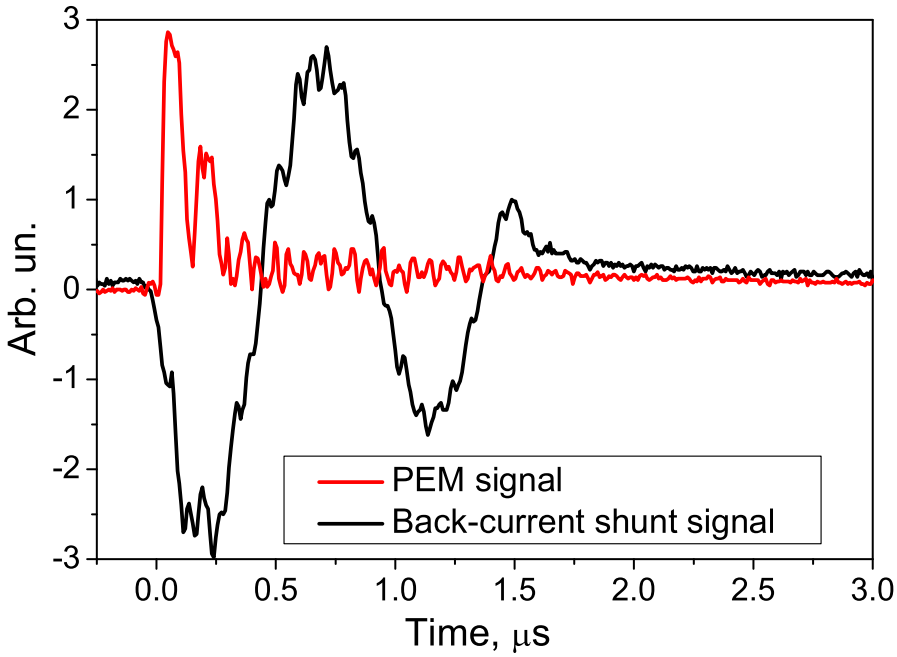


Fig. 1.6: PEM signal (red line), proportional to emission intensity, and back-current shunt signal (black line). Air, 1 torr.

responding spatially resolved ICCD images of the discharge are presented in figure 1.7. Time is counted off from the moment of electrical pulse reaching the electrode. It is seen that the discharge development occurred in a large portion of discharge cells not sooner than 80 ns after the pulse had reached the electrode. Due to the long rise time of the high-voltage pulse, the overvoltage on the discharge gap was not as high as in the case of the nanosecond discharge, which led to a streamer discharge formation. The streamers then reached the low-voltage electrode closing the discharge gap. Because of the scattering of the streamers properties there was one high-conducting channel, which was where the main portion of the discharge current passed. This led to the channel overheating and spark formation. As it is seen from the ICCD images, the spark could last for several microseconds, though the emission intensity was not high enough for the PEM to detect it.

At air pressure of 1 bar the discharge developed essentially differently. Temporal dependence of discharge emission registered by the PEM together with the back-current shunt signal and ICCD images of the discharge are presented in figures 1.8 and 1.9, respectively. In images (a) and (b) of figure 1.9, the streamer phase of discharge development at 1 bar is presented. The intensity of emission at this stage was extremely low. Unlike in the case

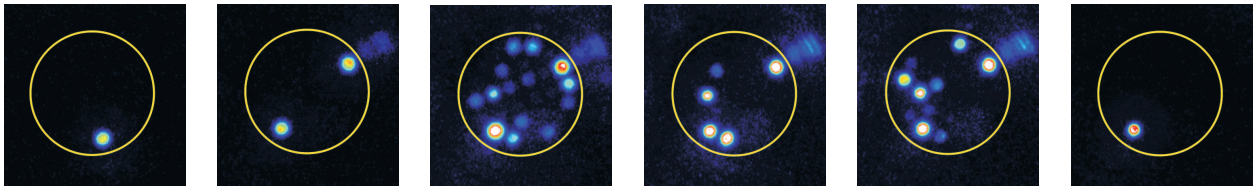

(a) 40 ns (b) 50 ns (c) 80 ns (d) 300 ns (e) 870 ns (f) 3500 ns

Fig. 1.7: Images of the microsecond discharge development in air at 1 torr at different moments in time. Yellow line corresponds to the edge of the discharge chamber. Camera gate 1 ns.

of discharge development at low pressure, the discharge localization and spark formation due to ionization instability occurred sooner than ∼50 ns after the pulse had reached the electrode. The spark stage of discharge development is presented in images (c), (d), and (e). It was these stages when most of the pulse energy consumption occurred. Homogeneous discharge phase was not observed at all in most of the discharge cells. Such discharge development pattern is a result of relatively long pulse rise time (∼100 ns).

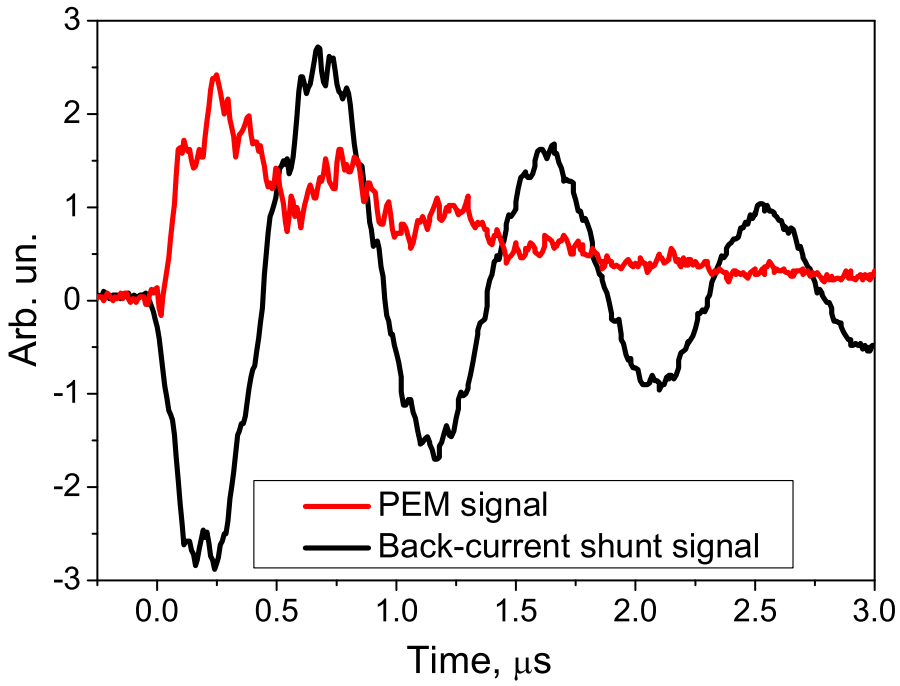


Fig. 1.8: PEM signal (red line), proportional to emission intensity, and back-current shunt signal (black line). Air, 1 bar.

Experiments on detonation initiation by a high-voltage microsecond discharge were carried out in two propane/butane mixtures ($C_3H_8/C_4H_{10}$ + $5O_2$ + $xN_2$ with x=0 and x=4) at initial pressures up to 1 bar. The mode

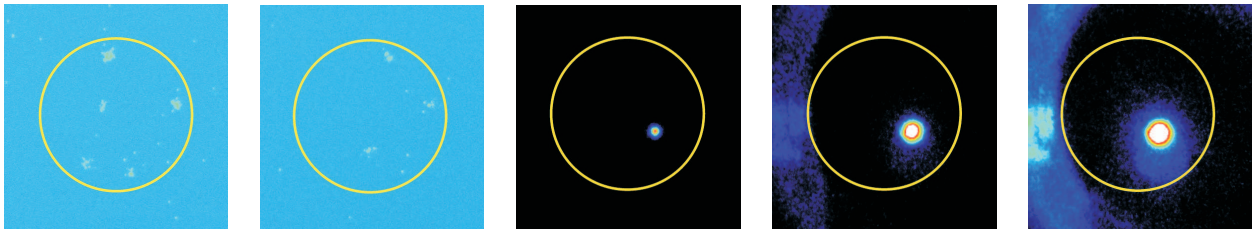

(a) 25–50 ns
Gate 25 ns
Intensity x 16

(b) 25–50 ns
Gate 25 ns
Intensity x 16

(c) 50 ns
Gate 1 ns
Intensity x 1

(d) 65 ns
Gate 1 ns
Intensity x 1

(e) 230 ns
Gate 1 ns
Intensity x 1

Fig. 1.9: Images of the microsecond discharge development in air at 1 bar at different moments in time. Yellow line corresponds to the edge of the discharge chamber.

of flame propagation was determined by shock wave velocity measured with pressure transducers. As has been shown in Section 1.1, flame front velocity coincides with shock wave velocity in all supersonic modes of propagation. The results of these experiments are presented in figure 1.10 (solid lines, solid symbols) in terms of the dependencies of shock wave velocity 600 mm away from the discharge chamber upon initial mixture pressure, for different mixture compositions. The results are presented in comparison with the ones in the same mixtures obtained under initiation by a nanosecond discharge and described in Section 1.1 (dashed lines and hollow symbols of the same color). It needs to be noted that these results are only to be compared in the region of supersonic propagation velocities.

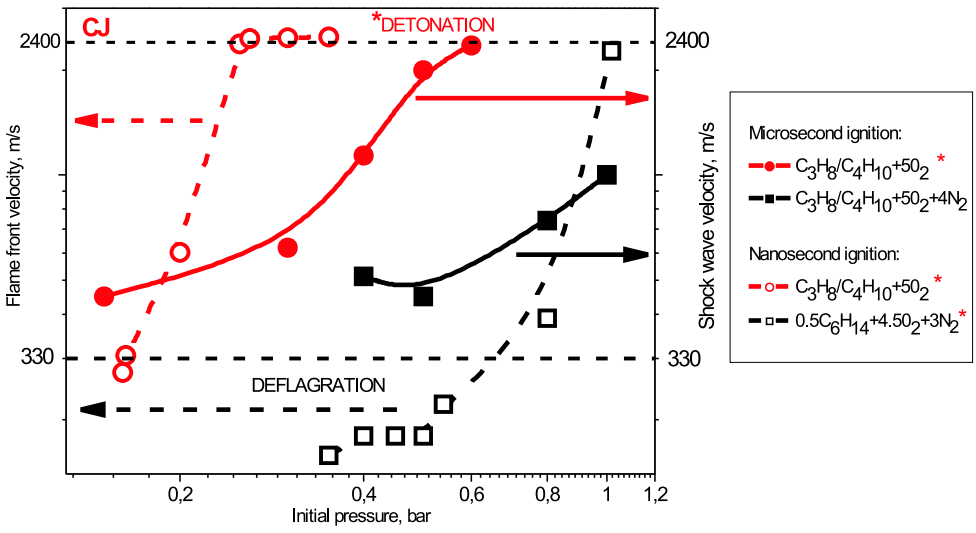


Fig. 1.10: Flame front velocity dependence upon initial mixture pressure for different mixture compositions. Solid lines and solid symbols for microsecond initiation, dashed lines and hollow symbols for nanosecond initiation. Same colors correspond to the same mixtures.

The same modes of flame propagation were observed in these experiments:

deflagration, transient detonation, and C-J detonation. For the undiluted mixture (red lines), detonation was observed at 0.6 bar of initial pressure under initiation by a microsecond spark, whereas in the case of initiation by a non-equilibrium nanosecond discharge the DDT was obtained at essentially lower pressure of 0.25 bar. For the mixture with nitrogen dilution level x=4, detonation was only observed under nanosecond initiation. In the case of microsecond spark initiation, at maximum initial pressure of 1 bar transient detonation mode with flame front velocity of ∼1000 m/s was observed. This indicates essentially higher efficiency of a distributed quasihomogeneous non-equilibrium discharge as a detonation initiator.

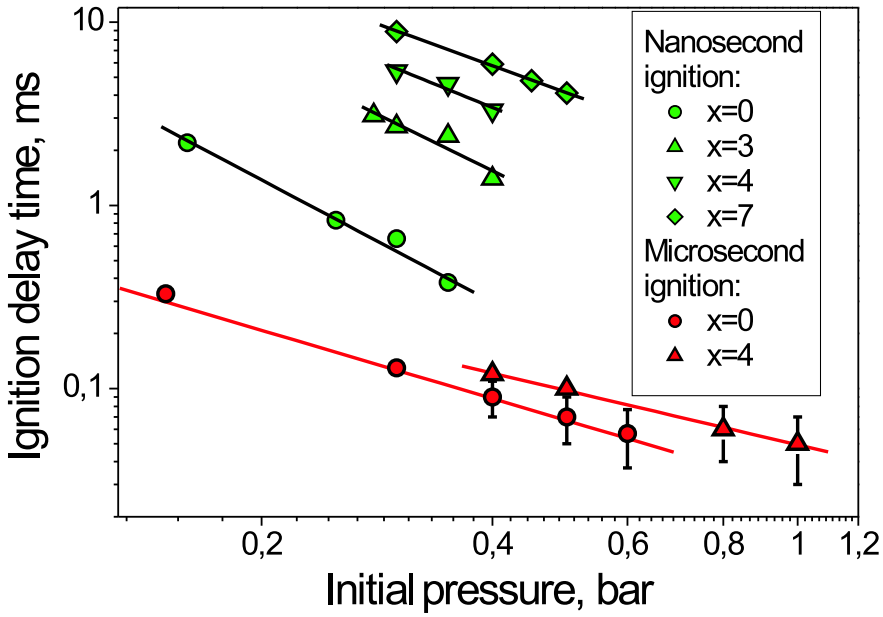


Fig. 1.11: Ignition delay time dependence upon initial pressure in $C_3H_8/C_4H_{10} + 5O_2 + xN_2$ mixtures for various nitrogen dilution levels. Green symbols for nanosecond ignition[1, 2], red symbols for microsecond ignition.

Simultaneously in the same experiments, mixture ignition was studied by measurement of ignition delay time dependence upon initial mixture pressure and nitrogen dilution level. Ignition delay time was determined from the delay between discharge initiation and the onset of signal of the first pressure transducer located 23 mm away from the discharge chamber. This ignition delay time dependence in various mixtures is presented in figure 1.11. The results for ignition by a microsecond spark discharge are represented by red symbols. Green symbols correspond to ignition by a non-equilibrium quasi-homogeneous nanosecond discharge in the first experimental setup described

in section 1.1. The latter results are described in detail in Refs. [1, 2]. It is seen that in log-log scale the dependencies are straight lines, the slopes being different for different ignition types. Noteworthy is that the values of ignition delay times are substantially lower for the microsecond ignition in all the mixtures at initial pressures up to $\sim$0.5 bar.

# Chapter 2

# Single–Cell Discharge Chamber

## 2.1 Experimental Setup

For a detailed experimental study of the deflagration–to–detonation transition under variable conditions and pulse parameters, a detonation tube with a single–cell geometry discharge chamber and nanosecond initiation has been assembled (see the scheme in Fig. 2.1 and the overall look in Fig. 2.2). The discharge cell is a Plexiglas cylinder (1) with a coaxial cylindrical channel. The pin–like high–voltage electrode (2) is placed inside the channel with a diameter of 6.5 mm. The length of the electrode can be varied, thus varying the interelectrode gap from 30 to 150 mm. The grounded electrode is at the outlet of the channel. The cell is covered with a grounded shield (3). A narrow gap in the shield along the discharge cell axis allows to perform direct optical imaging of the processes occurring inside the channel. The discharge is initiated by a high–voltage pulse delivered to the electrode from a nitrogen–filled Marx pulse generator with spark–gap commutators via a 50 Ohm coaxial line. The high–voltage pulse is 50 ns wide at half–maximum; its amplitude can be varied from 50 to 160 kV. The pulse shape and amplitude is controlled by a back-current shunt with an attenuation of 2000. The shunt is installed in a gap in the coaxial line shield close to the midpoint of the 50–meter long line. Such line length corresponds to a signal propagation time of 250 ns, which well exceeds the pulse width. This allows one to distinguish the incident pulse from the one reflected back off the discharge gap and propagating towards the generator. The pulse energy $W$ was calculated as $W = \int I^2 Z dt$, where $I$ is the current in the line measured by the shunt and $Z$ is the wave impedance of the line (equal to 50 Ohm). The difference between incident and reflected pulse energies was regarded as the energy input in the discharge.

The smooth detonation tube mounted at the output of the discharge cell

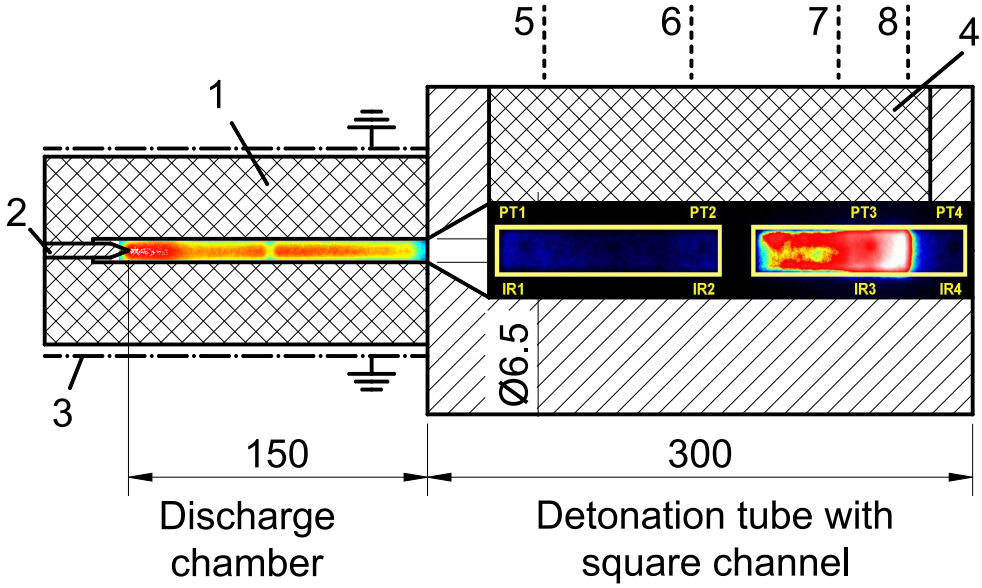


Fig. 2.1: Detonation tube with single–cell discharge chamber: the scheme.

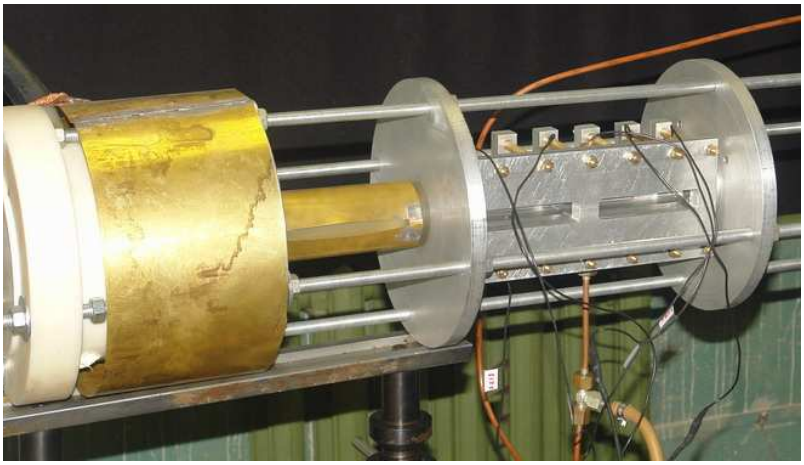

Fig. 2.2: Detonation tube with single–cell discharge chamber: the appearance.

has a 20×20 mm square cross–section and is 300 mm long. The tube is connected to the discharge cell channel with a conical nozzle with a full cone angle of 40°, which ensures flow attachment to the cone walls. The nozzle also serves as the ground electrode for the discharge. One sidewall of the detonation tube is made of Plexiglas (4), which allows one to perform direct optical measurements. Before each experiment the detonation tube was separated from the atmosphere by a membrane and vacuumized. The mixture under study was prepared and mixed in advance. For the current investigation, stoichiometric mixtures of propane–oxygen, propane–oxygen–nitrogen, and propane–air were used. The experiments were carried out at initial pressures varying from 0.1 to 1 bar but, for easier comparison, the results of DDT

initiation under different discharge conditions will be mostly presented for two pressure values: 0.3 and 1 bar. Four pairs of infra–red sensors (IR) and pressure transducers (PT) are installed in the sidewalls for accurate flame front and shock wave velocity measurements (5–8). The sensors are positioned 40, 130, 220, and 265 mm away from the nozzle inlet. An example of a set of traces obtained at different cross-sections is presented in Fig. 2.3. The traces are normalized to unity for easier representation. The time is counted off from the moment the nanosecond discharge developed. From these source data, the temporal delays of the arrival of flame and pressure waves at different positions can be obtained and plotted on an x–t diagram. The time instant of a wave arrival is defined as the moment when the intensity reaches 0.05 of the maximum level. The uncertainties in the determination of these delays are related to the finite signal rise time. For a detonation mode, the error value is insignificant due to the steepness of the wave front whereas, for deflagration modes, the error is within 10 $\mu$s. The main results of this paper are presented and interpreted in terms of x–t diagrams.

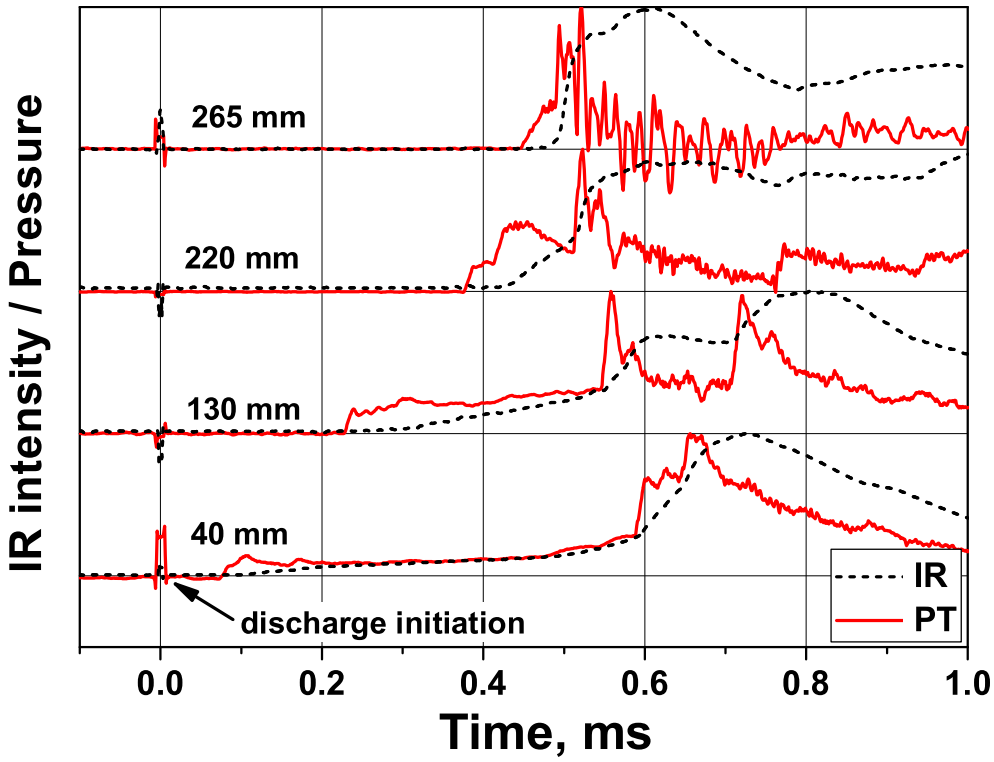


Fig. 2.3: Diagnostics example: infra–red sensor and pressure transducer traces at different cross–sections of the detonation tube. Propane–oxygen, 0.3 bar.

## 2.2 Discharge Study: Development Modes

### 2.2.1 Spatially Resolved Imaging

Spatially resolved images of the discharge development in air at pressures of 0.1 and 1 bar have been obtained through the plexiglas sidewall of the chamber with LaVision Picostar 12HR ICCD camera. The MCP-intensified images were taken with a camera gate of 1 ns at different moments during the discharge development. Simultaneously, the pulse parameters were registered with a back-current shunt in the 50 Ohm feeding line. The back-current shunt was assembled of 40 resistors, each with a 3 Ohm resistance, thus the shunt division factor being equal to 2000.

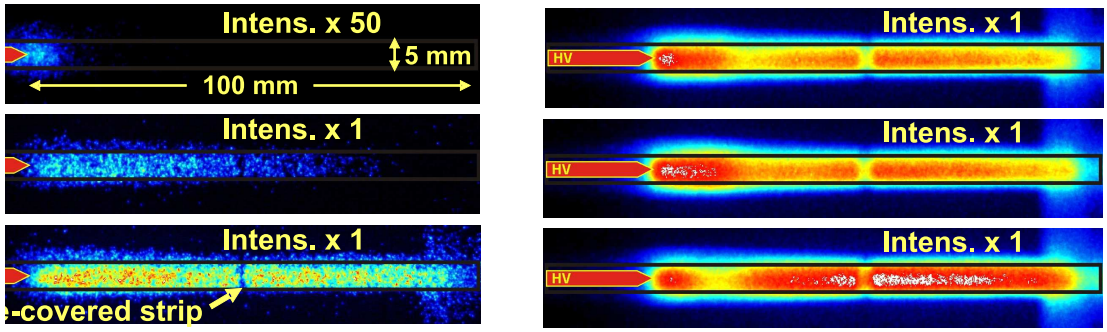


(a) 0–5 ns: streamer stage (b) 15–30 ns: gap closure stage

Fig. 2.4: ICCD-images of discharge development in single-cell geometry. Air, 0.1 bar.

The images corresponding to 0.1 bar and the discharge gap of 100 mm are presented in Fig. 2.4. The discharge was initiated by a positive 160 kV pulse from the Marx generator. The back-current shunt signal with the incident and the reflected pulses is shown in Fig. 2.5. The values of energy input in the discharge are calculated from the shapes of the pulses. It is seen that during the first 5 ns of the discharge propagation of streamers occurs. The velocity of streamer propagation exceeds 20 mm/ns, which is the result of the high values of reduced electric field ($E/N \approx 1200$ Td). The electric field $E$ was roughly estimated as $E \approx U/d$, where $U$ is the voltage over the gap and $d$ is the interelectrode distance.

The gap closure occurs within 5-10 ns after the discharge start, which agrees with the reflected pulse shape. A high-current channel is formed at this stage; the radiation intensity is significantly higher than during the streamer stage. The gap resistance diminishes rapidly, leading to almost complete reflection of the incident pulse off the shorted gap.

The images corresponding to 1 bar and the discharge gap of 100 mm under

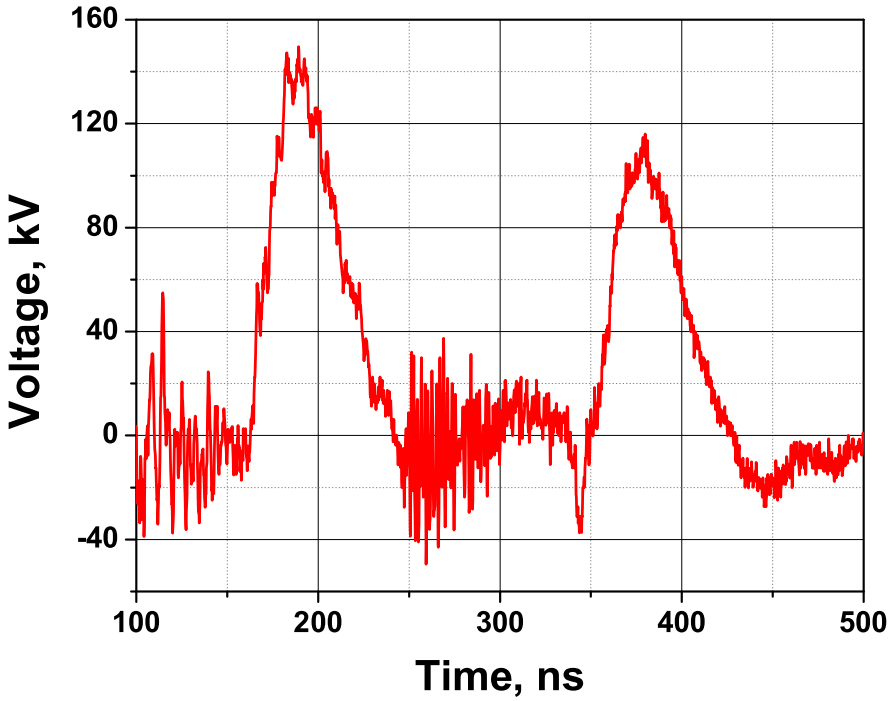


Fig. 2.5: Back-current shunt signal for incident and reflected pulses. Air, 0.1 bar.

the same pulse parameters are presented in Fig. 2.6. It is seen that at this pressure the streamers propagate along the discharge cell with a lower velocity of about 5 mm/ns. The reduced electric field value for the case is by an order of magnitude lower (∼120 Td). The gap closure in this case occurs after about 30 ns (see Fig. 2.7 for the shunt signal with the incident and reflected pulse shapes), followed by the high-current channel formation and rapid gas overheating.

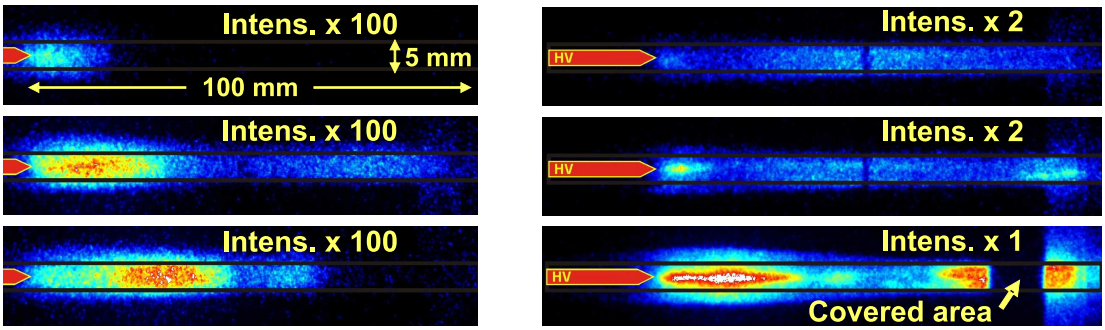


(a) 0–15 ns: streamer stage (b) 15–30 ns: gap closure stage

Fig. 2.6: Images of discharge development in single-cell geometry. Air, 1 bar.

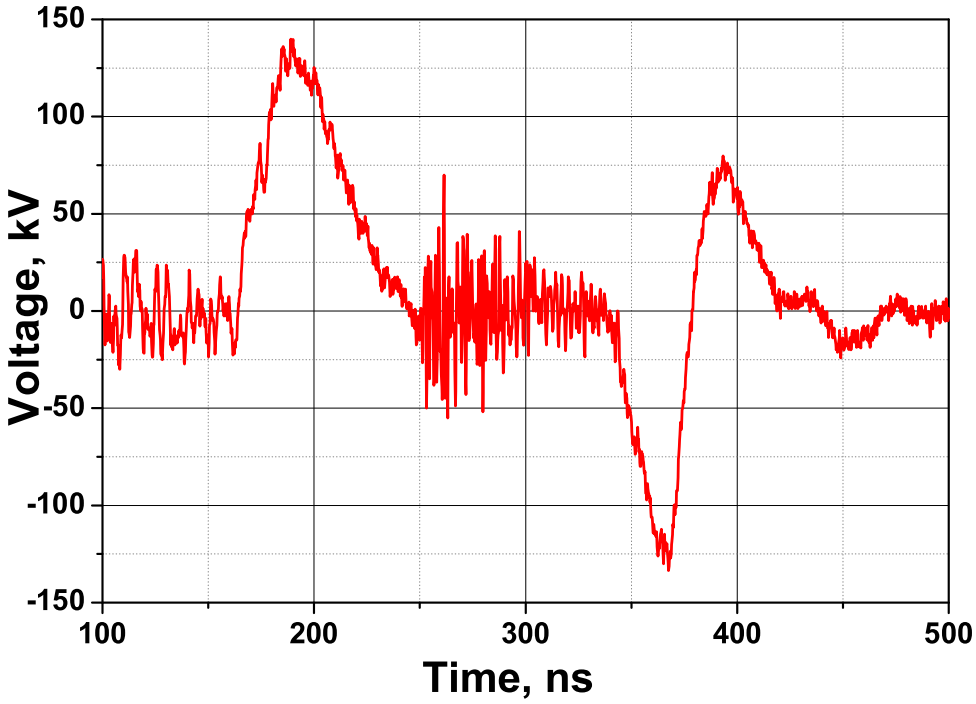


Fig. 2.7: Back-current shunt signal for incident and reflected pulses. Air, 1 bar.

### 2.2.2 Time–Resolved Imaging

More detailed information about the discharge development has been acquired with a Hamamatsu C5680 streak camera. The maximum available MCP gain is $5\times10^3$, the spectral response is in the wavelength region between 200 and 800 nm. The camera streak sweep time can be varied from 5 ns to 1 ms. This allows to perform highly time-resolved measurements of a developing nanosecond discharge.

In these experiments, the discharge was initiated by an 80 kV pulse formed by the Marx generator. The discharge gap was set at a maximum of 150 mm. The discharge cell channel, with transverse dimensions of 6.5×150 mm, was projected with a short-focus lens onto the rectangle photocathode with a size of 0.15×6 mm. The streak imaging through the plexiglas sidewall has been performed for discharge development in air at different initial pressures from 0.03 to 737 Torr. The corresponding images are shown in Figs. 2.8—2.15, along with the back-current shunt signals which contain information on the energy stored in the pulse and deposited into the gas. The discharge is propagating from the positive high-voltage electrode on the left towards the ground electrode on the right. The sweep is being performed downwards, that is, the time axis is directed downwards as well. Different sweep times from 5 to 50 ns have been used to obtain the results. The yellow line in the images

corresponds to the velocity of signal propagation in plexiglas (160 mm/ns) and provides a reference velocity.

The discharge development in air at the lowest pressure studied (0.03 Torr) is given in Fig. 2.8 along with the corresponding back-current shunt signal. The initial streamer (or ionization wave) is clearly seen propagating with a velocity of about 8 mm/ns. After its reaching the grounded electrode, a high-current channel is formed in the discharge gap. It is also seen that the channel formation occurs seemingly intermittently. An image of the same process with higher temporal resolution is given in Fig. 2.9; the sweep time for the case is 5 ns.

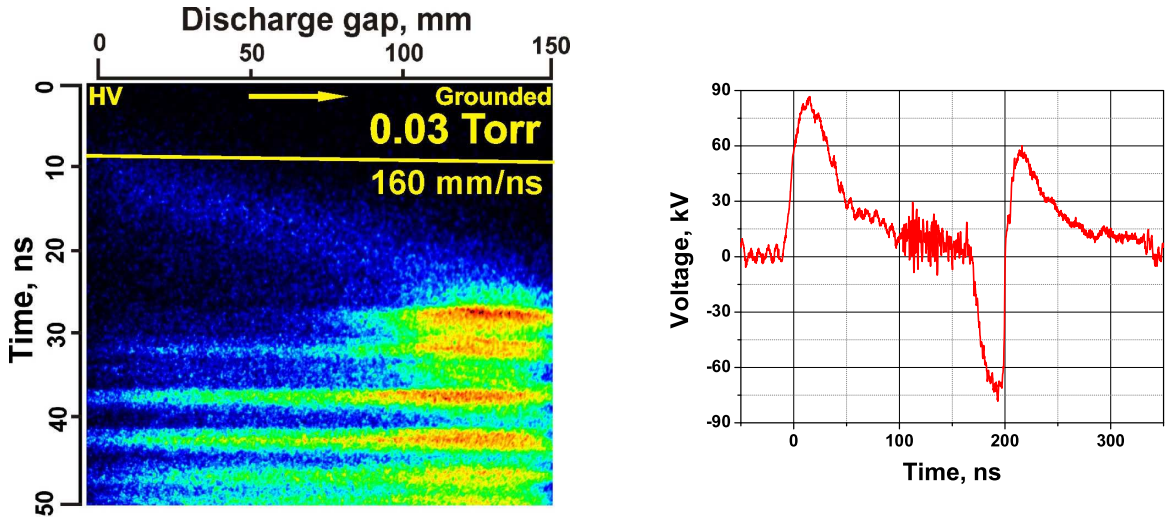


(a) Streak image

(b) Back-current shunt signal

Fig. 2.8: Discharge development in the single-cell geometry. Air, 0.03 Torr, E/N = $10^6$ Td, streamer velocity — 8 mm/ns.

The discharge development pattern at a pressure of 1 Torr is shown in Fig. 2.10 along with the corresponding back-current shunt signal. The initial streamer is seen propagating with a substantially higher velocity of about 60 mm/ns. The energy input in the discharge is also different due to the higher gas pressure, as is seen from the reflected pulse shape. A similar intermittent pattern can still be observed.

In the pressure range from 30 to 250 Torr the observed patterns of discharge development were quite similar, as is seen from Figs. 2.11—2.13. The streamer propagation velocity decreased gradually from 30 to 13 mm/ns as the pressure increased, due to the corresponding decrease of the reduced electric field. At 122 Torr and, especially, at 250 Torr, a return stroke is distinctively seen propagating backwards at a velocity exceeding that of the forth–propagating streamer.

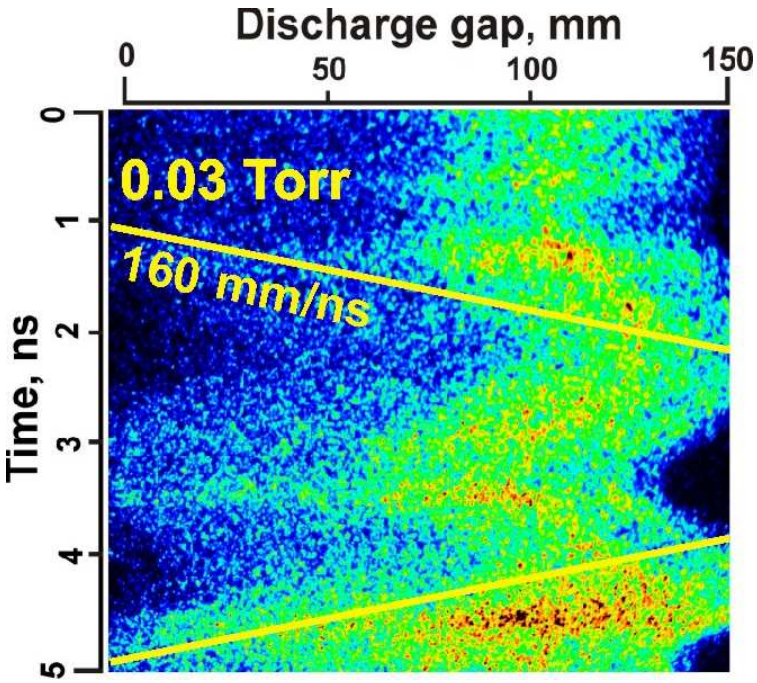


Fig. 2.9: Streak image of discharge development in the single-cell geometry at a sweep time of 5 ns. Air, 0.03 Torr, $10^6$ Td.

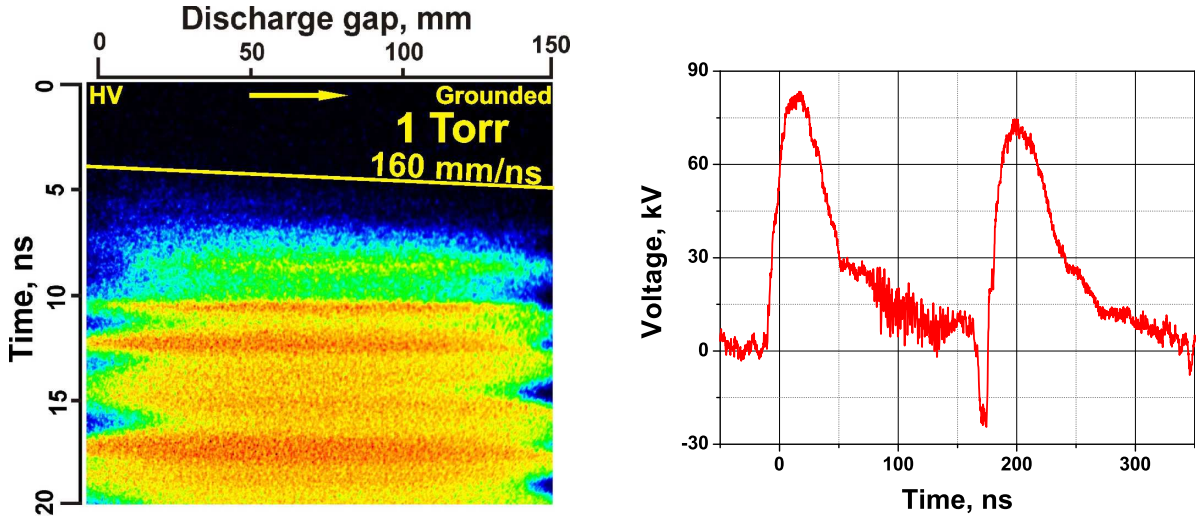


(a) Streak image (b) Back-current shunt signal

Fig. 2.10: Discharge development in the single-cell geometry. Air, 1 Torr, E/N = 30000 Td, streamer velocity — 60 mm/ns.

At higher pressures, the streamer velocity falls below the value necessary for the gap closure: the incident pulse is too short for the streamer to reach the grounded electrode when the pressure is as high as 500 and 737 Torr. The streamer propagation is shown in Figs. 2.14 and 2.15. The streamer velocities for 500 and 737 Torr amounted to 5 and 3.5 mm/ns, respectively.

Thus, we have observed two distinctively different modes of discharge prop-

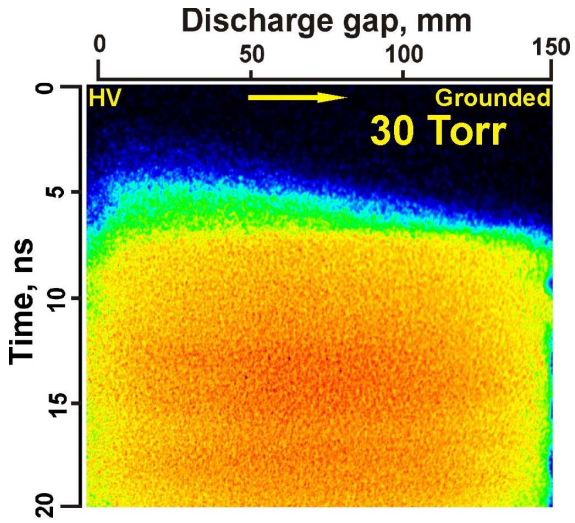


(a) Streak image

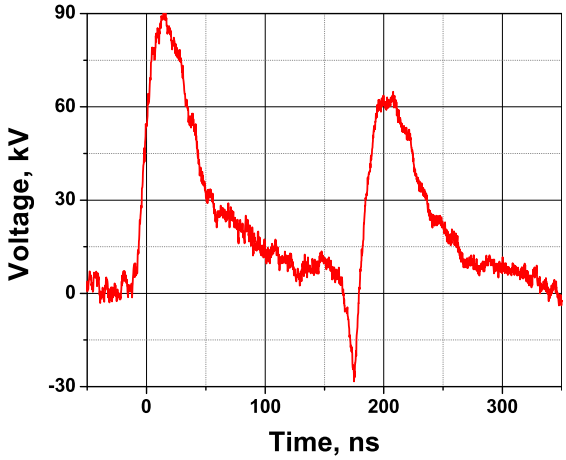


(b) Back-current shunt signal

Fig. 2.11: Discharge development in the single-cell geometry. Air, 30 Torr, E/N = 480 Td, streamer velocity — 30 mm/ns.

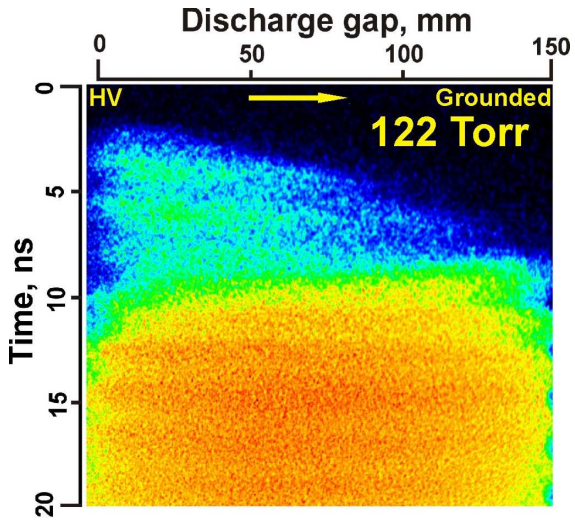


(a) Streak image

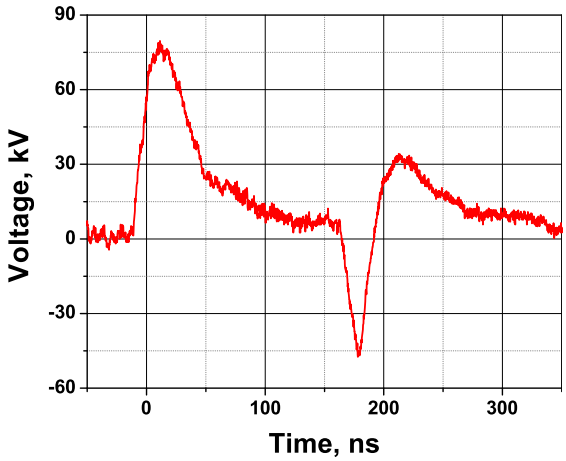


(b) Back-current shunt signal

Fig. 2.12: Discharge development in the single-cell geometry. Air, 122 Torr, E/N = 240 Td, streamer velocity — 25 mm/ns.

agation under our experimental conditions. Under high enough values of reduced electric field the streamer reaches the grounded electrode, which results in a return stroke propagation and a high–current channel formation with rapid gas heating all over the volume of the discharge cell. When the reduced electric field is insufficiently high, the streamer does not reach the grounded electrode. No return stroke propagation and high–current channel formation was observed. Rather, the gas was seen to be excited nonuniformly, forming an excited species concentration gradient along the discharge gap.

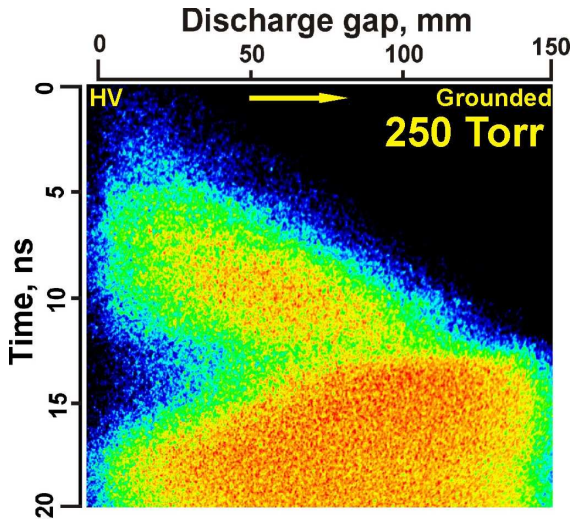


(a) Streak image

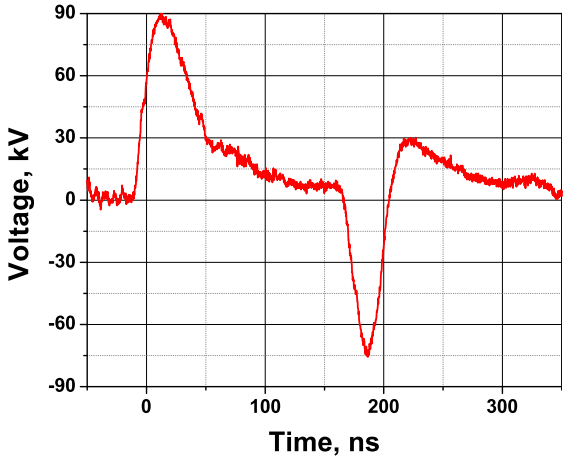


(b) Back-current shunt signal

Fig. 2.13: Discharge development in the single-cell geometry. Air, 250 Torr, E/N = 120 Td, streamer velocity — 13 mm/ns.

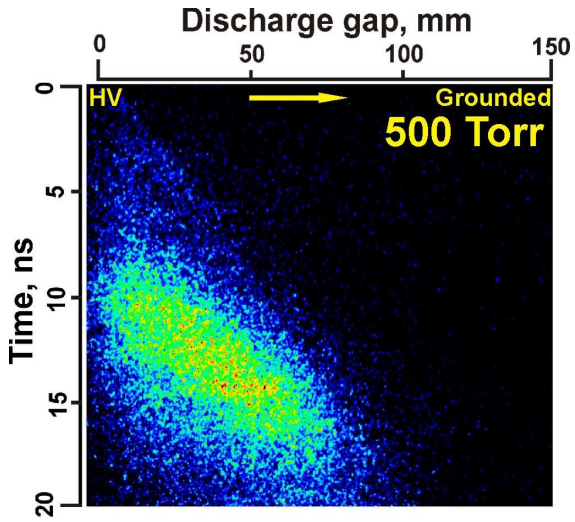


(a) Streak image

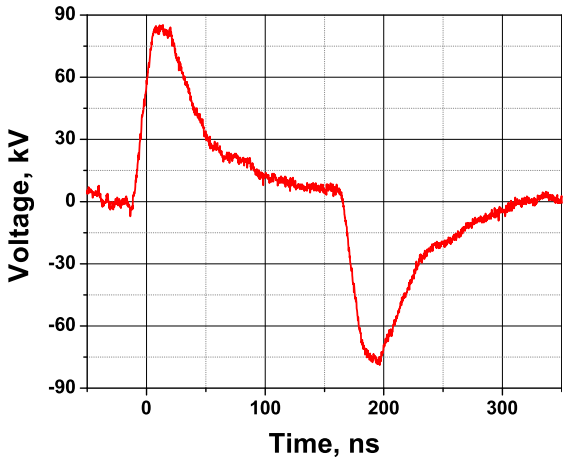


(b) Back-current shunt signal

Fig. 2.14: Discharge development in the single-cell geometry. Air, 500 Torr, E/N = 60 Td, streamer velocity — 5 mm/ns.

In the current report, these two modes of discharge development are referred to as the spark and the streamer mode, respectively. The effect of the different modes of discharge development on detonation initiation efficiency under these conditions will be studied during the following sections.

As was shown in [5], ignition by non–equilibrium plasma is mainly governed by atomic oxygen produced by the discharge. In our experiments, the shape of the O atoms density gradient could be estimated basing on the emission intensity distribution. The discharge emission in air corresponds to the

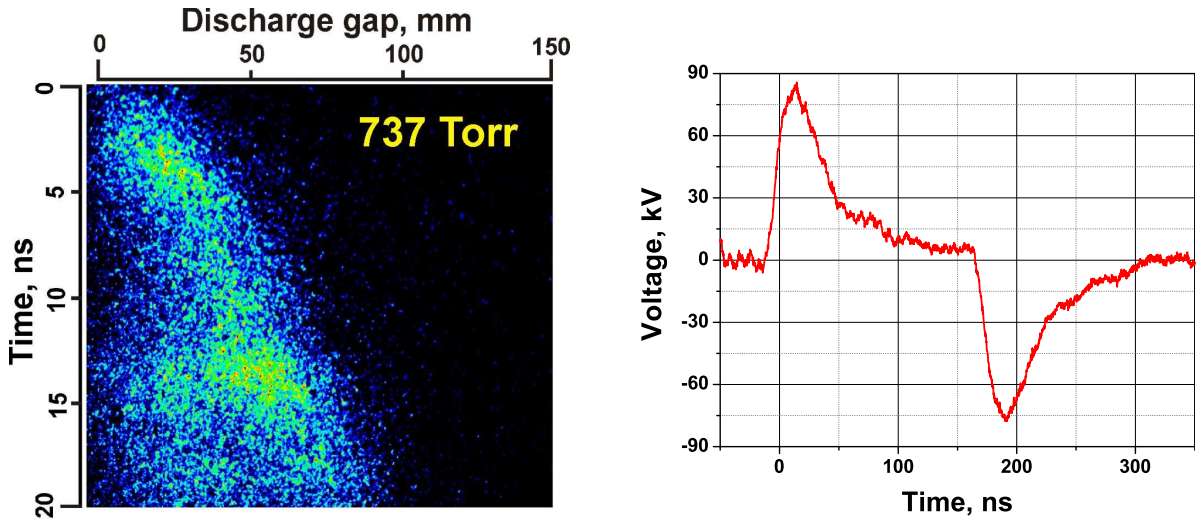


(a) Streak image (b) Back-current shunt signal

Fig. 2.15: Discharge development in the single-cell geometry. Air, 737 Torr, E/N = 40 Td, streamer velocity — 3.5 mm/ns.

second positive system of molecular nitrogen ($N_2(C^3) - N_2(B^3)$ transition). It is well known that the production of atomic oxygen in pulsed nanosecond discharges mainly occurs through 2 processes: quenching of triplet states of nitrogen [6] and direct dissociation by electron impact through the state at 8 eV [5]. The rates of these processes are approximately proportional to $N_2(C^3)$ excitation rate, which is in turn proportional to the emission intensity. Thus, analyzing the temporal dynamics of the second positive system emission, one can obtain relative concentrations of atomic oxygen in the discharge gap as $[O](z) \sim \int I(z)dt$, where $I(z)$ is the emission intensity at point $z$ of the interelectrode gap. Such analysis was performed for the streak image in Fig. 2.15 (streamer mode in air at 1 bar). The result is presented in Fig. 2.16 in terms of a normalized O atoms distribution along the interelectrode gap obtained by integrating the intensity over the discharge duration. It is seen that the gradient spans over ∼10 cm under these conditions.

Under certain experimental conditions, a transient initiation mode was also observed. After the discharge initiated by the incident high–voltage pulse had developed in the streamer mode, the pulse was reflected off the gap, having lost 10–25% of its energy on gas ionization, dissociation, and excitation. The pulse then travelled back towards the generator, where it was re–reflected again, losing a significant portion of its energy in the generator. After ∼500 ns, the pulse reached the gap for the second time. Under the experimental conditions (0.3–1 bar), this time period was not enough for complete plasma recombination; thus, the gas in the discharge channel

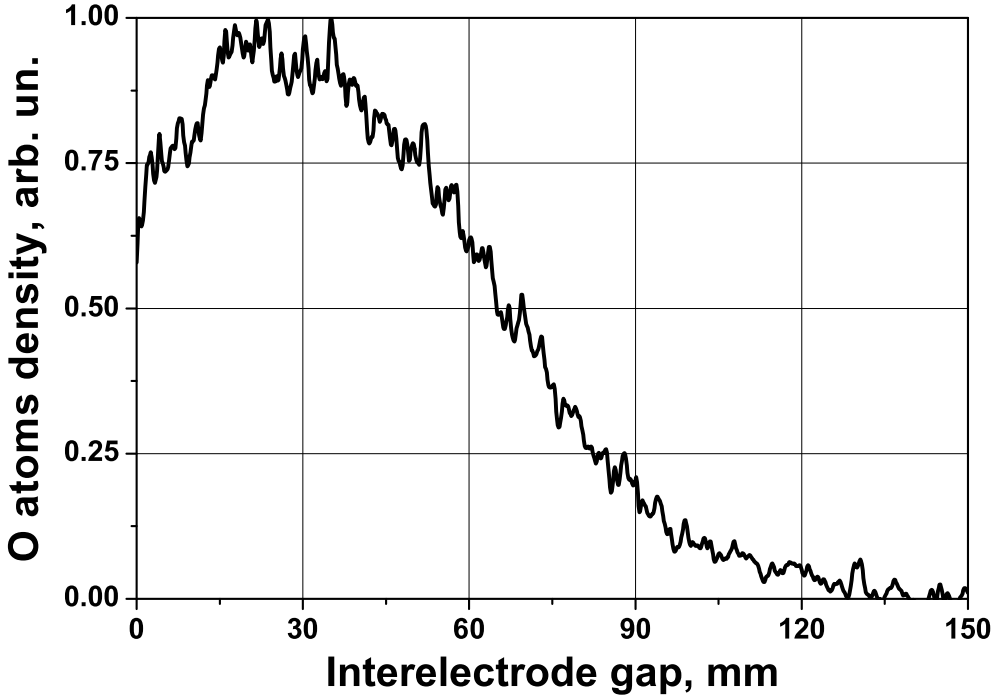


Fig. 2.16: O atoms density distribution over the interelectrode gap.

remained partially ionized. This resulted in the development of the second discharge under lower reduced electric field ($E/N$) values and the formation of a relatively hot conducting channel, which was clearly seen from the back–current shunt signal (see Fig. 2.17). Under this kind of initiation, the energy of the discharge was subdivided between translational and internal degrees of freedom of the gas, forming a typical transient plasma. The heating level was still expected to be significantly lower than under spark initiation, since the energy input in the discharge was lower due to the low energy of the second pulse. However, it did make a distinct effect on the detonation initiation parameters when compared to both basic modes.

The discharge development modes were primarily investigated in air since the absence of nitrogen resulted in a low level of emission intensity in a propane–oxygen mixture. However, the three modes were also observed in all fuel–oxidizer mixtures at slightly different parameters. The actual discharge mode was controlled by the back–current shunt signal in every experiment.

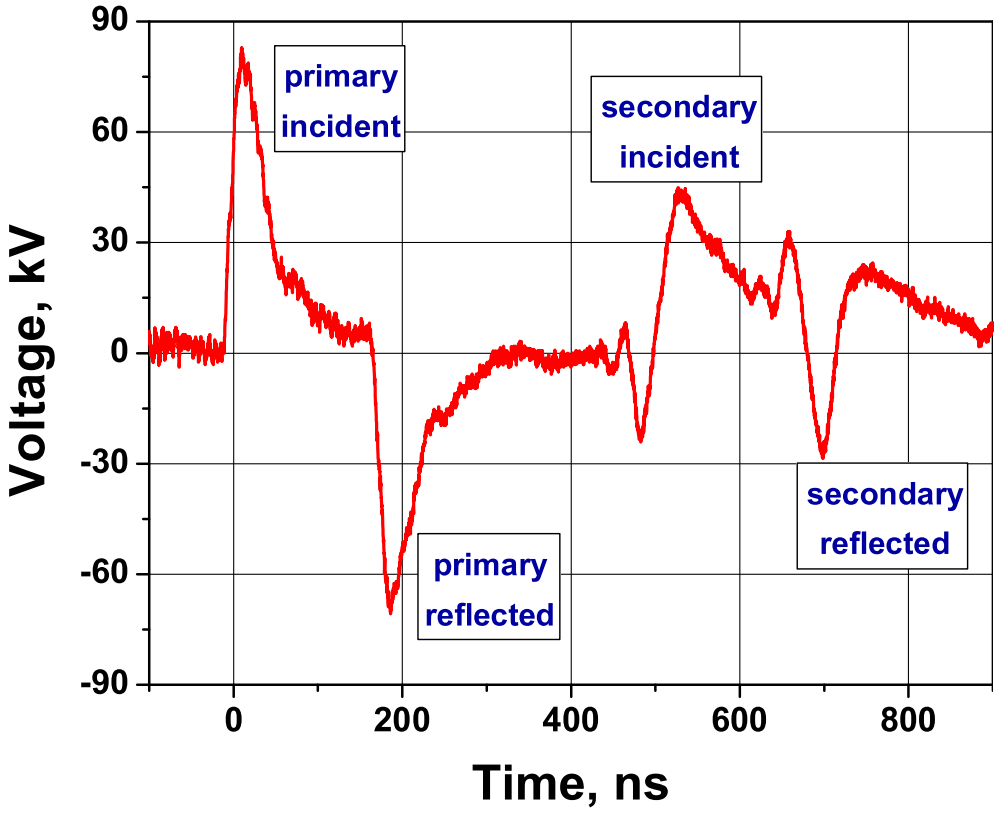


Fig. 2.17: Typical back–current shunt signal in a transient plasma initiation mode.

## 2.3 DDT Study Under Different Discharge Modes

### 2.3.1 Initiation by Spark Discharge

The spark mode of discharge development in the single–cell geometry was realized in the whole pressure range under a maximum pulse amplitude of 160 kV, which corresponded to a pulse energy of 15 J. The discharge gap in the experiments at an initial pressure of 0.3 bar was 100 mm. This resulted in an energy input into the gas of ∼10 J. Typical traces of the pressure transducers (PT) and the infra–red sensors (IR) and the corresponding x–t diagram are presented in Fig. 2.18 and Fig. 2.19, respectively. The origin of the X–coordinate in the x–t diagram coincides with the grounded electrode of the discharge gap and, hence, with the nozzle inlet. The negative X–values correspond to the discharge channel and are used to represent the ignition process dynamics captured with ICCD cameras. Each data set in the positive X-values region corresponds to a pair of pressure transducers and infra–red sensors installed at different distances from the nozzle inlet. It is seen from the x–t diagram that, by the first measuring interval between sensors 1 and 2, the flame front was closely coupled with the shock wave and propagated with

a supersonic velocity of over 700 m/s. Assuming that the flame front and the shock wave travelled at that velocity between the nozzle inlet and the first sensor would yield their propagation with zero delay after the discharge. Such a pattern resulted in a successful DDT between the 3rd and the 4th sensor, 230 mm from the nozzle inlet, which is 11–12 transverse tube sizes. The average velocity in this region — 2100 m/s — was slightly lower than the calculated CJ value. Also, a retonation wave was clearly seen propagating backwards with an average velocity of 1700 m/s. The DDT time did not exceed 300 $\mu$s.

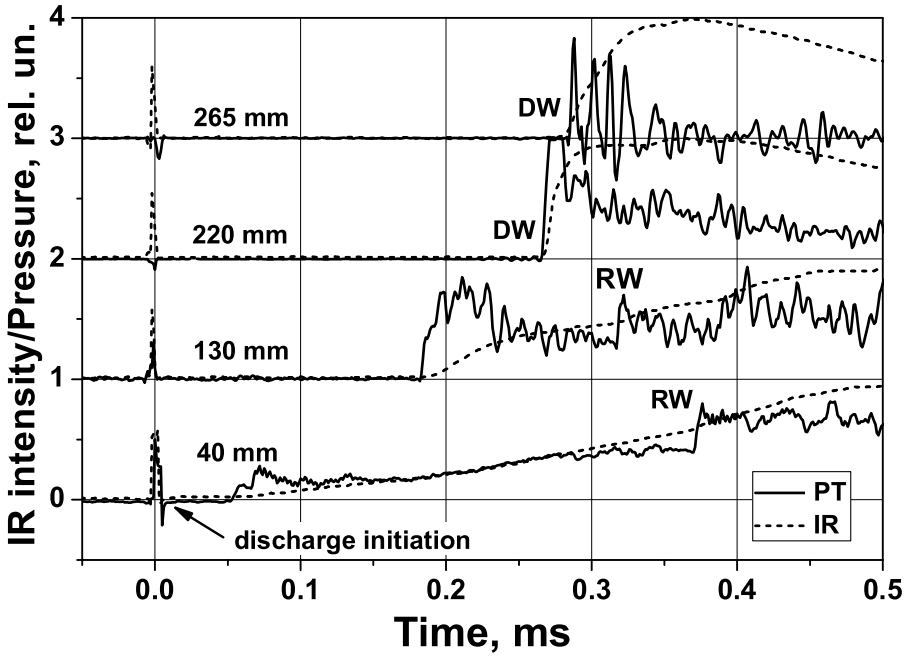


Fig. 2.18: Infra–red sensors (IR) and pressure transducers (PT) traces. DDT at an initial pressure of 0.3 bar, spark mode.

The ignition process inside the discharge channel was studied with a LaVision Picostar HR 12 ICCD camera. One image with a 1 ns gating was taken during each experiment through an interference filter with the maximum transmittance at 431.1 nm and a full width at half–maximum of 2.6 nm. The ICCD image taken 5 $\mu$s after the discharge is shown in Fig. 2.20. The image intensity corresponds to flame emission inside the discharge channel. The yellow line in the image designates the channel, with its high-voltage electrode being on the left and the detonation tube being on the right. The transverse channel size is 6.5 mm, the longitudinal dimension is the interelectrode gap (equal to 100 mm). The dark vertical strip in the image corresponds to a

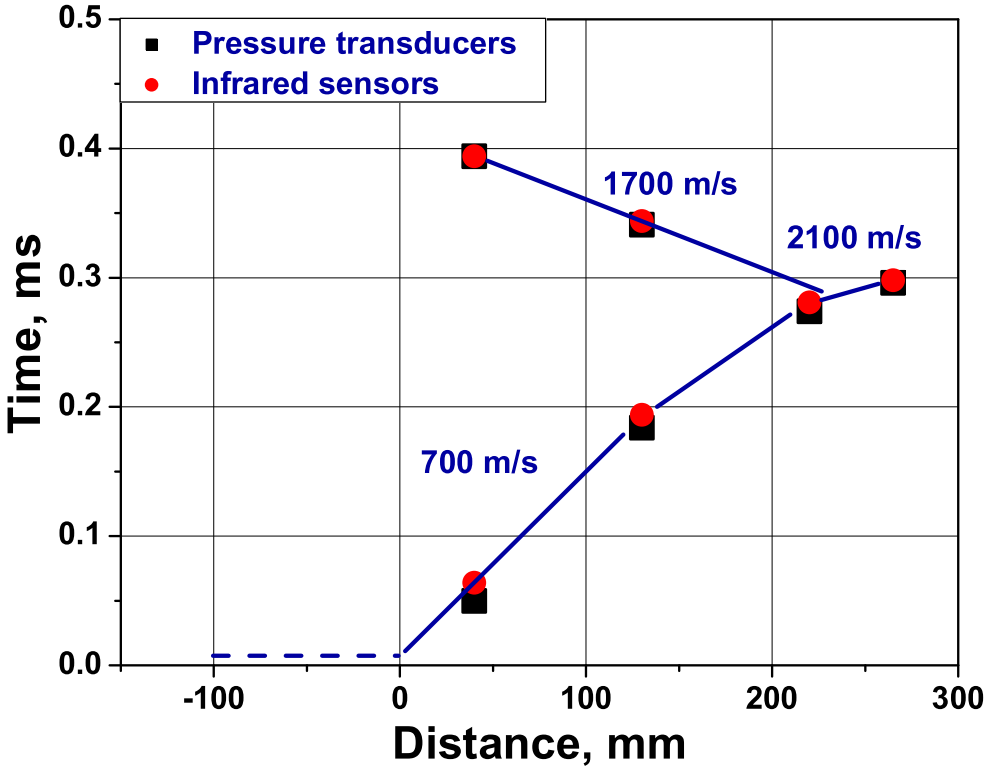


Fig. 2.19: X–t diagram of DDT at an initial pressure of 0.3 bar, spark mode.

fixing wire outside the grounded shield, which blocks the view in this area. It is seen that 5 $\mu$s after the discharge the mixture was already ignited almost all over the cell volume, which is represented by the horizontal dashed line in Fig. 2.19. This implies simultaneous ignition of the mixture in terms of the typical temporal scale of gas–dynamic processes and confirms the assumption that the propagation of both the flame wave and the shock wave occurred without a significant delay.

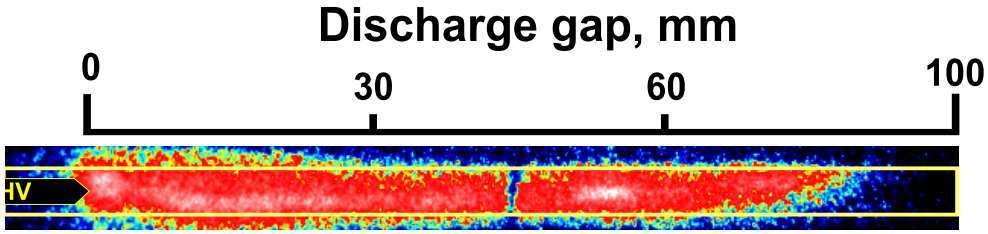


Fig. 2.20: ICCD image of the discharge cell 5 $\mu$s after the discharge. DDT at an initial pressure of 0.3 bar, spark mode.

After simultaneous ignition inside the cell, a DDT occurred in the detonation tube. This process was also captured with the ICCD camera through the plexiglass window. A series of these images taken in different experiments at different moments in time is presented in Fig. 2.21. The window consists

of two parts designated by yellow frames, each spanning 110 mm lengthwise. The width of the window is 20 mm, which is equal to the transverse size of the detonation tube. The time is counted off from the discharge initiation. The discharge cell and the conical nozzle are on the left. It is seen that, at the early stages (0–200 $\mu$s), a deflagration wave propagated with a velocity of approximately 700 m/s, which agrees well with the sensors data. After 200 $\mu$s, a hot spot formed. The location of the hot spot varied among different experiments. Again in agreement with the sensor data, a detonation wave was formed less than 300 $\mu$s after the discharge.

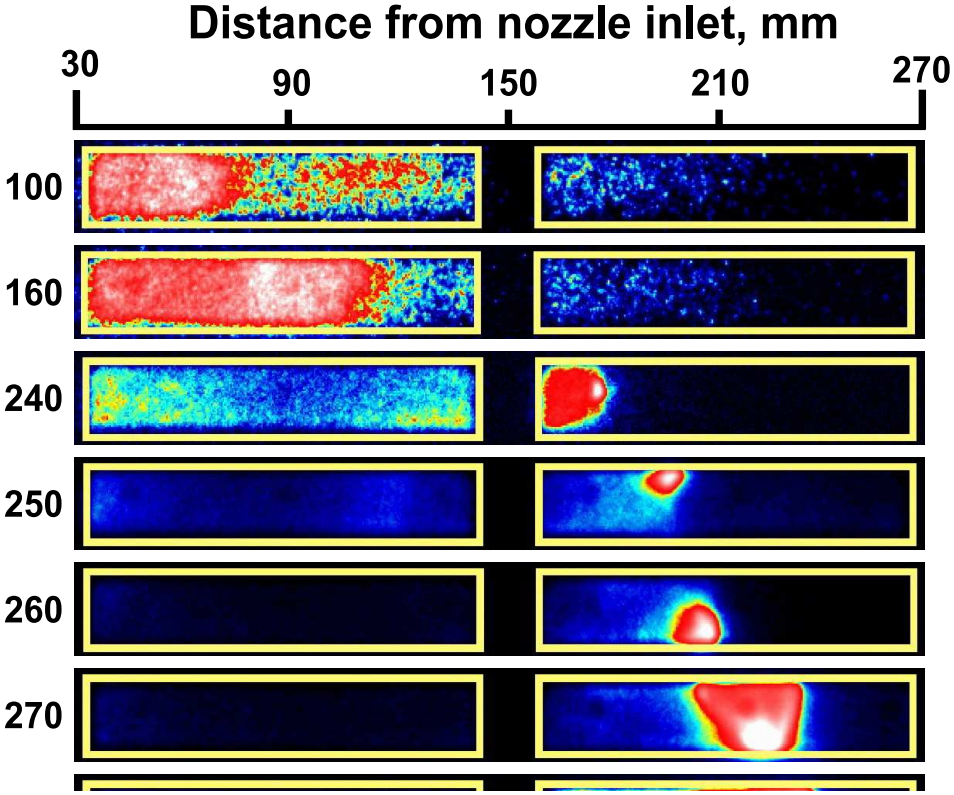


Fig. 2.21: ICCD images of the detonation tube at different moments in time. DDT at an initial pressure of 0.3 bar, spark mode.

The spark mode of DDT initiation at an initial pressure of 1 bar resulted in a significantly shorter DDT time and run–up distance, though under the same energy input of 10 J from the high–voltage pulse. The discharge gap in these experiments was 150 mm. The corresponding pressure transducers traces and the x–t diagram are presented in Figs. 2.22 and 2.23. The average velocity became equal to the CJ value between sensors 1 and 2, which implied that the detonation wave was formed before or shortly after sensor 1. Thus, the DDT time amounted to 50 $\mu$s and the run–up distance was 50 mm or less.

Since we have shown that the ignition in the spark mode occurs earlier than 5 $\mu$s after the discharge, the average velocity between the nozzle inlet and the first sensor can be estimated as ∼800 m/s, as illustrated by the dashed line in Fig. 2.23.

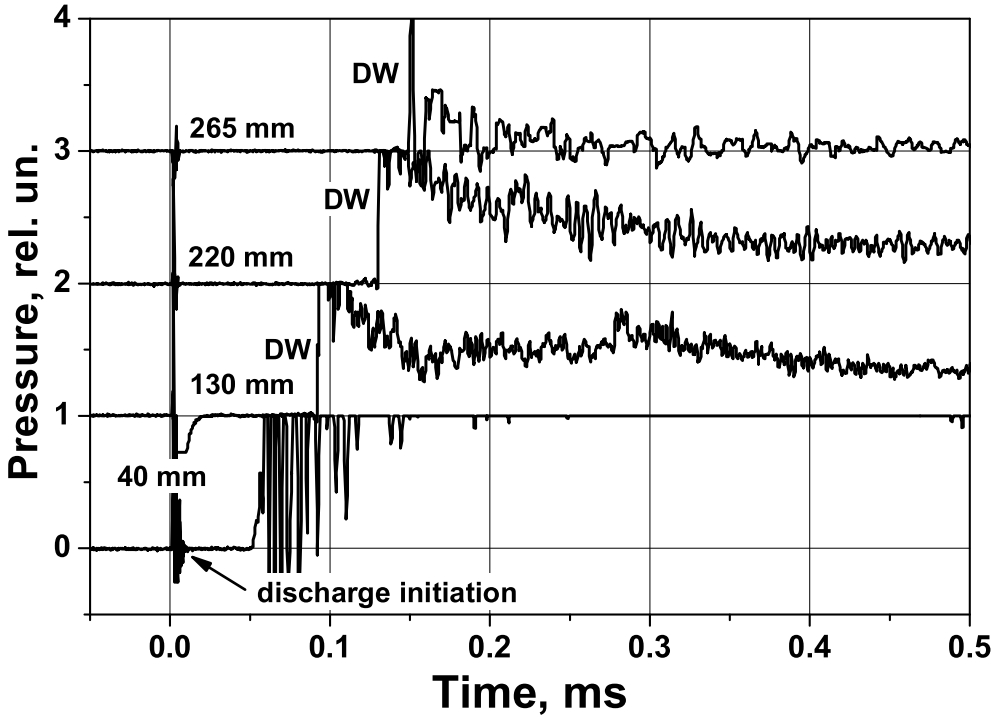


Fig. 2.22: Pressure transducers (PT) traces. DDT at an initial pressure of 1 bar, spark mode.

### 2.3.2 Initiation by Transient Plasma

At a pressure of 0.3 bar, the combined transient initiation mode was realized with a pulse amplitude of 80 kV and under a longer discharge gap of 150 mm. The energy of the pulse amounted to 4–5 J, whereas the energy input in the initial streamer discharge was less than 1.5 J. The accurate amount of energy deposited in the mixture during the second discharge is difficult to calculate due to the overlapping of the incident and the reflected pulses, but an estimate yields ∼1 J. The DDT pattern for this kind of initiation in terms of IR and PT traces and an x–t diagram is shown in Figs. 2.24 and 2.25. The initial velocity of the shock wave is equal to 600 m/s, which is slightly lower than that for the spark initiation at the same initial pressure. During the initial stages, the flame wave was following the shock wave with the same velocity, but with a notable delay of 30–40 $\mu$s. The flame wave then accelerated and caught up with the shock wave shortly after sensor 3. The acceleration took more

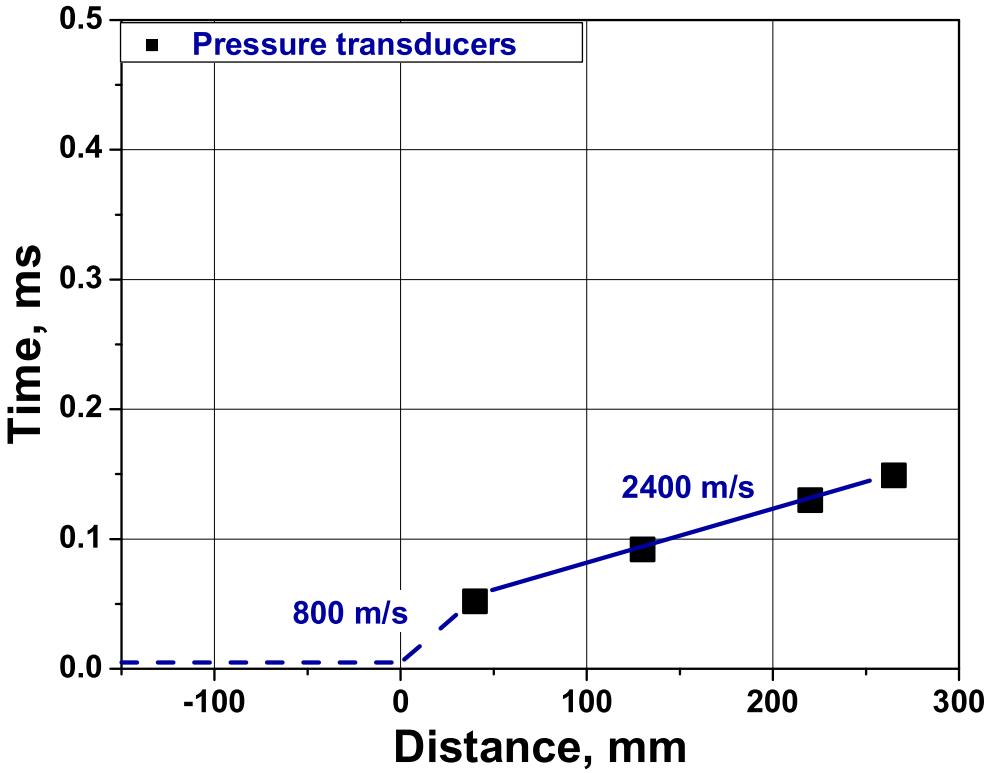


Fig. 2.23: X–t diagram of DDT at an initial pressure of 1 bar, spark mode.

time and distance to occur in comparison with the spark mode: the average velocity between sensors 3 and 4 amounted to only 1150 m/s. However, the DDT did occur between these sensors since a retonation wave is clearly seen propagating backwards from some point in that region. The DDT length and time amounted to approximately 250 mm and 400 $\mu$s, respectively.

In order to investigate the ignition process in detail, time–resolved ICCD imaging of the discharge chamber was performed with a LaVision Ultra-SpeedStar16 camera. The camera is capable of capturing a sequence of up to 16 frames with a 512×512 resolution at a maximum frame rate of 1 MHz. The minimal gate value is determined by the image intensifier and is equal to 100 ns. Apart from these limitations, the frame sequence may be arbitrary. This allowed us to capture the temporal development of the ignition process inside the discharge chamber during a single experiment. The imaging was performed in the spectral region between 200 and 800 nm. The results for the transient initiation mode at 0.3 bar are presented in Fig. 2.26 in terms of a 12–frame sequence of images taken each 5 $\mu$s with a 2 $\mu$s gate. The first image was supersaturated due to the discharge afterglow. The subsequent images confirmed that ignition did occur almost simultaneously over all the volume of the channel and with an ignition delay of ∼30 $\mu$s after the dis-

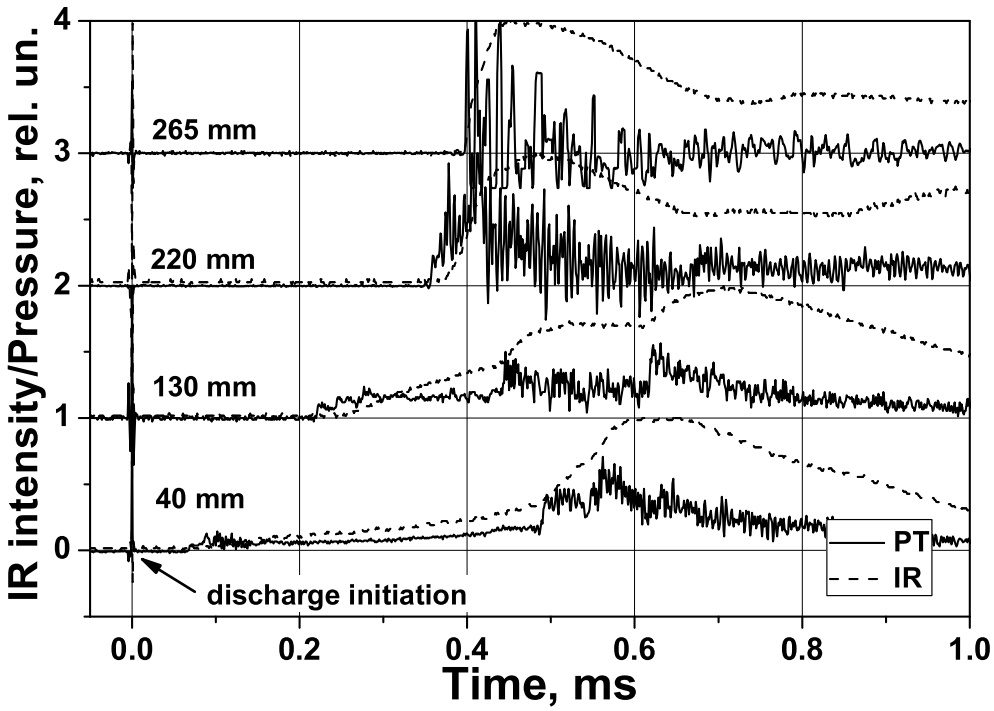


Fig. 2.24: Infra–red sensors (IR) and pressure transducers (PT) traces. DDT at an initial pressure of 0.3 bar, transient mode.

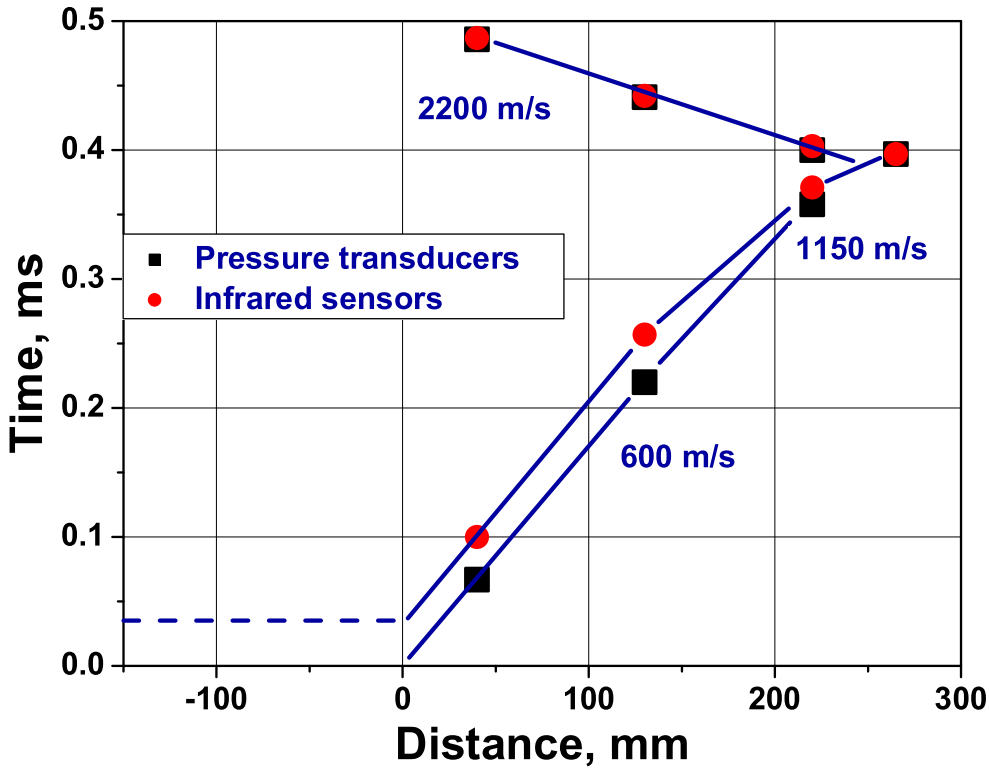


Fig. 2.25: X–t diagram of DDT at an initial pressure of 0.3 bar, transient initiation mode.

charge. At this instant, a flame front was formed at the discharge channel

output and started to propagate towards the detonation tube, which agrees very well with the IR sensor data presented in the x–t diagram in Fig. 2.25.

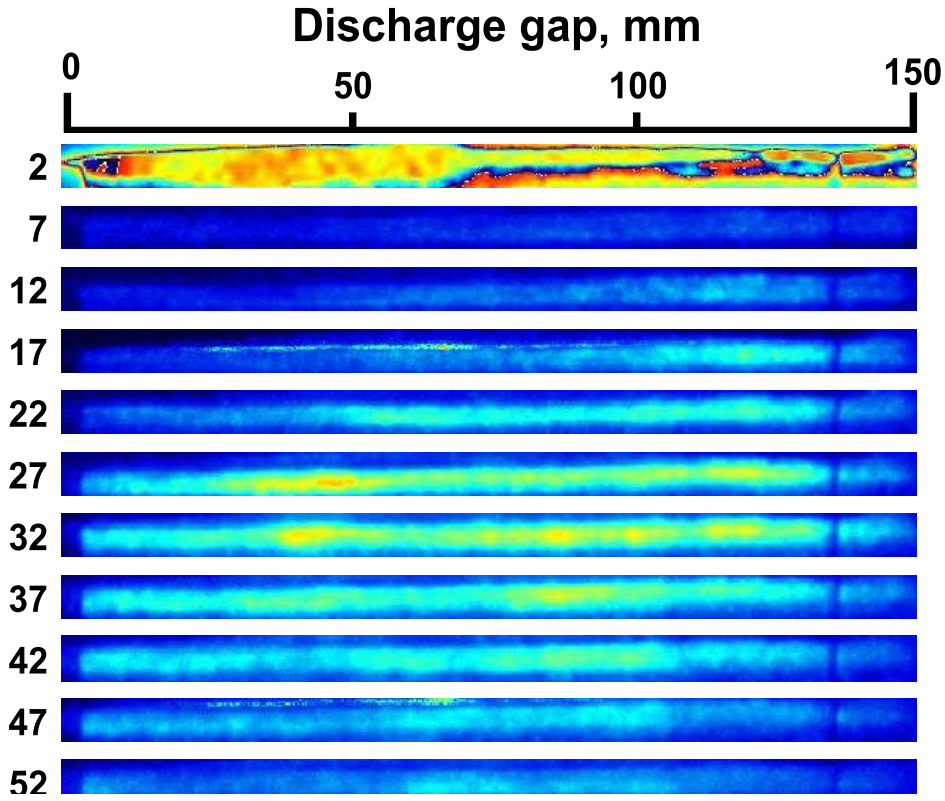


Fig. 2.26: Time-resolved ICCD imaging of fuel mixture ignition inside the discharge chamber. DDT at an initial pressure of 0.3 bar, transient initiation mode.

In order to realize this initiation mode at an initial pressure of 1 bar, the pulse amplitude was raised up to 120 kV under the same interelectrode gap of 150 mm. The pulse energy was 12 J, 1.2 J of which was deposited in the plasma by the first streamer discharge. A significant portion of the pulse energy — over 3 J — was deposited during the second discharge. The IR and PT traces and the x–t diagram under these conditions are presented in Figs. 2.27 and 2.28. At the higher pressure, the flame wave caught up with the shock wave sooner: the delay was only 10 $\mu$s at sensor 1, completely diminishing later on. The average velocity value corresponded to the CJ value already between sensors 1 and 2. The DDT time was slightly over 60 $\mu$s and the run–up distance was $\sim$50 mm, which is quite close to the values observed for the spark initiation under the same conditions. A backwards propagating wave seen in the x–t diagram corresponds to the wave reflected off the membrane located 300 mm from the nozzle inlet.

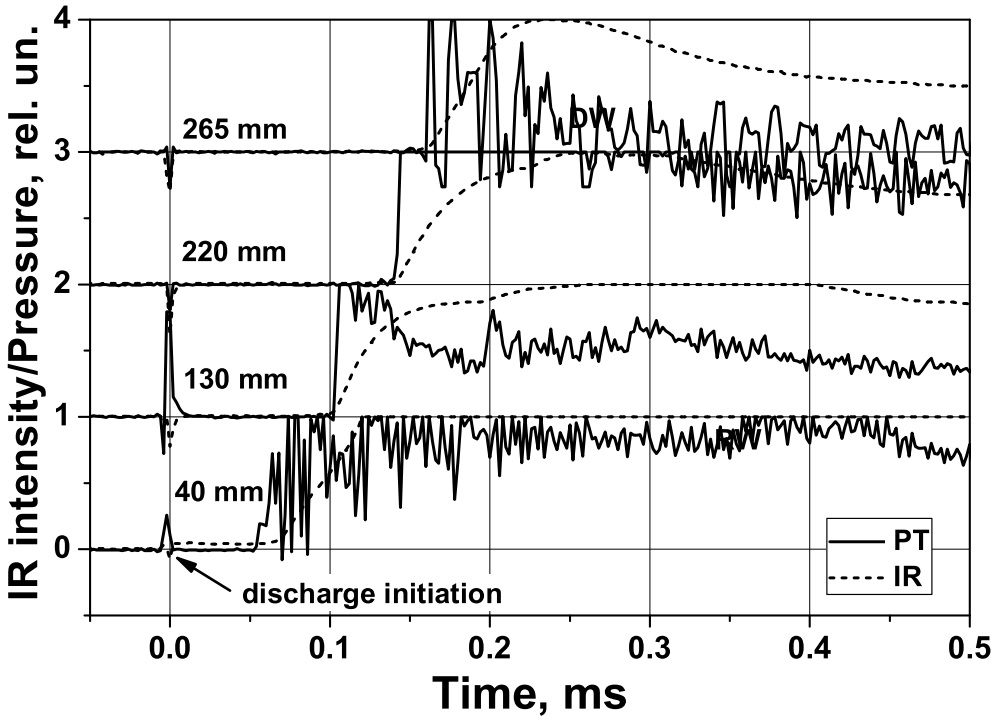


Fig. 2.27: Infra–red sensors (IR) and pressure transducers (PT) traces. DDT at an initial pressure of 1 bar, transient mode.

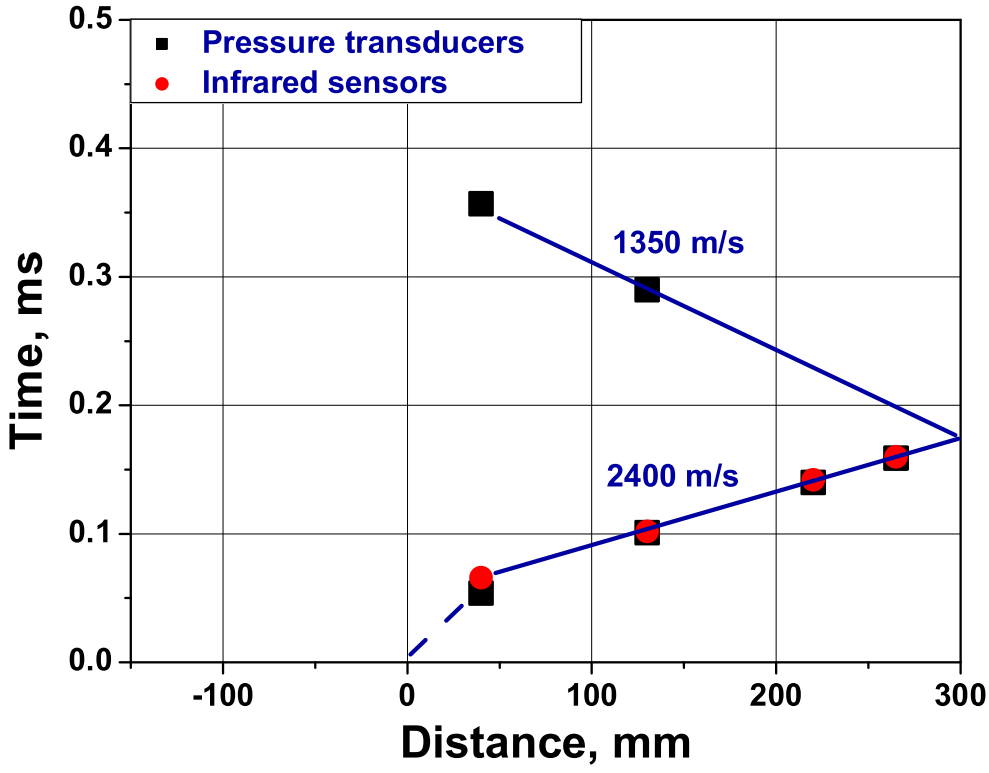


Fig. 2.28: X–t diagram of DDT at an initial pressure of 1 bar, transient initiation mode.

### 2.3.3 Initiation by Streamer Discharge: Gradient Mechanism

The streamer mode of discharge development could only be realized at a maximum discharge gap of 150 mm, a maximum initial pressure of 1 bar, and a minimum possible pulse voltage of 80 kV. The pulse energy amounted to 3—5 J under these conditions. The streamer mode of discharge propagation without the formation of a hot channel resulted in a different DDT pattern. The results are presented in terms of the PT and IR sensors traces in Fig. 2.29. From the sensors data, it is seen that a detonation wave already propagated at CJ velocity between sensors 1 and 2. The DDT time was significantly longer and amounted to 150 $\mu$s.

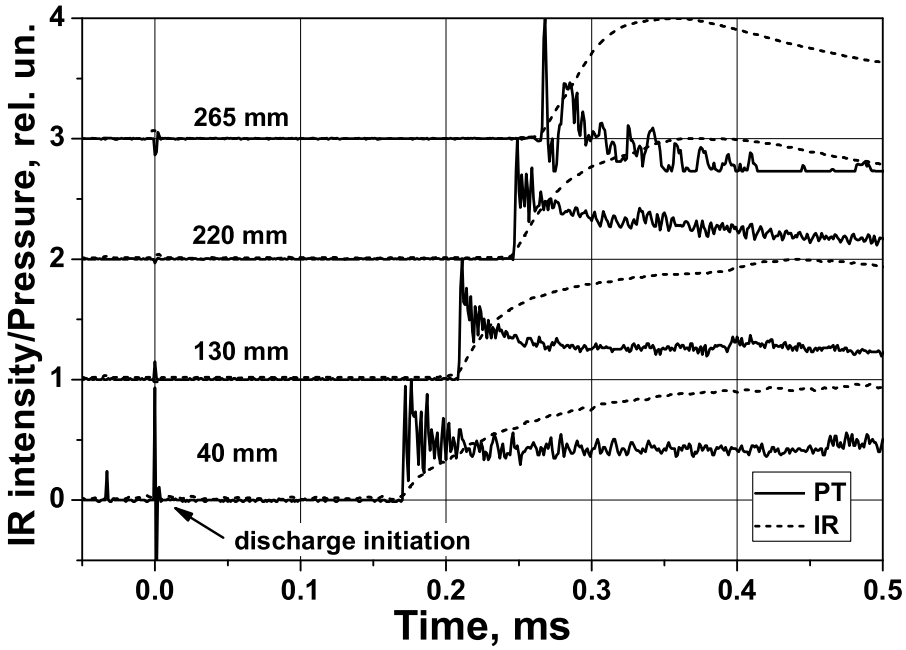


Fig. 2.29: Infra–red sensors (IR) and pressure transducers (PT) traces. DDT at an initial pressure of 1 bar, streamer mode. Test 1.

In order to investigate the ignition process dynamics, time–resolved ICCD imaging of the discharge chamber was performed with the LaVision UltraSpeedStar16 camera. The results for the streamer initiation mode at 1 bar are presented in Figs. 2.30 and 2.31 in terms of a 12–frame sequence of images taken with a 4 $\mu$s gate. The images were taken during two tests under identical gas conditions. The observed difference is due to the pulse shape variation intrinsic to gas–filled Marx type generators. The traces in Fig. 2.29 correspond to test 1 and, thus, to the image sequence in Fig. 2.30. The time–resolved ICCD imaging showed that the ignition did not occur simulta-

neously over the channel. Instead, a flame was seen originating in the region closest to the high–voltage electrode after a delay of over 50 $\mu$s and then propagating and accelerating along the channel. The initial flame front velocity exceeded 1500 m/s, and accelerated up to 2000 m/s at the channel outlet. The corresponding data points for both tests were plotted in the x–t diagram in Fig. 2.32 in the negative X–values region. It is seen that the x–t trajectories of the flame waves inside the discharge channel agree well with the ones measured by the pressure transducers and the IR sensors inside the detonation tube.

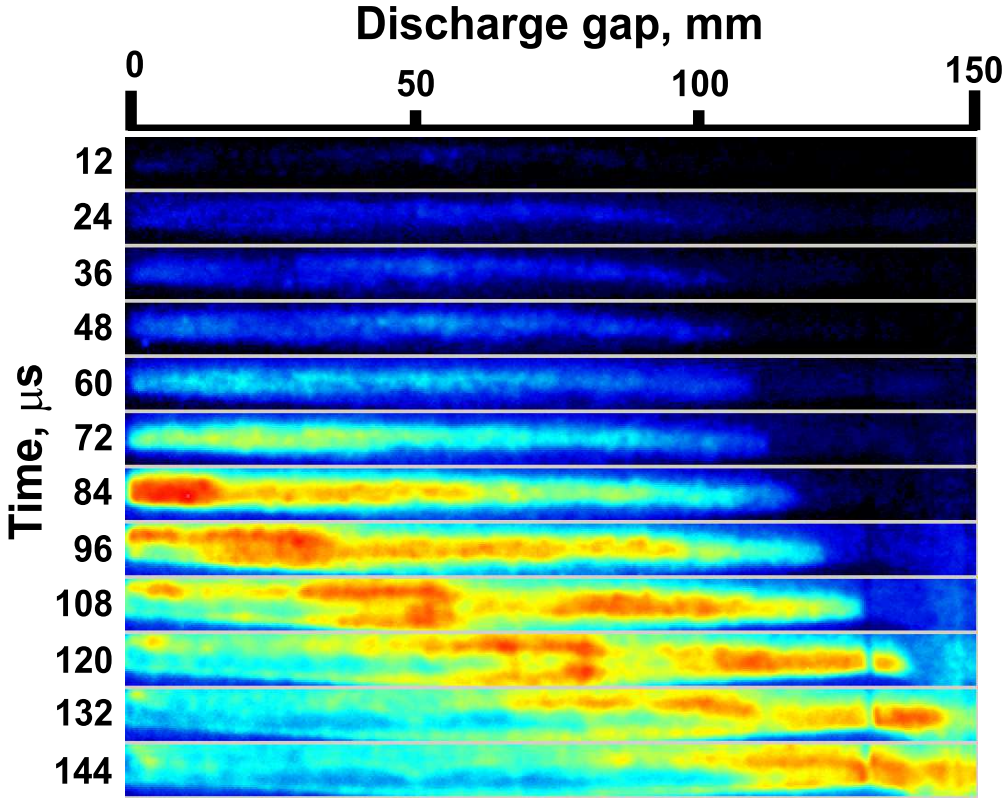


Fig. 2.30: Time-resolved ICCD imaging of fuel mixture ignition inside the discharge channel. DDT at an initial pressure of 1 bar, streamer mode. Test 1.

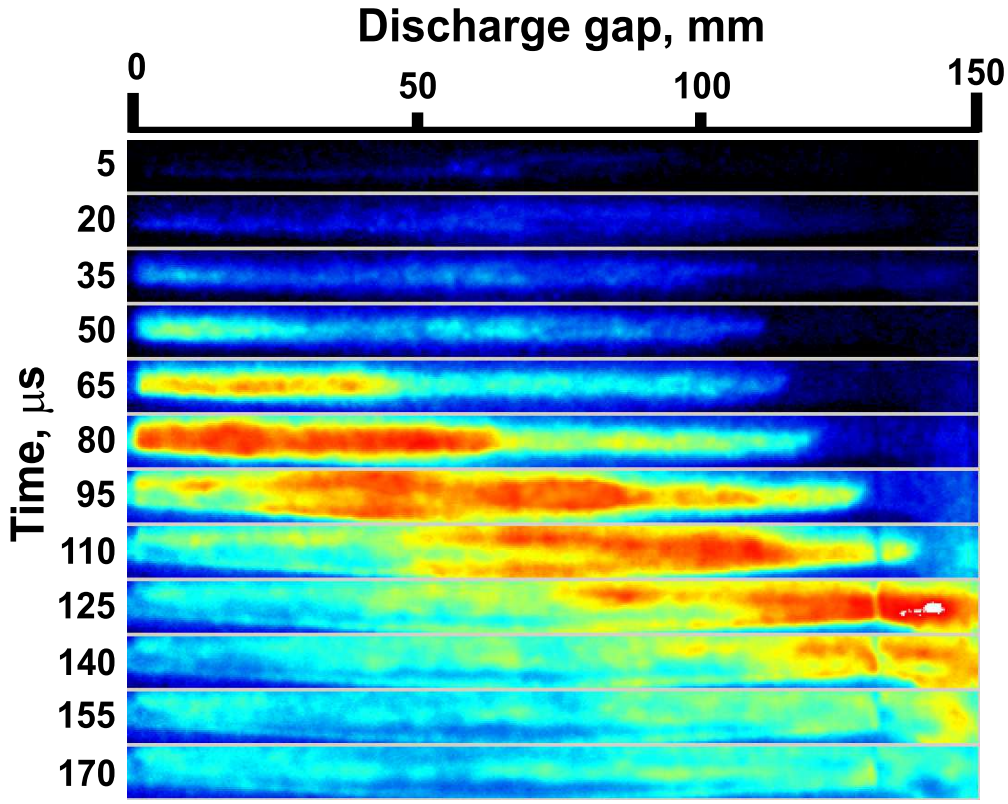


Fig. 2.31: Time-resolved ICCD imaging of fuel mixture ignition inside the discharge channel. DDT at an initial pressure of 1 bar, streamer mode. Test 2.

## 2.4 Discussion: Discharge Modes vs DDT Modes

The current section includes an experimental study of DDT initiation in a detonation tube with a discharge chamber of single–cell geometry under three different discharge development modes: a nanosecond spark, a streamer, and a combined transient discharge, which is a streamer followed by a spark–like breakdown after 0.5 $\mu$s. The experiments were carried out in a stoichiometric propane–oxygen mixture. The results for two initial pressure values (0.3 and 1 bar) are presented and discussed. Detonation cell sizes for that mixture at 0.3 and 1 bar are 3 and 1.5 mm, respectively [7]. The latter value was obtained by extrapolation of data from Ref. [7] into a higher pressure region. Both values are noticeably lower than the discharge cell diameter (6.5 mm) and the detonation tube transverse size (20 mm). The critical energy of direct planar detonation initiation in the current detonation tube is ∼100 J at an initial pressure of 1 bar and ∼150 J at 0.3 bar [7]. The initiating energies are at least an order of magnitude lower in all the experiments presented. In this section of the paper, a comparison between different DDT mechanisms under different modes of discharge development will be given.

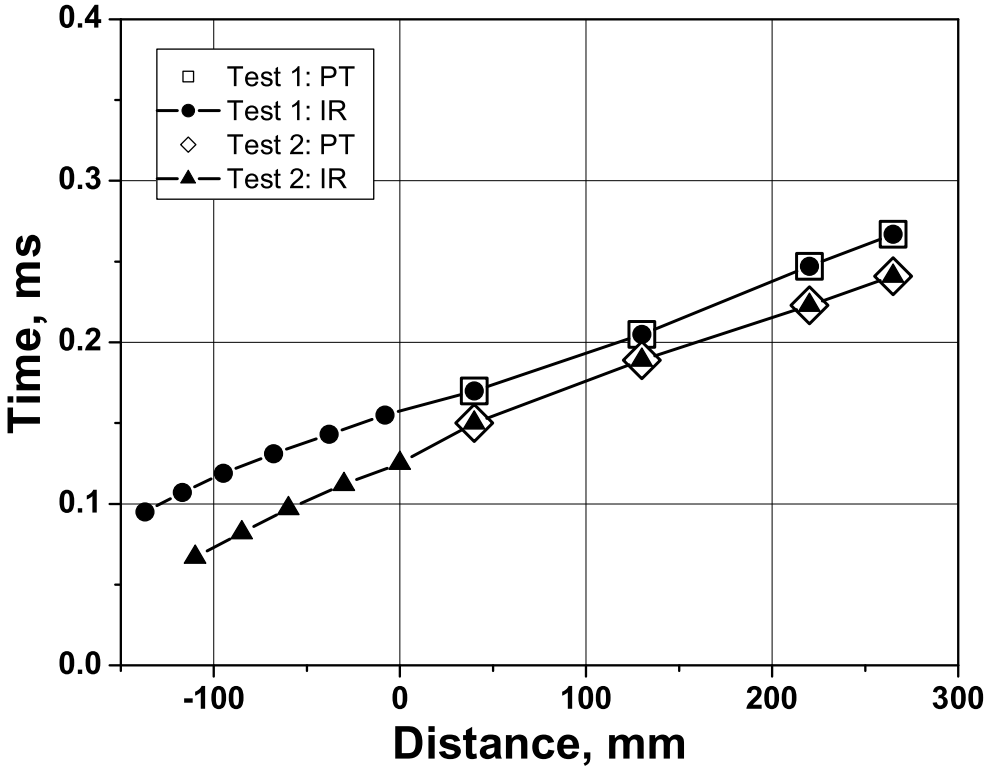


Fig. 2.32: X–t diagrams of DDT at an initial pressure of 1 bar, streamer mode.

The spark mode of discharge development is distinguished by a greater amount of energy deposited into the gas. For both initial pressures studied, the energy input amounted to approximately 10 J. Considering that the discharge channel volume for the experiment at 0.3 bar is 3.3 $cm^3$, this energy is enough to heat the mixture by over 10000 K. However, it is known that in high–voltage nanosecond discharges, the most energy is deposited into electronic excitation and ionization and not into translational degrees of freedom. A calculation of the energy distribution was performed in a two–term expansion of the Boltzmann equation. Self–consistent sets of cross–sections for electron collisions with $O_2$ [8] were used. No reliable, self–consistent sets of electron cross–sections are available for propane. In our simulation, they were assumed to be similar to those for $C_2H_6$ [9]. We took into account dissociation, ionization, and vibrational and electronic excitation of $O_2$ and hydrocarbon molecules, as well as elastic scattering of electrons. The calculation yielded that under a reduced electric field value of 320 Td, which is the case for this experiment, over 80% of the energy is deposited into excitation of electronic levels. As has been estimated in [10], approximately 30% of this energy is transferred into translational degrees of freedom within a time period much shorter than 1 $\mu$s. In the current experiment, this means

that the fuel mixture is being instantly (within 1 $\mu$s) heated up by $\sim$3000 K. Such rapid and significant heating leads to instant formation of a shock wave propagating at a Mach number above 2 and to mixture ignition all over the discharge channel without any delay. This rapid volumetric ignition has been confirmed by the single–frame ICCD imaging performed 5 $\mu$s after the discharge (Fig. 2.20). Thus, being closely coupled from the very initial stages of the process, the shock wave and the flame wave start propagating together as a fast deflagration wave with supersonic velocity. These considerations are confirmed by the sensors data provided in the x–t diagram in Fig. 2.19. Since the ignition occurs in a long channel (10 to 15 cm in all the experiments), the rarefaction wave originates at a considerable distance from the shock wave, allowing the coupled waves to accelerate along the detonation tube. However, it is seen from the temporally resolved image sequence in Fig. 2.21 that the flame never accelerates to above 800–1000 m/s. Instead, after reaching such a velocity (after $\sim$250 $\mu$s for the current experiment), an explosion occurs from a hot spot forming a planar detonation front. After that, a stationary Chapman–Jouguet detonation wave propagates with a velocity of $\sim$2400 m/s. Such a DDT pattern is well–known and has been described in a number of works [11]. The position where the adiabatic explosion occurs can also be determined as the origin point of the retonation wave plotted in Fig. 2.19. This value is 230 mm under these conditions, which agrees very well with the image sequence in Fig. 2.21.

The mechanism of detonation wave formation under spark initiation at an initial pressure of 1 bar is quite the same. Due to the higher gas concentration and longer discharge gap, the reduced electric field value is lower and amounts to 70 Td. The calculation still yields $\sim$80% of the energy deposition into electronically excited species since the lower $E/N$ value results mostly in lower ionization rates and greater energy deposition into vibrational and rotational degrees of freedom. On the other hand, the portion of energy deposited into electronic excitation does not decrease significantly. Considering that fact and that the value of the total energy input is 10 J, the gas heating can be estimated as $\sim$800 K, which is still enough to rapidly ignite the mixture and produce a shock wave. It has to be noted here that it is unlikely for the discharge to be completely uniform over the cross–section of the channel. The non–uniformities of discharge current lead to a lower value of the effective gas volume being heated and, hence, to even higher temperature values in these regions. As a consequence, a shock and a flame wave are again formed with zero delay and then propagate with supersonic velocity. But,

due to the higher pressure and concentration of the fuel mixture, the acceleration and the consequent transition to detonation occur earlier; the pressure trace at the first transducer 40 mm away from the discharge chamber output corresponds to a CJ detonation wave. That also implies a shorter DDT time of 50 $\mu$s, which is noticeably less than for the experiment at 0.3 bar.

The transient discharge initiation mode is specific to the current experimental setup. The shape of the secondary re–reflected pulse is governed by the processes inside the spark gaps of the Marx generator; its delay relative to the initial pulse depends on the length and type of the feeding line chosen. The distinguishing feature of this initiation mode is the way the pulse energy is transferred to the gas. The initial discharge develops as a regular streamer at relatively high reduced electric field values: the most energy is deposited into the ionization and excitation of the gas. But, under the typical experimental conditions, the energy input in streamer mode is only 10–25% and the total energy input proves to be lower than in the spark mode, thus not heating the gas significantly. The total energy input during the secondary discharge is comparable or even greater than that of the streamer. In addition, since its amplitude is lower and the discharge gap is filled with preionized, partially conducting gas, the effective reduced electric field value proves to be considerably lower. This results in a greater energy deposition into translational degrees of freedom and gas heating, which is more typical for a spark discharge; under high enough pulse amplitude, the secondary discharge develops in a way similar to the nanosecond spark observed in the first mode.

Such discharge development accounts for the observed DDT pattern reasonably well. At an initial pressure of 0.3 bar, the total energy of the incident pulse under this initiation mode is 5 J, which leads to an energy input of only 1.5 J in the first streamer and of 1 J in the secondary discharge. This energy proves to be sufficient to produce a shock wave propagating at 600 m/s (see Fig. 2.25 for the x–t diagram) but, in contrast to the spark mode, it is not coupled with the flame wave. The latter does start propagating after the simultaneous ignition inside the discharge channel after a significant ignition delay of $\sim$30 $\mu$s. This consideration has been clearly confirmed by the time–resolved imaging with an UltraSpeedStar16 camera (Fig. 2.26). Such an ignition delay is due to the insufficient heat release by the discharge in comparison with the spark mode. What is important is that the ignition still occurs almost simultaneously along the discharge gap, which is illustrated by the horizontal dashed line in Fig. 2.25. Due to the ignition delay, it takes

time for the flame wave to catch up with the shock wave. After that, the acceleration occurs quite soon, leading to a successful DDT at a distance of 250 mm, though after a noticeably longer time of 400 $\mu$s in comparison with the 300 $\mu$s in the spark mode.

The results of transient initiation under an initial pressure of 1 bar are very close to those obtained in the spark mode, at least in terms of x–t diagrams (see Figs. 2.23 and 2.28). That fact is accounted for by the relatively large energy input in the transient mode; the total energy input is 4.2 J, of which 3 J was deposited during the secondary discharge. The energy input in the spark mode is yet larger and exceeds 10 J. However, the second discharge in the transient mode develops under lower $E/N$ values, which results in significantly more efficient gas heating. Any numerical estimate is extremely complicated due to the gas preionization remaining after the first streamer. It is most likely that the heating level is eventually enough to form a strong shock wave together with a flame wave propagating at a velocity of $\sim$800 m/s with a short delay. This makes the transient mode very similar to the spark mode in terms of the DDT mechanism as well, although it is under lower absolute values of incident and deposited energy.

The energy input in the streamer mode is yet lower: 1 J under the total incident pulse energy of 4.5 J. Furthermore, the calculations of the discharge phase demonstrate that only $\sim$0.3 J is deposited into gas heating, which corresponds to a uniform temperature shift of only 70 K. However, the imaging performed with the UltraSpeedStar16 camera proves that the energy input is not uniform along the discharge gap in the streamer discharge (see Fig. 2.31). It is clearly seen that the mixture is first ignited in the region next to the high–voltage electrode 50–60 $\mu$s after the discharge. The hot spot is formed here, at the tip of the electrode, due to the highest $E/N$ and current values, which is typical for streamer discharges starting from pin–like electrodes; the increased temperature implies shorter ignition delay time. The spontaneous combustion front then propagates along the discharge channel with an extremely high velocity of over 1500 m/s, gradually accelerating up to 2000 m/s. Such an ignition pattern is accounted for by an ignition delay time gradient in the mixture, which corresponds to the excited species concentration gradient formed by the streamer. Eventually, a detonation wave is formed shortly after the channel output before 40 mm from the nozzle inlet. In comparison to the spark mode, the DDT time is relatively long and amounts to $\sim$150 $\mu$s due to the longer ignition delay under a lower energy input. Also, under streamer initiation, the flame front has to propagate

over the length of the discharge channel before entering the detonation tube, which takes up almost half the DDT time.

The comparison of all three initiation modes shows that there are actually two general mechanisms of DDT initiation under our experimental conditions. The first one implies simultaneous ignition of the fuel mixture inside the discharge channel and the formation of a shock wave propagating at a Mach number over 2. When ignited by a strong enough spark, the flame wave is coupled with the shock wave from the very early stages of the process. The coupled waves then accelerate up to a certain velocity value, at which point an adiabatic explosion occurs from a hot spot. Shortly after the explosion, a plane CJ detonation wave is formed. If the energy input is not that high and the heating level does not allow the mixture to ignite instantly, the flame wave starts propagating after an ignition delay. It then takes additional time for the flame wave to catch up with the shock wave and to further accelerate up to the necessary velocity value. It is worth noting that the discharge channel length and, hence, the volume of the excited mixture, is significant for spark initiation; the large ignited volume does not allow the rarefaction wave to catch up with the leading shock before the DDT occurs.

The second mechanism observed in the experiments is a combination of the Zeldovich [12] and the SWACER [13] mechanisms, also studied numerically in [14]. That mechanism does not require the ignition of all the mixture inside the discharge channel. Instead, the mixture is non–uniformly excited, so that an ignition delay gradient is formed. It has to be noted that, according to Zeldovich, the ignition delay gradient is formed through a temperature gradient in the mixture whereas, in our experiments, it is also due to the active species concentration distribution. This results in lower values of temperature and, hence, sound speed in the gradient region. The ignition first occurs at the hot spot at the tip of the high–voltage electrode after a delay. The spontaneous wave then propagates along the channel at $V_{sp} < V_{CJ}$, gradually accelerating up to the CJ velocity, in agreement with the mechanisms cited above. Such weak ignition leads to a longer DDT time in comparison with the spark mode under the same conditions. However, the DDT length is below 2 transverse tube sizes for the both mechanisms. Furthermore, the deposited initiation energy in the experiments with streamer initiation is lower, by an order of magnitude, than that necessary for the spark mode, and is two orders of magnitude lower than the energy of direct planar detonation initiation. It is clear also that the efficiency of the gradient mechanism depends on experimental parameters, such as the discharge cell geometry, the pulse

shape and amplitude, gas properties, and others. These aspects are discussed in detail in the following section.

# Chapter 3

# Four–Cell Discharge Chamber

## 3.1 Experimental Setup

For a more detailed study of the gradient mechanism, a four–cell Plexiglas discharge chamber was designed. The scheme is shown in Fig. 3.1. The geometry of each discharge cell remained the same. Each cell contains a pin–like high–voltage electrode (1) which is immersed into a 6.5 mm–diameter channel (2). The channels length is 150 mm. Replacement of the electrodes allows to vary the interelectrode distance and, thus, the reduced electric field value under the same pulse parameters. The four channels are led into the same square detonation tube (see Fig. 2.1) through a converging reducer (3). The diameter of the channels inside the reducer is 9 mm. The convergence angle is 24deg. The diameter of the reducer outlet is 20 mm, which matches with the inlet of the detonation tube. The reducer is manufactured of aluminium and is grounded, serving as the ground electrode. The whole Plexiglas discharge section is also covered with grounded shield (4). The shield includes a longitudinal gap for visual observation of the processes inside one channel. Discharge propagation is also enhanced by four grounded plates (5) which are fixed into narrow slits inside the chamber between the discharge channels. The plates stretch along the whole chamber, increasing the capacitance of the electrode system and the transverse reduced electric field in the channels. In comparison to the single–cell geometry, the volume of the potentially excited gas mixture is increased fourfold. The overall appearance of the discharge chamber is shown in Fig. 3.2.

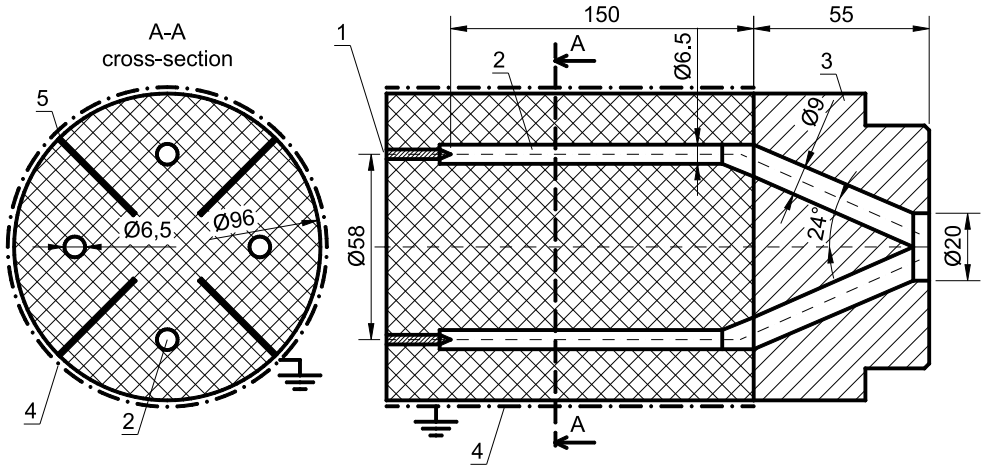


Fig. 3.1: Four–cell discharge chamber: the scheme. (1) — high–voltage electrode, (2) — discharge channel with a diameter of 6.5 mm, (3) — converging reducer, (4) — coaxial grounded shield, (5) — grounded plates.

Fig. 3.2: Detonation tube with four–cell discharge chamber: the appearance.

## 3.2 Discharge Development: Gradient Shape

The construction of the four–cell discharge chamber implied that only relatively low–amplitude pulses could be used. The vast majority of DDT experiments was carried out under a pulse amplitude of ∼50 kV. Under such conditions, the discharge propagated as a streamer in a wide pressure range above ∼0.1—0.15 bar depending on the gas. It allowed to study the gradient mechanism extensively. At the same time, it would demonstrate how that kind of DDT occurred under low energy inputs.

The discharge propagation mode was controlled in every experiment by the same back–current shunt used with the single–cell chamber. The shunt provided the data on both the propagation mode and the energy input value in the experiment. Both the spark mode and the streamer mode were registered. However, due to the different geometry and pulse amplitude, the pressure ranges differed substantially from those observed for the single–cell chamber. The typical back–current shunt traces for the two modes are presented in Figs. 3.3 and 3.4. The incident pulse energy, the reflected pulse energy, and the energy input are shown in the figures. It is seen that almost 90% of the pulse energy is deposited into the gas in spark mode, which is accounted for by the multi–cell geometry of the discharge chamber.

In order to estimate the shape of the excited species gradient, streak imaging has also been performed for the discharge in air at 1 bar using the same technique as in 2.2.2. The imaging could only be performed in the one discharge channel not completely covered by the shield. However, the discharge was expected to develop similarly in all the channels due to the symmetry of the chamber. The resulting streak image is presented in Fig. 3.5 together with the shunt data illustrating the incident and reflected pulse shapes. The pulse voltage was typical for the DDT experiments and amounted to ∼50 kV. An estimation of the O atoms concentration gradient along the interelectrode gap was obtained by integrating the intensity over the discharge duration. The resulting distribution is presented in Fig. 3.6. The relatively low reduced electric field value (25 Td) results in a low streamer velocity (1.5 mm/ns). For that reason, the streamer only propagates over the portion of the channel next to the high–voltage electrode. That is also clearly seen from the O atoms concentration gradient shape, which spans over ∼5 cm in comparison with the 10 cm in the single–channel case under a higher reduced electric field value (40 Td).

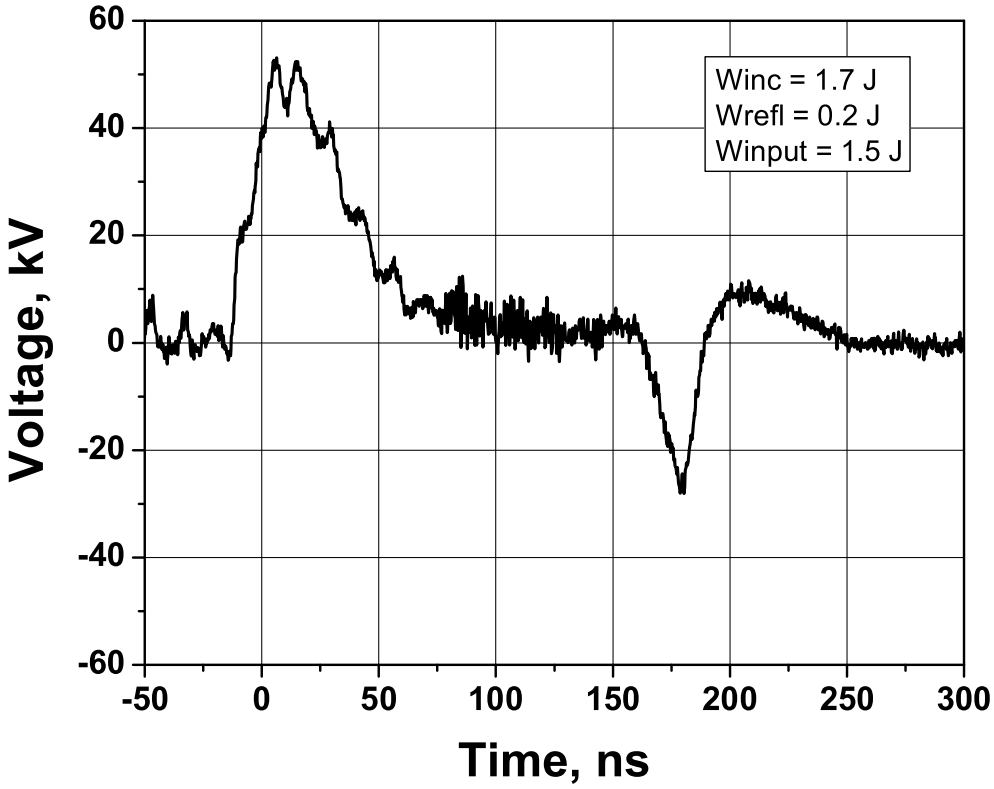


Fig. 3.3: Typical back–current shunt signal in spark mode in the four–cell DC. Air, 0.09 bar.

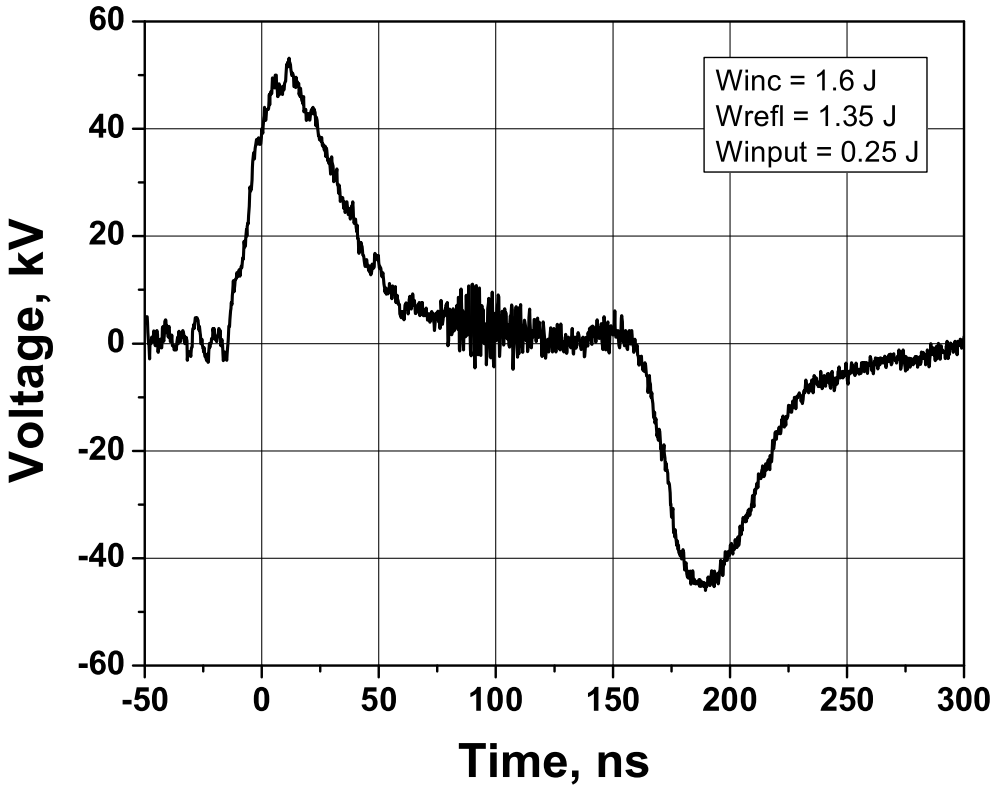


Fig. 3.4: Typical back–current shunt signal in streamer mode in the four–cell DC. Air, 1 bar.

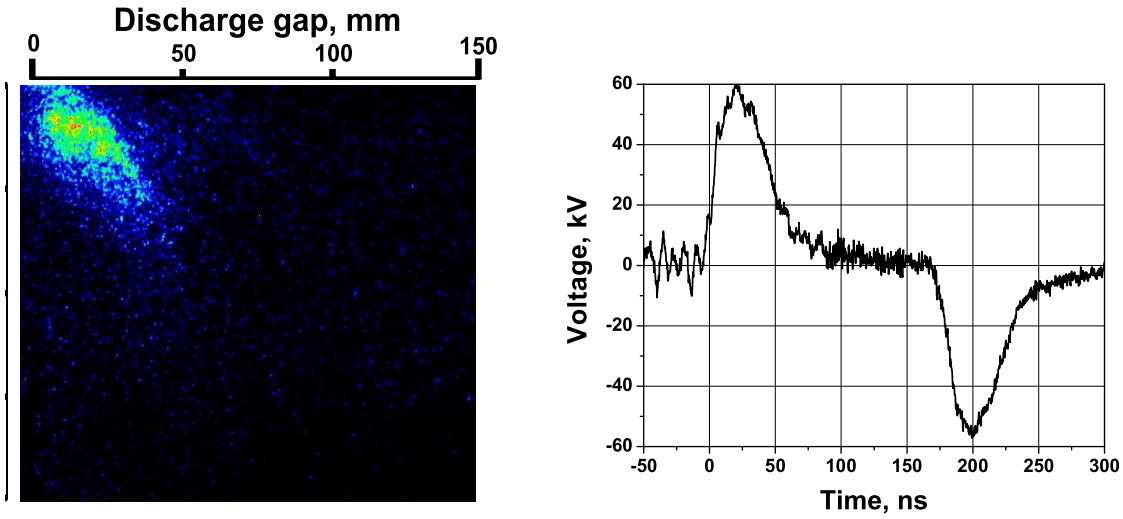


(a) Streak image (b) Back-current shunt signal

Fig. 3.5: Discharge development in the four–cell geometry. Air, 737 Torr, E/N = 25 Td, streamer velocity — 1.5 mm/ns.

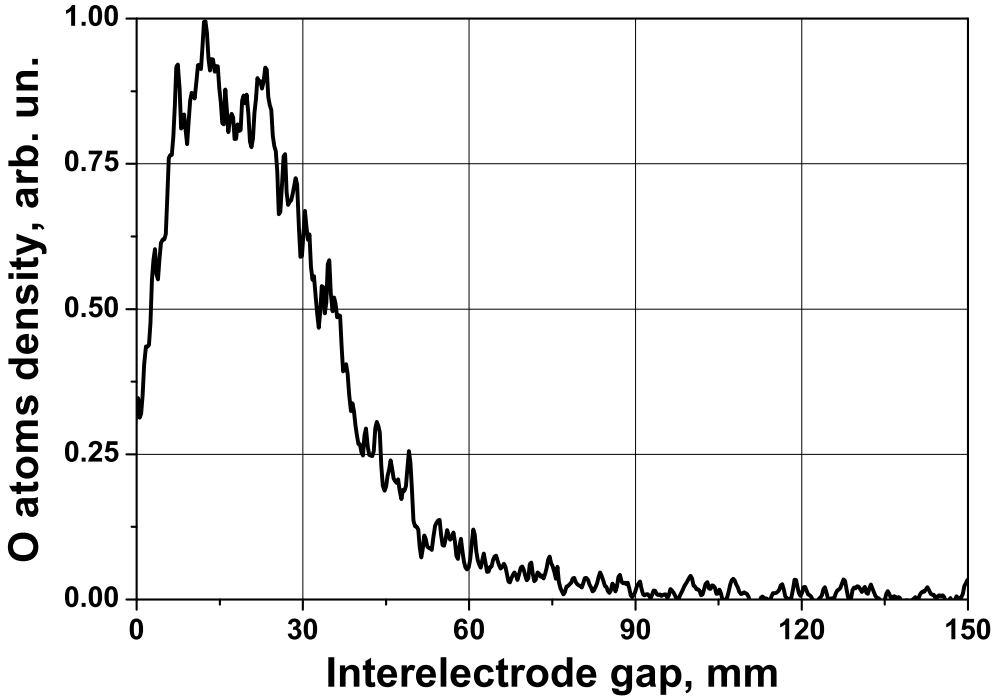


Fig. 3.6: O atoms density distribution over the interelectrode gap in one of the four channels.

## 3.3 Gradient Mechanism Study Under Different Conditions

For the experiments in the four–cell DC, the same smooth detonation tube with a square cross section was used. The tube was now connected to the discharge channels with the reducer with four converging channels. The same set of infra–red sensors (IR) and pressure transducers (PT) was used in the DDT experiments. The sensors were positioned 80, 170, 260, and 305 mm from the discharge channel outlet and the reducer inlet, which is 40 mm further downstream in respect to the channel outlet due to the insertion of the reducer. The experiments were carried out in three different mixtures: $C_3H_8 + 5O_2$ (undiluted), $C_3H_8 + 5O_2 + 4N_2$ (40% nitrogen), and $C_2H_2$ + air (stoichiometric). The interelectrode gap was 150 mm in all the experiments. The pulse amplitude was 40—60 kV in all the presented experiments except one in the acetylene–air mixture. The results are again presented in terms of x–t diagrams. The original IR and PT traces are provided for additional information.

### 3.3.1 Undiluted Propane–Oxygen Mixture

#### Initiation by spark and transient discharge

The first experiments were carried out in undiluted propane–oxygen mixture at a relatively low pressure of 0.09 bar under which the discharge developed as a spark. The detonation cell size for this mixture under these conditions is 14 mm [7], which is comparable to the tube transverse size. The incident pulse voltage was varied, so that results under different initiation energies (energy input in the discharge) could be compared. The energy input in the discharge was defined from the back–current shunt signal. The IR and PT traces for the experiments under initiation energies of 1.2 and 1.7 J are presented in Figs. 3.7 and 3.8, respectively. The x–t diagrams based on the PT data for the cases are plotted in Fig. 3.9 as full and hollow black squares. The energy values shown in the legend next to the pressure correspond to the energy input in the discharge. It is seen that in both cases there was a shock wave propagating along the tube with a velocity of 900 m/s. A flame wave was propagating behind the shock with the same velocity and with a delay of $\sim$30 $\mu$s. The waves reached the first measuring cross–section (80 mm from the reduces inlet) 300 $\mu$s after the discharge under the initiation energy of 1.2 J. The larger energy input of 1.7 J resulted in a decrease of the initial

delay to 200 $\mu$s. Such pattern is typical for a deflagration wave initiated by a spark discharge, which has also been observed in our previous experiments. For comparison, the x–t diagram of the experiment performed at 0.1 bar in spark mode in the single–cell DC is also plotted in Fig. 3.9 as grey triangles. The high value of energy input (9 J) lead to a significantly lower delay in that case, but the resulting flame velocity was only 600 m/s.

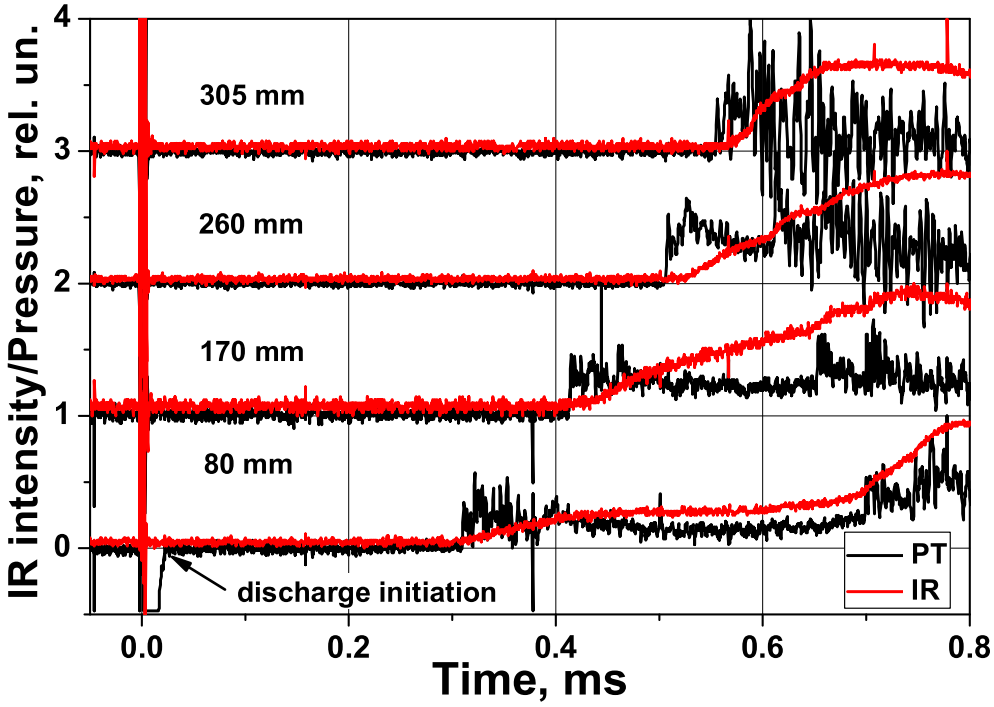


Fig. 3.7: Infra–red sensors (IR) and pressure transducers (PT) traces. DDT at an initial pressure of 0.09 bar, spark mode, energy input 1.2 J.

Under a slightly higher initial pressure of 0.13 bar, the discharge developed as a transient streamer. In that case, the gap gets closed by the streamer, but then the high–voltage pulse ceases before the current and the conductivity in the gap rises significantly. No reflection of the same polarity is observed on the back–current shunt signal, which indicates that there is a non–zero resistance in the gap. However, a large portion of the incident pulse energy (typically 80—90%) is deposited into the gas in this mode. The results of the experiments at this pressure in terms of IR and PT traces are presented in Figs. 3.10 and 3.11 for two values of initiation energy: 1.0 and 1.9 J. In the first case, the shock wave propagated along the tube at the CJ velocity after the second measuring cross–section or earlier. It is also seen from Fig. 3.10 that the flame wave was closely coupled with the shock wave in this region. This clearly testifies that a CJ detonation wave had been formed by this point.

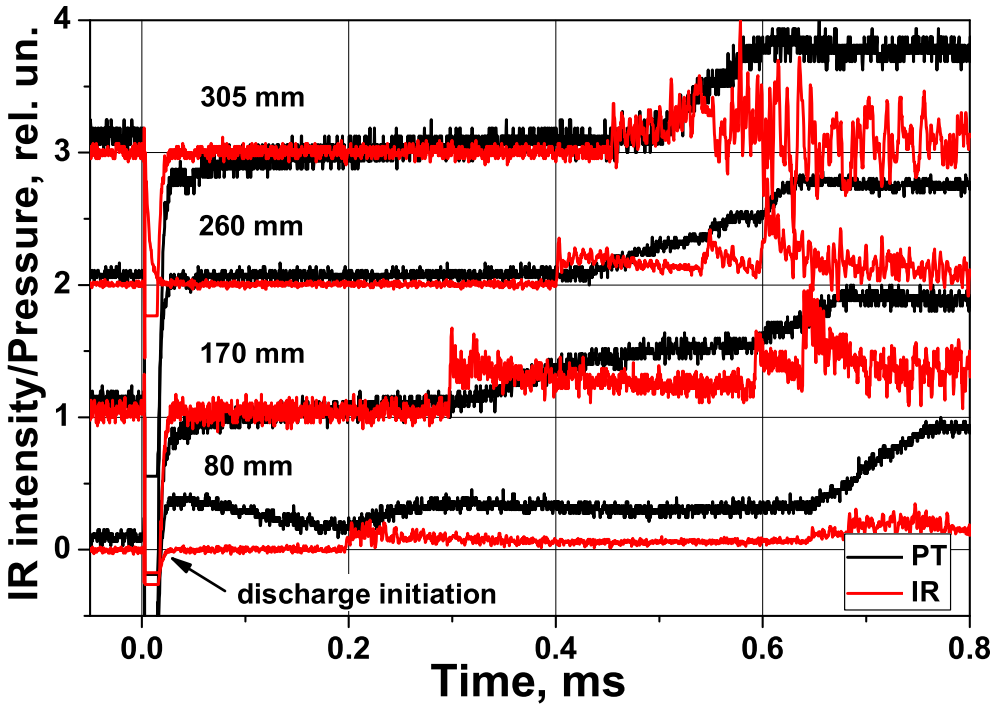


Fig. 3.8: Infra–red sensors (IR) and pressure transducers (PT) traces. DDT at an initial pressure of 0.09 bar, spark mode, energy input 1.7 J.

The formation of the detonation wave was captured with the LaVision UltraSpeedStar16 camera using the technique described in Sec. 2.3.2. The resulting 12–frame image sequence for the case under 1.0 J of initiation energy is shown in Fig. 3.12, demonstrating the temporal development of the ignition inside one of the four discharge channels. It is seen that, even under an energy input of 1 J in a transient mode, the gas was not overheated and ignited all over the volume of the chamber due to the large volume of the chamber. After the ignition occurred near the high–voltage electrode, a spontaneous combustion wave started propagating, accelerating along the channel. Approximately 100 $\mu$s before the wave reached the channel outlet, the mixture also ignited in the area next to the grounded electrode. It indicated that, under certain conditions, there was also a backward propagating streamer, which originated from a sharp edge of the grounded converging reducer. All these distinctive points are plotted in the x–t diagram in Fig. 3.9 (full red circles). Here, the x–t data points may be based on either the IR or the PT traces, because the arrival times of the flame and shock waves are identical on this temporal scale, as is seen from Fig. 3.10. It is clear from the x–t diagram that the flame wave originating from the grounded electrode reached the first sensor earlier than the accelerating spontaneous combustion wave could reach that point. However, the velocity of the latter at the end

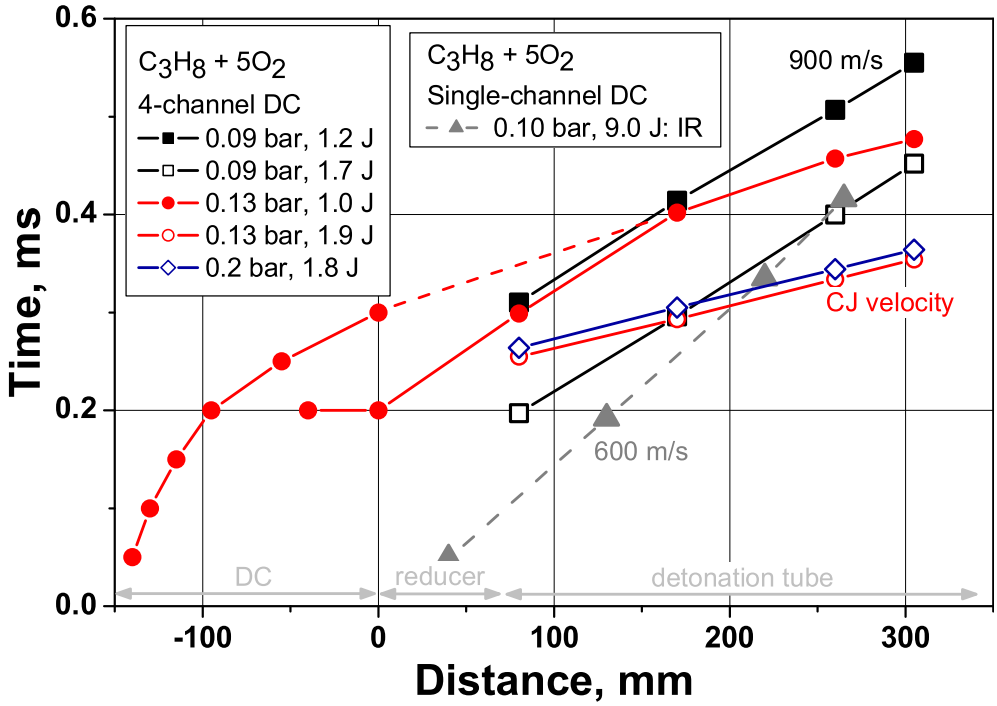


Fig. 3.9: X–t diagrams of DDT at initial pressures of 0.09—0.13 bar, spark and transient modes.

of the discharge channel was high enough to catch up with the initial flame wave before the second sensor ($\sim$ 1000 m/s), which resulted in a detonation wave formation.

A higher value of the initiation energy (1.9 J) under the same mode of discharge development resulted in the formation of a CJ detonation wave 100 $\mu$s earlier (see the traces in Fig. 3.11). It is illustrated by the PT data for this experiment plotted in the x–t diagram in Fig. 3.9 (hollow red circles). A very similar DDT pattern in terms of DDT time and distance was observed at a pressure of 0.2 bar under an initiation energy of 1.8 J (see the traces in Fig. 3.13 and the x–t diagram in Fig. 3.9, blue diamonds). In this case, the ignition delay remained the same due to an interplay between two trends. First, a pressure rise lead to a decrease of ignition delay time. At the same time, a pressure rise under the same energy input implied a lower specific energy per gas particle. In the current case, the specific energy input was two times lower in the high pressure experiments, which resulted in no overall DDT time decrease. However, this may as well be accounted for by a slightly different discharge development pattern under different pressures.

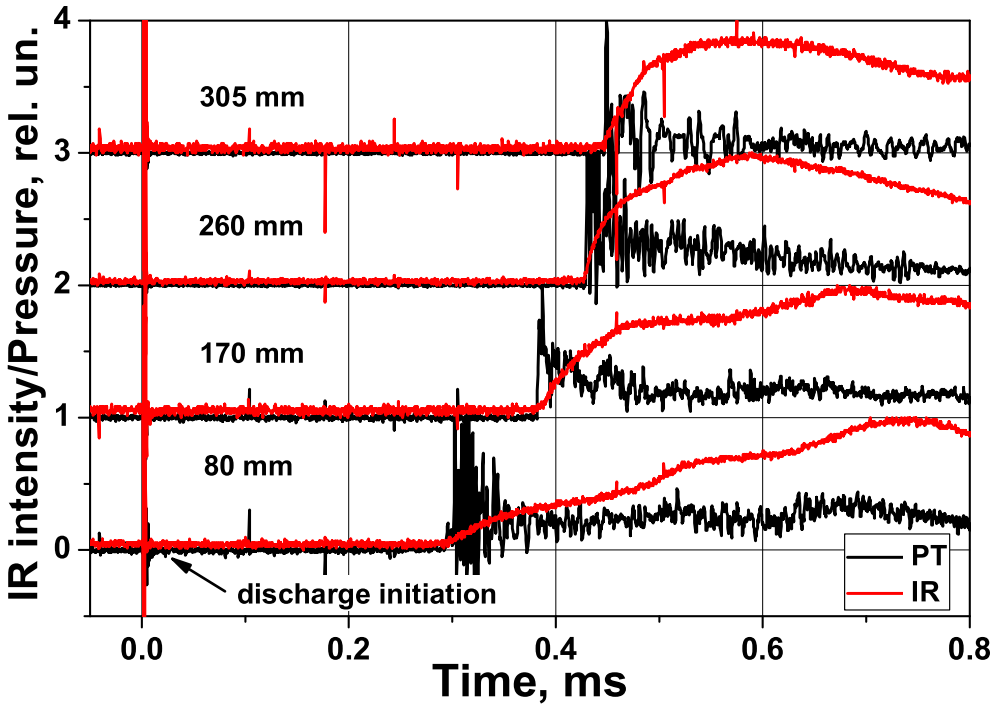


Fig. 3.10: Infra–red sensors (IR) and pressure transducers (PT) traces. DDT at an initial pressure of 0.13 bar, transient mode, energy input 1.0 J.

**Initiation by streamer discharge**

Under higher pressure values (0.2—1 bar), the discharge only developed as a streamer, due to the lower values of the reduced electric field. The energy input typically amounted to 0.2—0.3 J under these conditions. Under such low energy inputs, only the gas in the region next to the high–voltage electrode was excited, as is seen from Fig. 3.5. Since these conditions were suitable for detonation initiation by the gradient mechanism, a series of temporally resolved imaging of the ignition inside the discharge channels was performed in a number of experiments at different pressures. Below, the IR and PT traces are presented for the experiments at initial pressures of 0.2, 0.3, 0.6, and 1 bar (Figs. 3.14—3.17). All the traces show that a detonation wave was formed before the first sensor. The temporally resolved UltraSpeedStar imaging is presented for two pressure values of 0.3 and 0.6 bar (Figs. 3.18 and 3.19). It is seen from the image sequence in Fig. 3.18 for 0.3 bar that the mixture was ignited next to both electrodes. The ignition at the ground electrode occurred almost 300 $\mu$s after the discharge due to a lower value of reduced electric field in the region. The overall results for the streamer mode in the undiluted propane–oxygen mixture are presented in terms of x–t diagrams in Fig. 3.20.

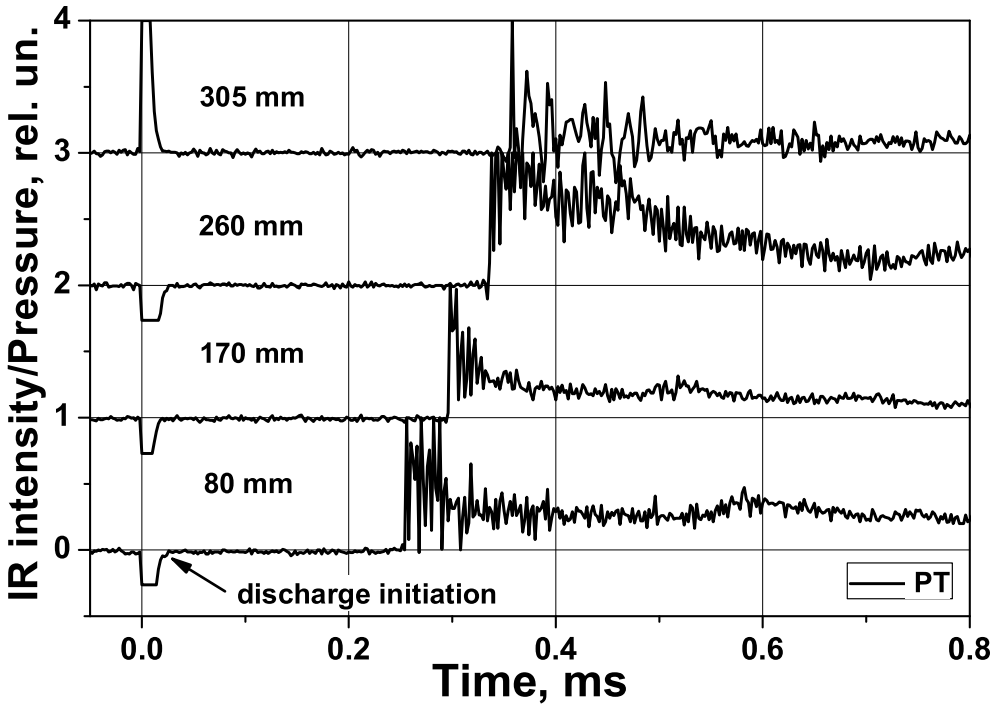


Fig. 3.11: Pressure transducers (PT) traces. DDT at an initial pressure of 0.13 bar, transient mode, energy input 1.9 J.

It is seen that the DDT time decreases with pressure rise under close energy input values. This is due to the similar dependency of ignition delay time upon mixture pressure. On the other hand, the DDT time also decreases with energy input rise. For a clear comparison, the data points for the experiment in transient mode at 0.2 bar are plotted in the same figure (blue triangles in Fig. 3.20. Under an initial pressure of 0.2 bar, the arrival time of the detonation wave to the position of the first sensor decreased from 400 $\mu$s under the initiation energy of 0.35 J to 260 $\mu$s under 1.8 J. Another comparison can be made with detonation initiation by streamer discharge in the single–cell discharge chamber. The x–t diagram for the case at 1 bar of initial pressure is also plotted in Fig. 3.20 as grey circles. The higher energy input of 2 J together with the smaller volume of the excited gas in the single–cell DC results in a slightly shorter delay than in the experiment in the four–cell DC at the same initial pressure. However, the DDT distance is below 3 transverse tube sizes in all the tests in streamer mode.

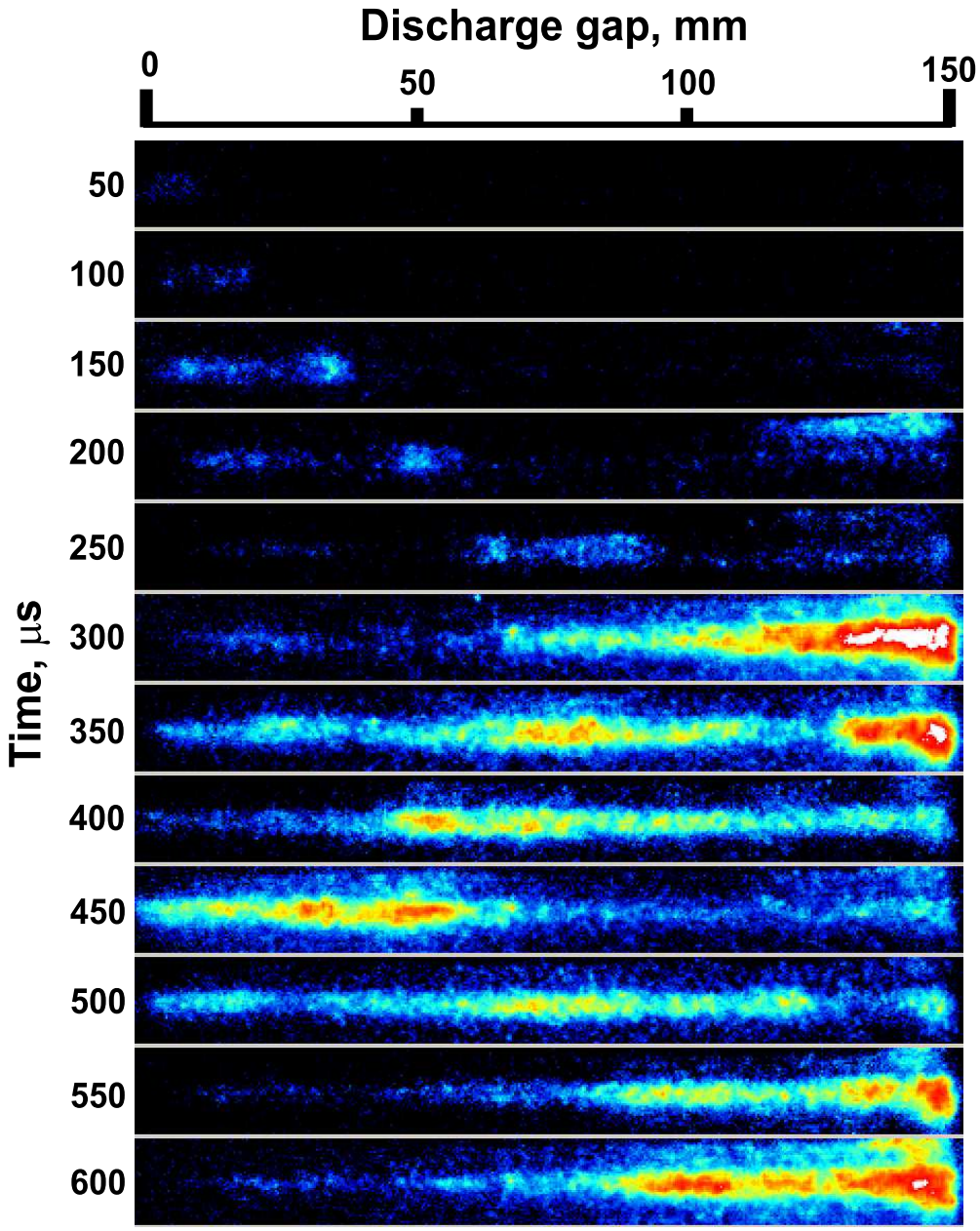


Fig. 3.12: Time–resolved ICCD imaging of propane–oxygen mixture ignition inside the discharge chamber. DDT at an initial pressure of 0.13 bar, transient initiation mode.

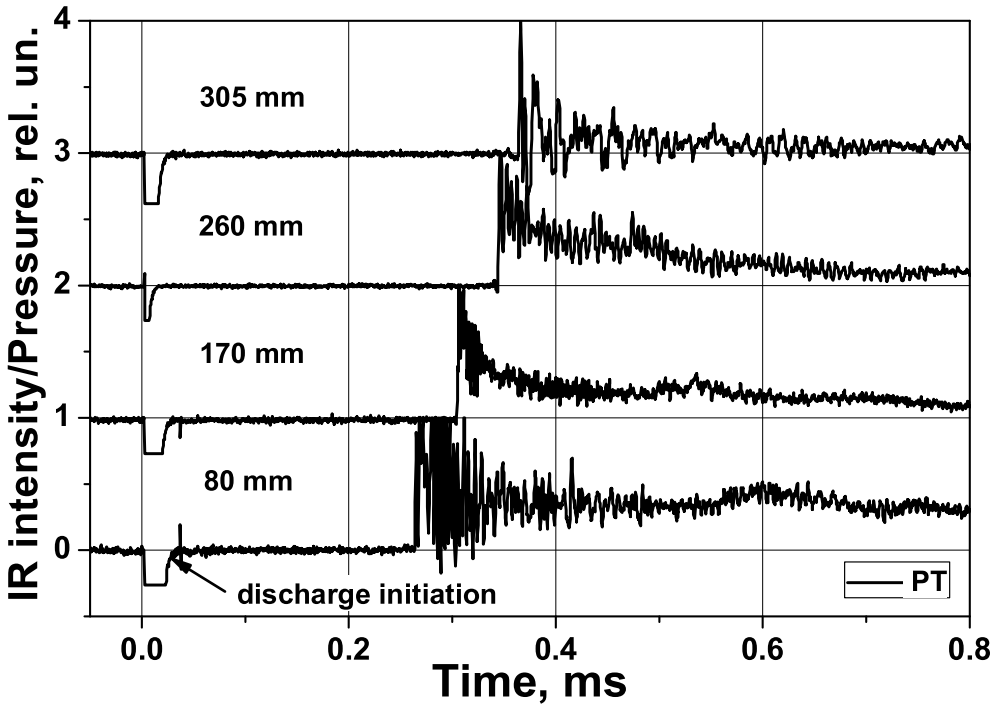


Fig. 3.13: Pressure transducers (PT) traces. DDT at an initial pressure of 0.2 bar, streamer mode, energy input 2.0 J.

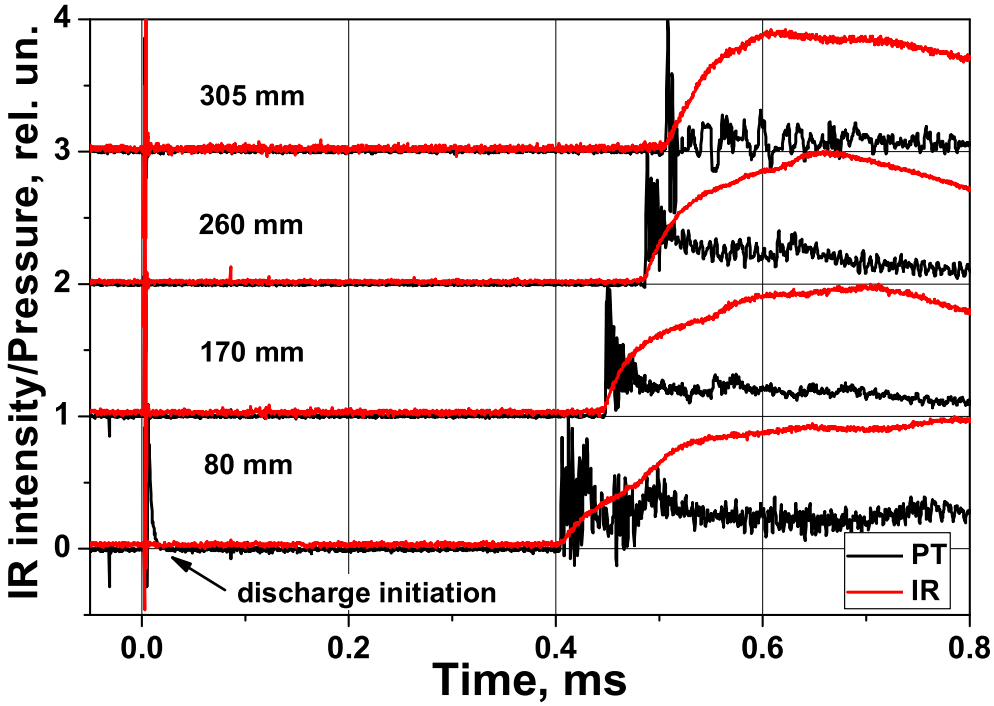


Fig. 3.14: Infra–red sensors (IR) and pressure transducers (PT) traces. DDT at an initial pressure of 0.2 bar, streamer mode, energy input 0.35 J.

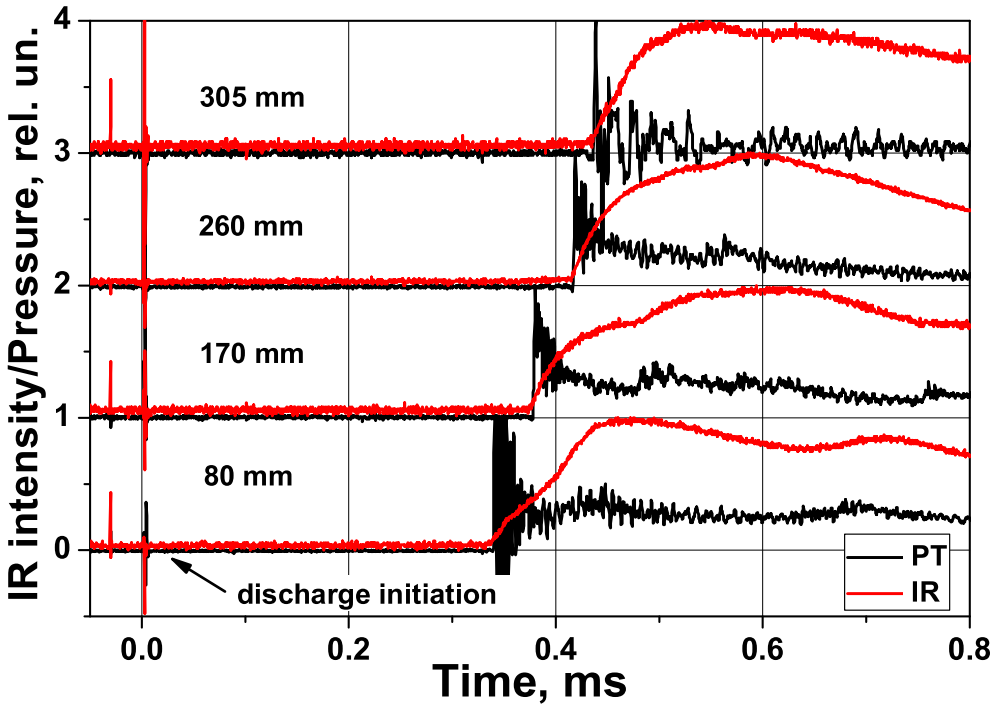


Fig. 3.15: Infra–red sensors (IR) and pressure transducers (PT) traces. DDT at an initial pressure of 0.3 bar, streamer mode, energy input 0.2 J.

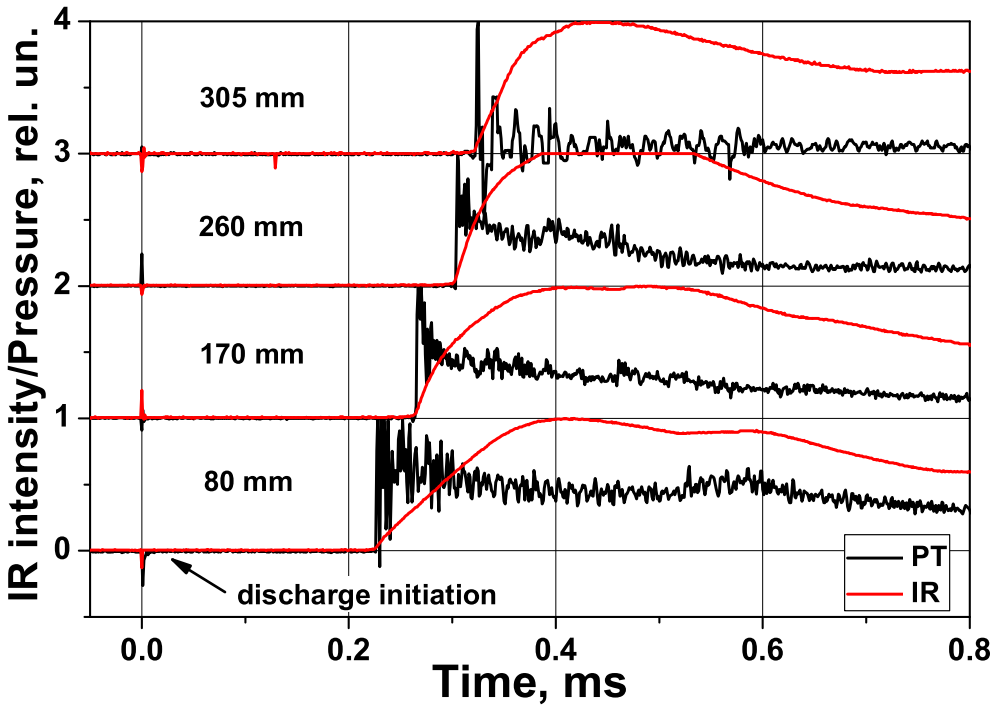


Fig. 3.16: Infra–red sensors (IR) and pressure transducers (PT) traces. DDT at an initial pressure of 0.6 bar, streamer mode, energy input 0.1 J.

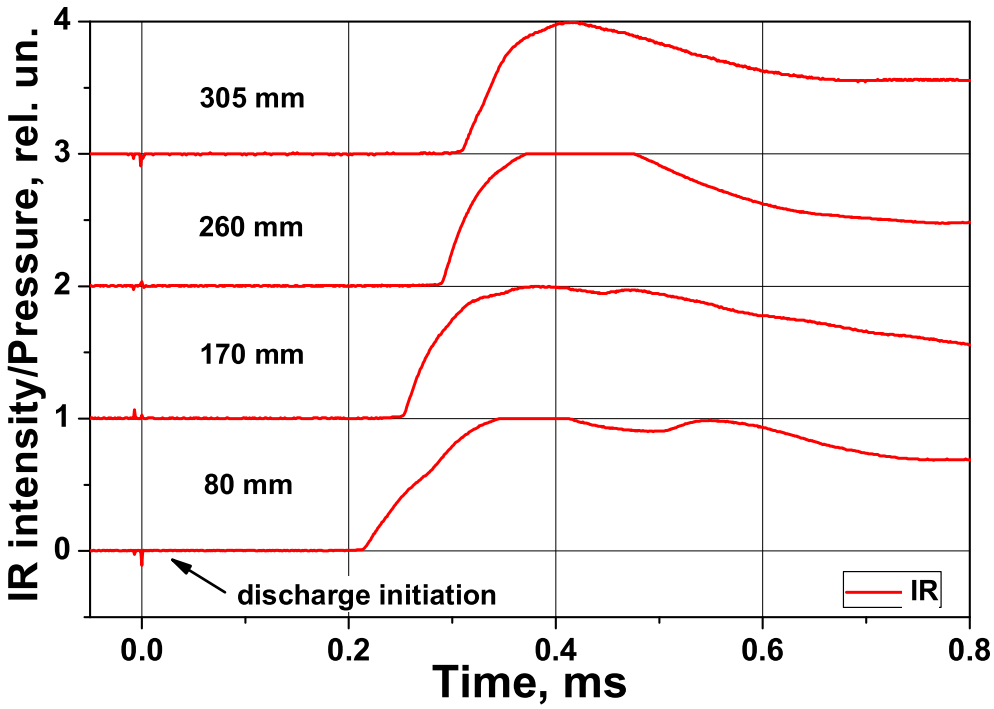


Fig. 3.17: Infra–red sensors (IR) traces. DDT at an initial pressure of 1 bar, streamer mode, energy input 0.2 J.

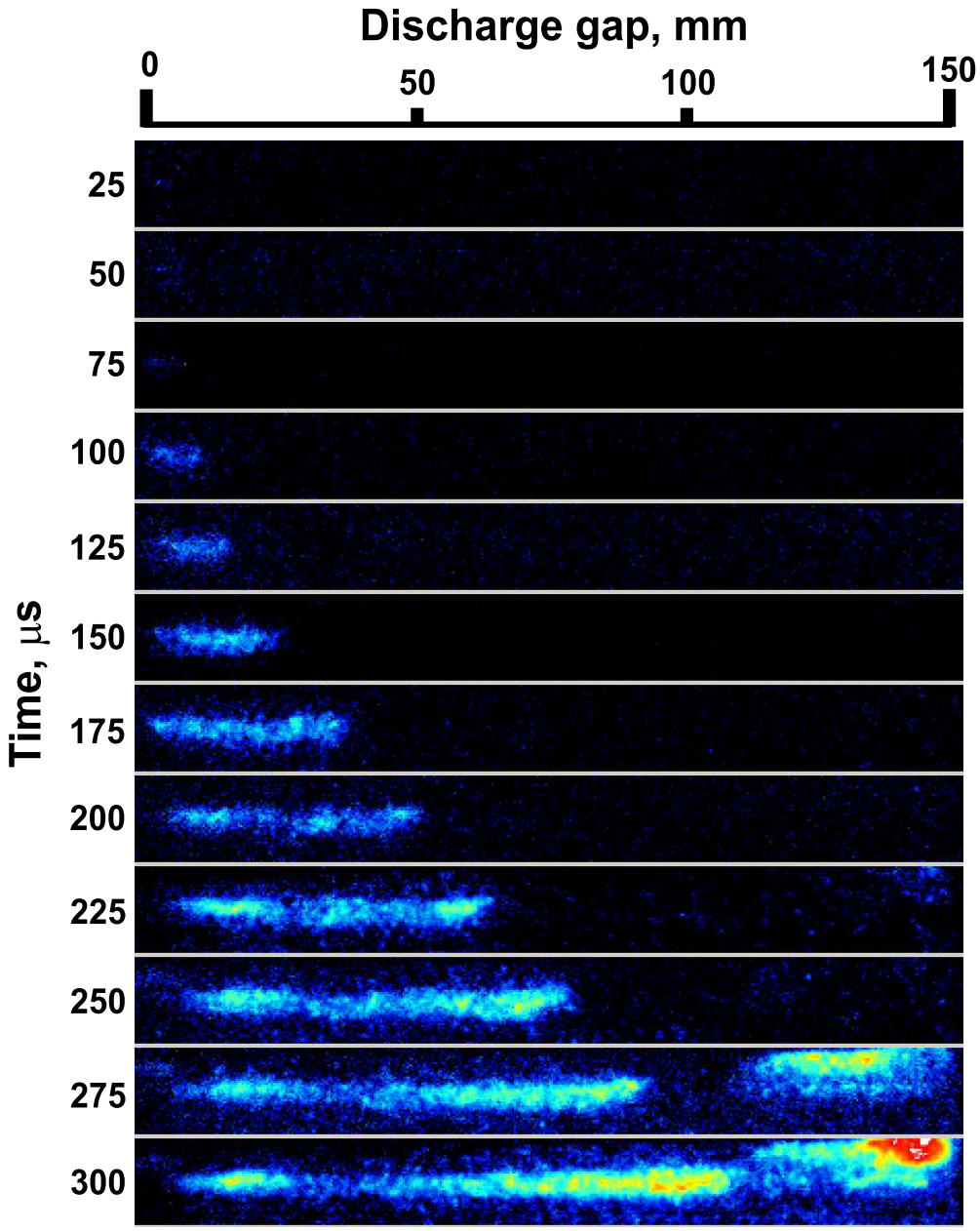


Fig. 3.18: Time–resolved ICCD imaging of propane–oxygen mixture ignition inside the discharge chamber. DDT at an initial pressure of 0.3 bar, streamer mode.

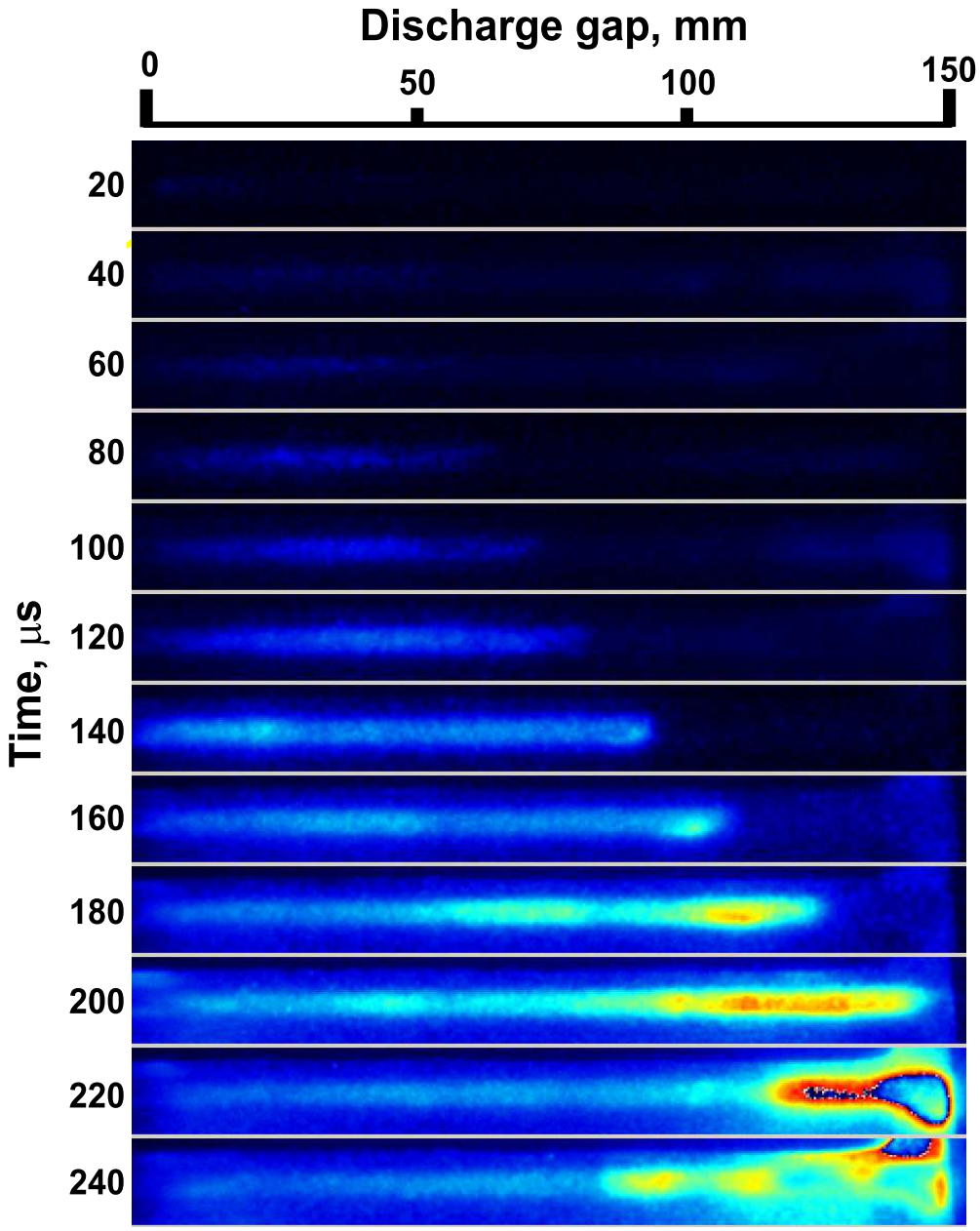


Fig. 3.19: Time–resolved ICCD imaging of propane–oxygen mixture ignition inside the discharge chamber. DDT at an initial pressure of 0.6 bar, streamer mode.

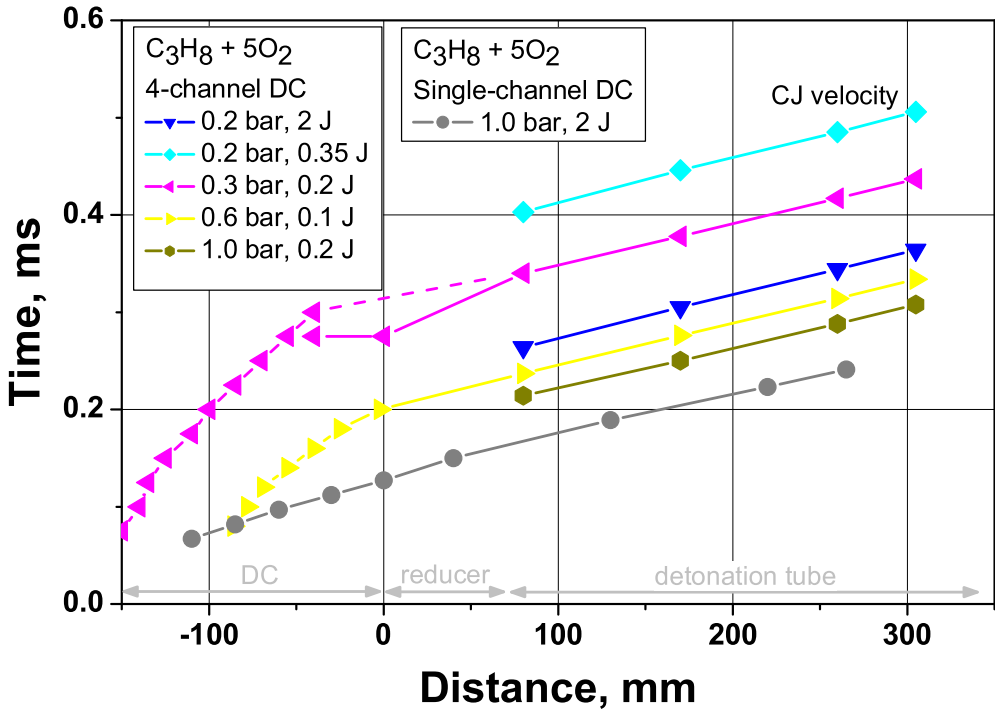


Fig. 3.20: X–t diagrams of DDT at initial pressures of 0.2—1 bar, streamer mode.

### 3.3.2 Propane–Oxygen Mixture with 40% Nitrogen Dilution

**Deflagration at initial pressures of 0.2—0.5 bar**

The experiments in the propane–oxygen mixture diluted with 40% of nitrogen were only carried out in streamer mode at initial pressures from 0.2 to 1 bar. The IR and PT traces are presented for the experiments at initial pressures of 0.2, 0.34, and 0.5 in Figs. 3.21—3.23). The temporally resolved UltraSpeedStar imaging is presented for the experiment at 0.5 bar (Fig. 3.24). The overall results for the this mode in the diluted mixture are presented in terms of x–t diagrams plotted based on the PT data in Fig. 3.25. Under such relatively low pressures, only deflagration mode was observed in this mixture. At the same time, a significant effect of initial pressure on both flame velocity and the arrival time is clear. The temporally resolved imaging at 0.5 bar also indicated, that the gradient mechanism is as well effective in diluted mixtures. It allowed the flame wave to accelerate inside the discharge channel up to ∼500 m/s, which resulted in a shock wave formation in the detonation tube, travelling at a velocity of ∼1000 m/s. Such deflagration velocity is typically enough for an adiabatic explosion to occur within a short distance further downstream, leading to an onset of a CJ detonation.

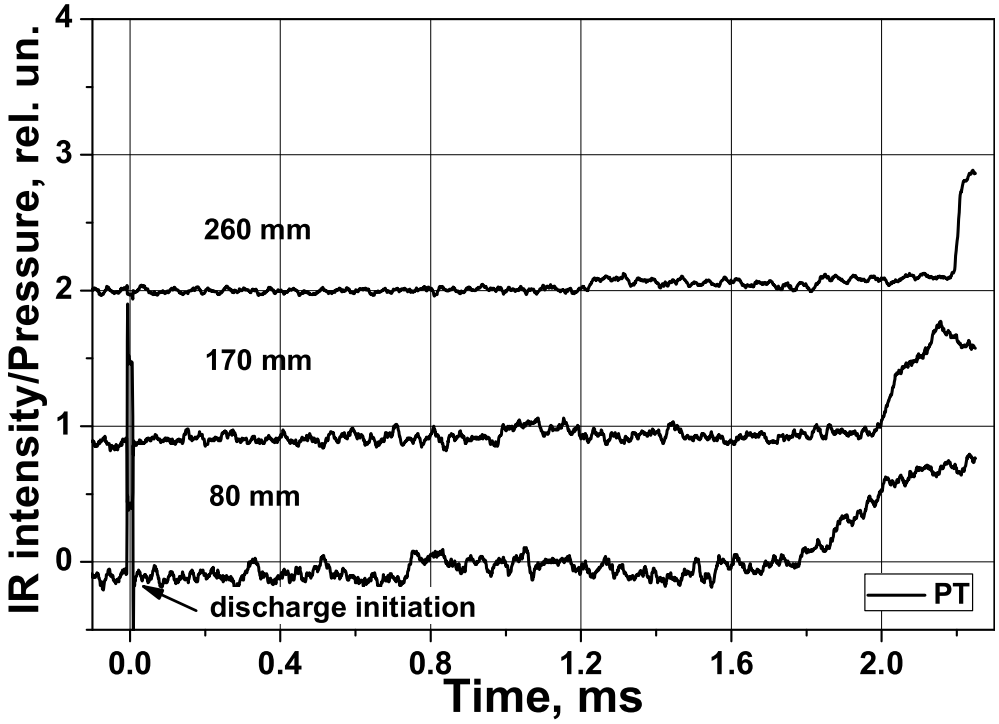


Fig. 3.21: Pressure transducers (PT) traces. DDT at an initial pressure of 0.2 bar, streamer mode, energy input 0.6 J.

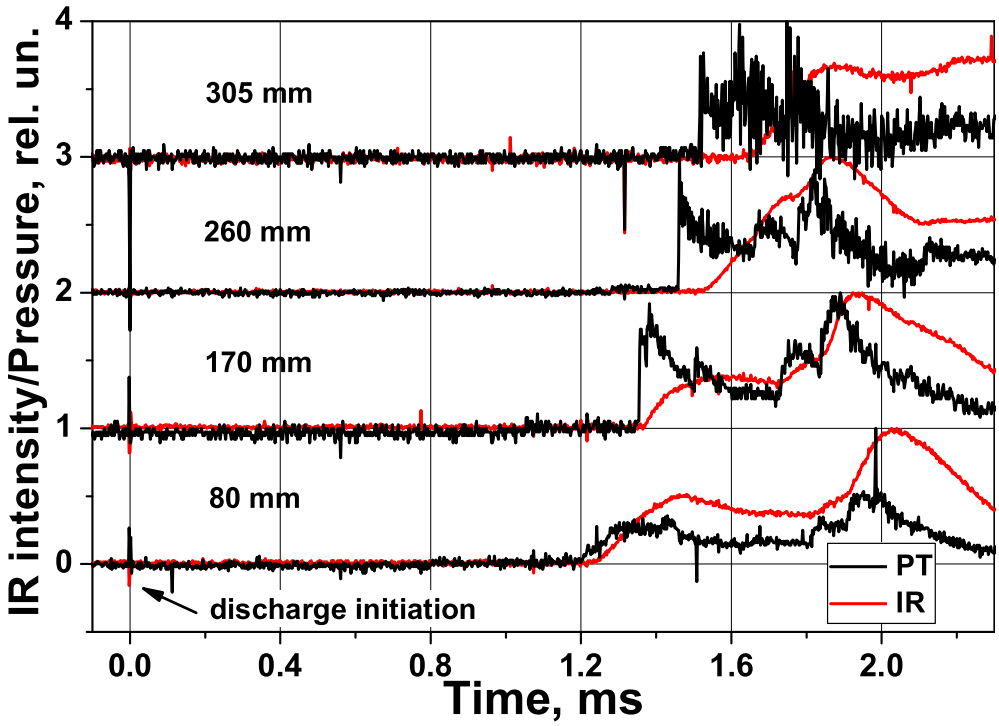


Fig. 3.22: Infra–red sensors (IR) and pressure transducers (PT) traces. DDT at an initial pressure of 0.34 bar, streamer mode, energy input 0.35 J.

**CJ detonation at initial pressures of 0.5—1 bar**

The increased initial pressure together with the gradient mechanism allowed to obtain CJ detonation in the diluted mixture under energy inputs of 0.2—0.3 J. The results are presented for three pressure values of 0.63, 0.8, and 1 bar. At 0.63 bar, the shock/flame velocity remained ∼1000 m/s, though the deflagration wave arrival time decreased as compared with the case at 0.5 bar (see IR and PT traces in Fig. 3.26). A CJ detonation wave was first observed at 0.8 bar of initial pressure (Fig. 3.27). Temporally resolved ICCD imaging confirmed the role of the gradient mechanism in detonation initiation (see UltraSpeedStar image sequence in Fig. 3.28). The spontaneous combustion wave again originated from the region next to the high–voltage electrode and then accelerated along the channel. At the initial pressure of 1 bar, the DDT pattern inside the tube was rather similar to that at 0.8 bar, the shock waves arriving at the first sensor simultaneously (see PT traces in Fig. 3.29), whereas a shorter delay was expected under a higher pressure. The effect of pressure rise could be compensated by a lower energy input (0.2 J for 1 bar experiment compared to 0.3 J for the case at 0.8 bar) or by a slightly different discharge development which would alter the gradient shape.

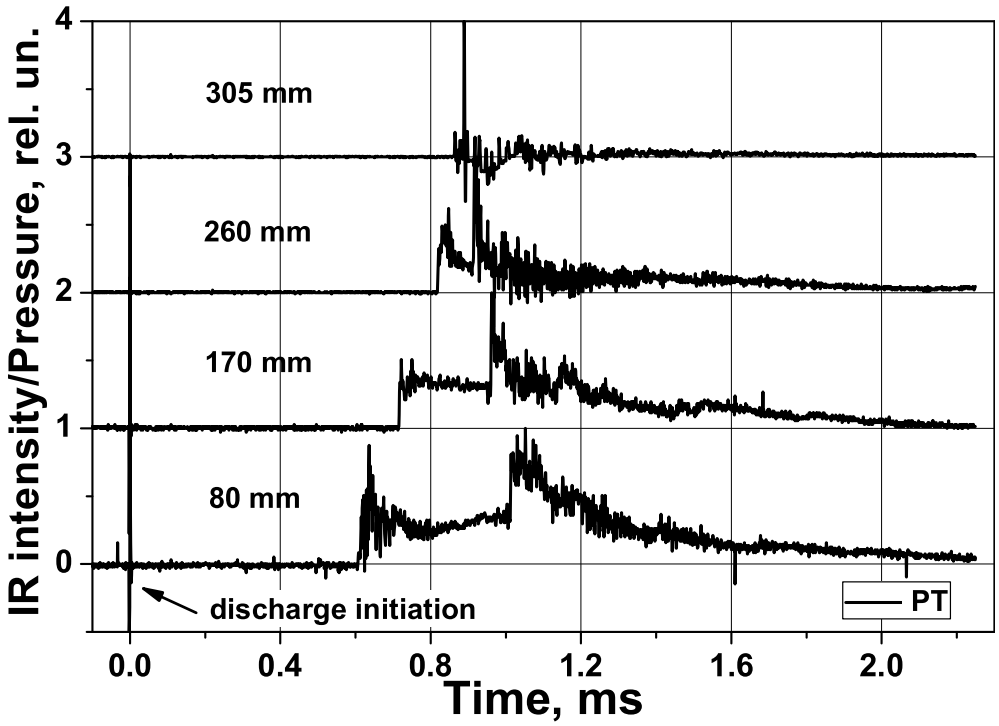


Fig. 3.23: Pressure transducers (PT) traces. DDT at an initial pressure of 0.5 bar, streamer mode, energy input 0.2 J.

The overall results of the experiments at higher pressures in the diluted mixture are presented in terms of x–t diagrams plotted based on the PT data in Fig. 3.30. The gradient mechanism of detonation initiation at 0.8 bar is clearly seen in the figure. Additionally, an x–t diagram of the experiment at 1 bar in the same mixture in the single–cell DC is plotted in the same figure for comparison (grey circles). The data points are based on the IR data and correspond to the flame wave propagation. Even though the initiation energy was by an order of magnitude higher (2 J), only a deflagration wave with a velocity of 600 m/s was observed. Furthermore, in this case the shock wave propagated ahead of the flame wave with a slightly higher velocity. That resulted in a decoupling of the shock–flame complex and in an eventual deceleration of both waves.

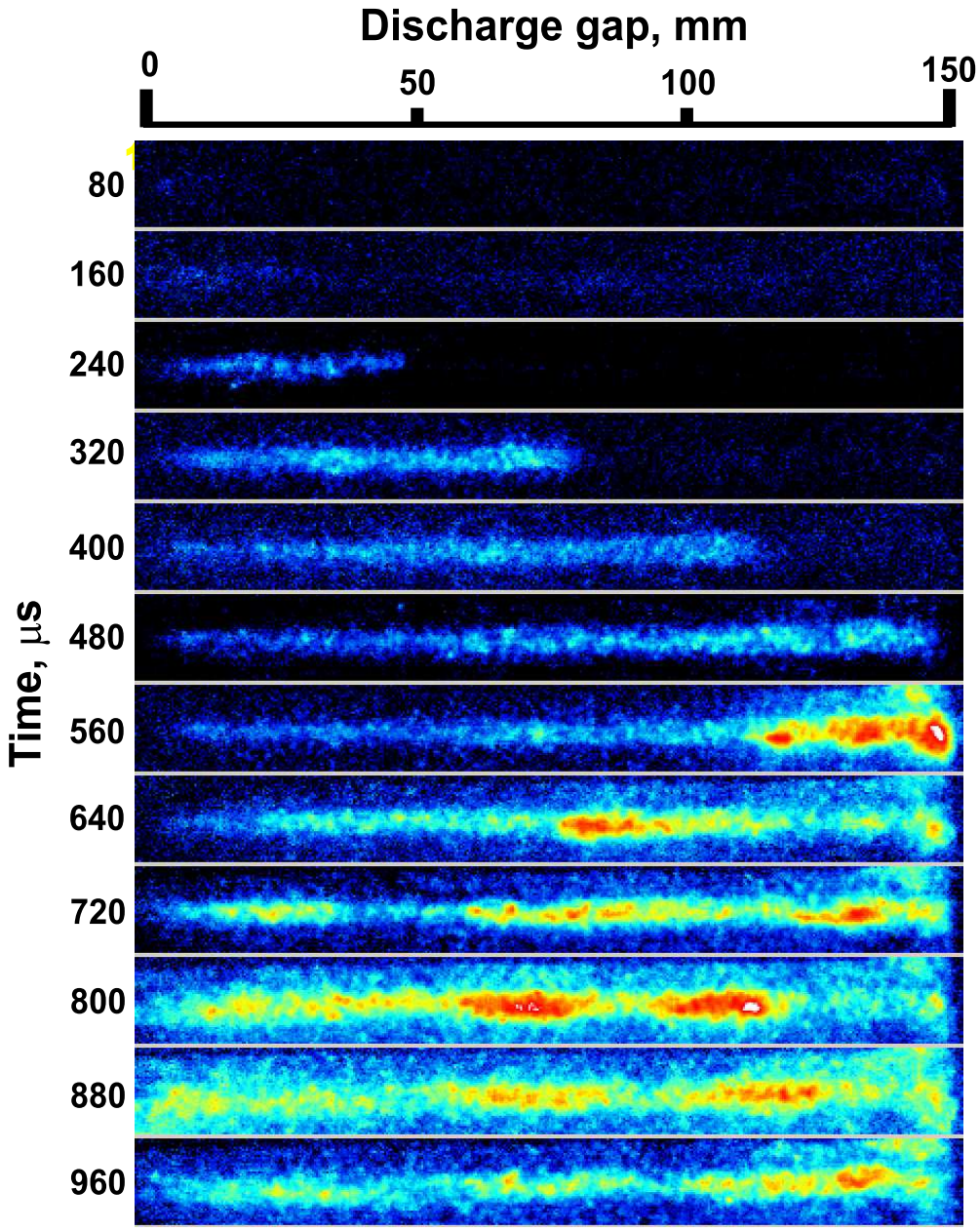


Fig. 3.24: Time–resolved ICCD imaging of propane–oxygen–nitrogen mixture ignition inside the discharge chamber. DDT at an initial pressure of 0.5 bar, streamer mode.

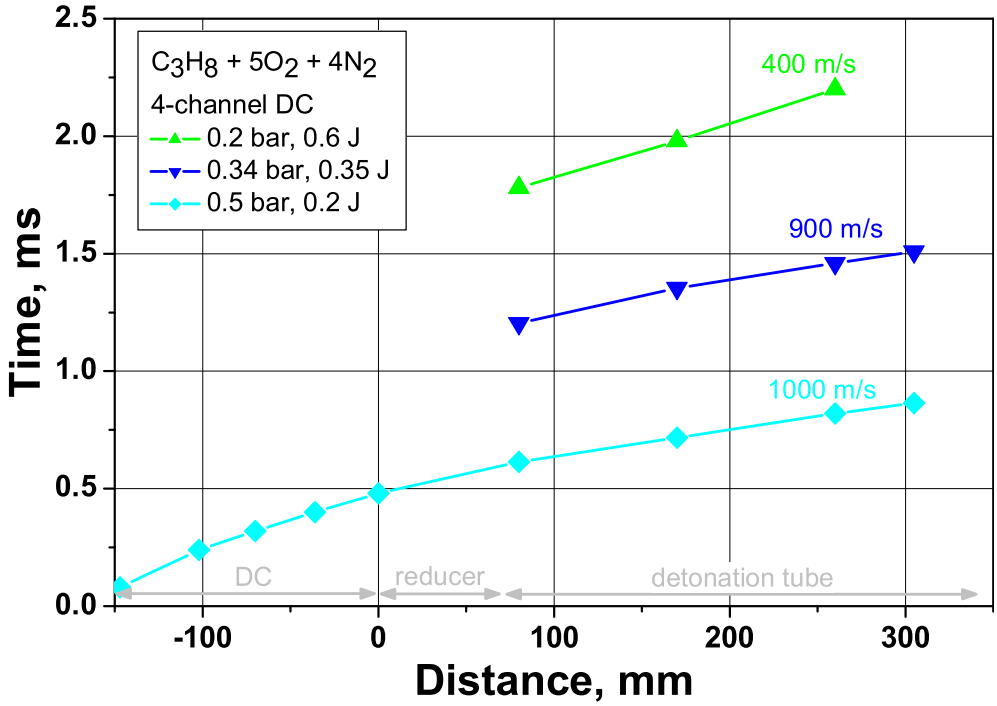


Fig. 3.25: X–t diagrams of DDT at initial pressures of 0.2—0.5 bar, streamer mode.

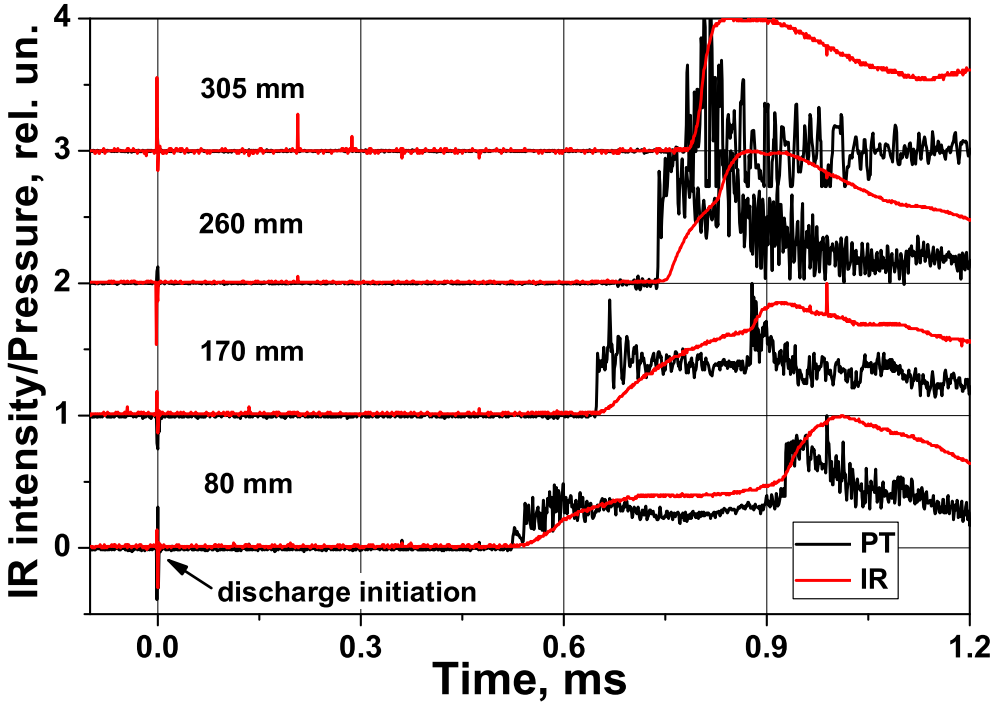


Fig. 3.26: Infra–red sensors (IR) and pressure transducers (PT) traces. DDT at an initial pressure of 0.63 bar, streamer mode, energy input 0.3 J.

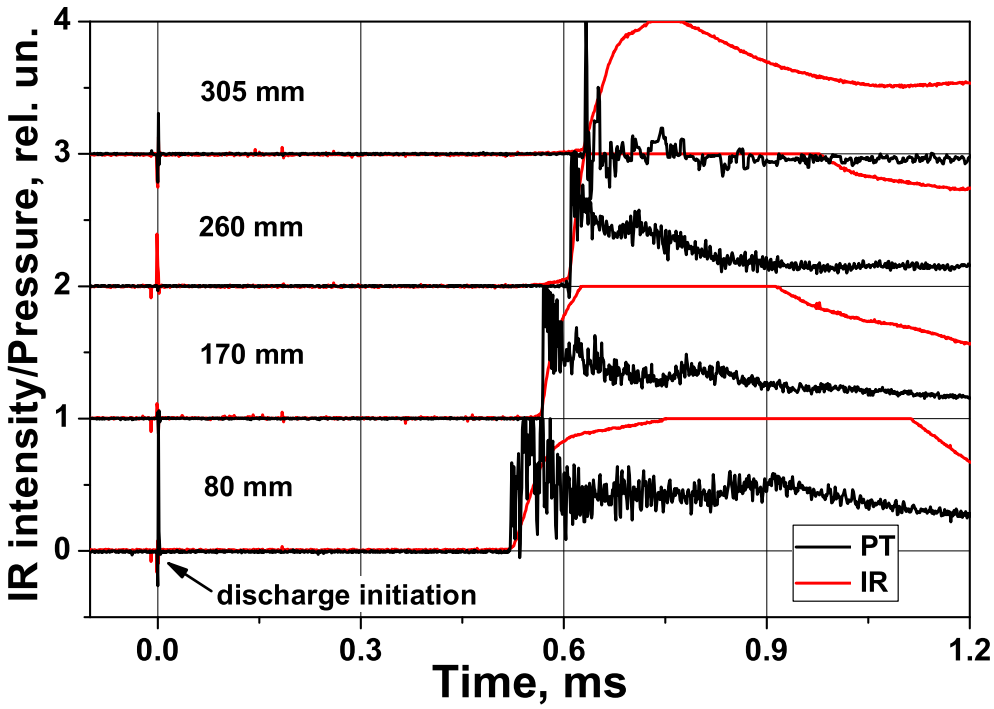


Fig. 3.27: Infra–red sensors (IR) and pressure transducers (PT) traces. DDT at an initial pressure of 0.8 bar, streamer mode, energy input 0.3 J.

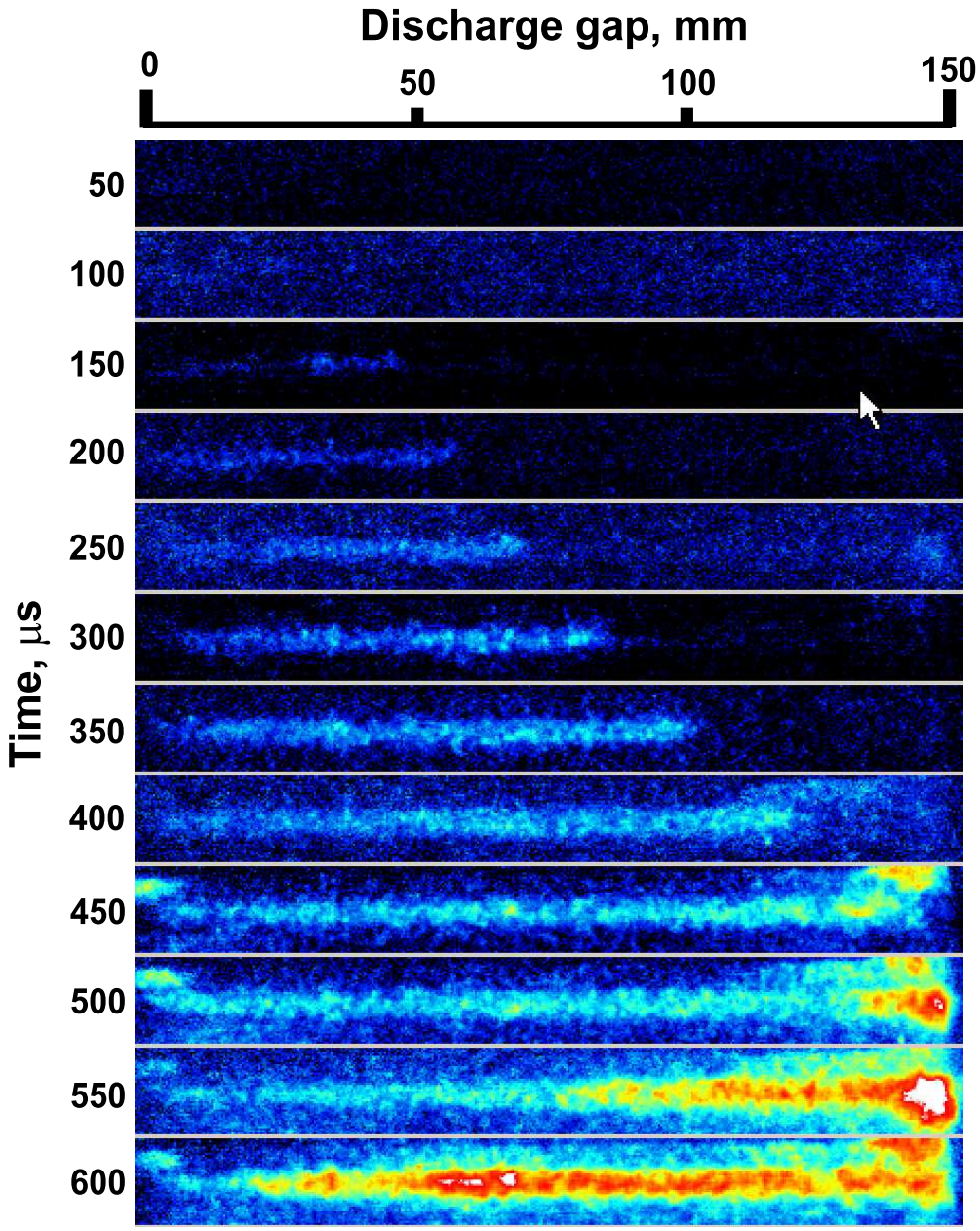


Fig. 3.28: Time–resolved ICCD imaging of propane–oxygen–nitrogen mixture ignition inside the discharge chamber. DDT at an initial pressure of 0.8 bar, streamer mode.

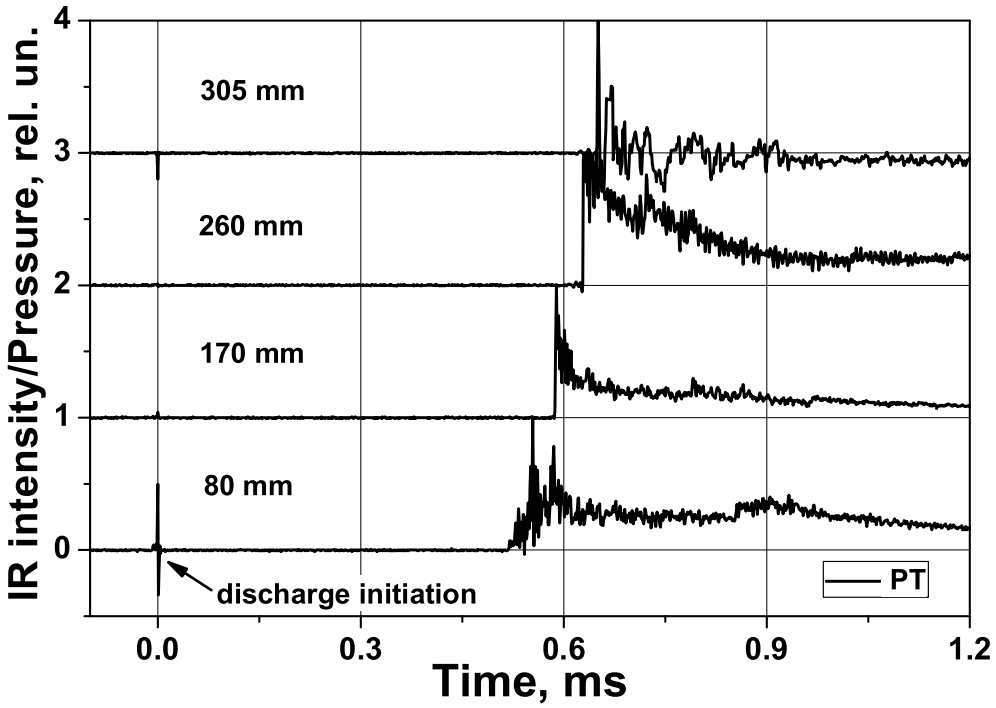


Fig. 3.29: Pressure transducers (PT) traces. DDT at an initial pressure of 1 bar, streamer mode, energy input 0.2 J.

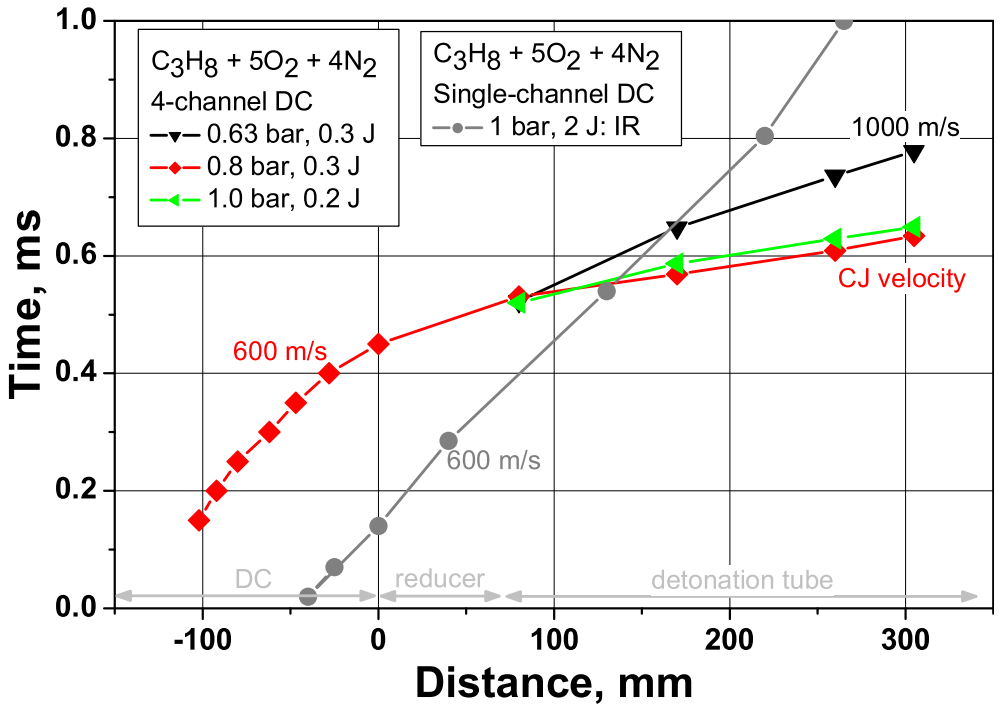


Fig. 3.30: X–t diagrams of DDT at initial pressures of 0.5—1 bar, streamer mode.

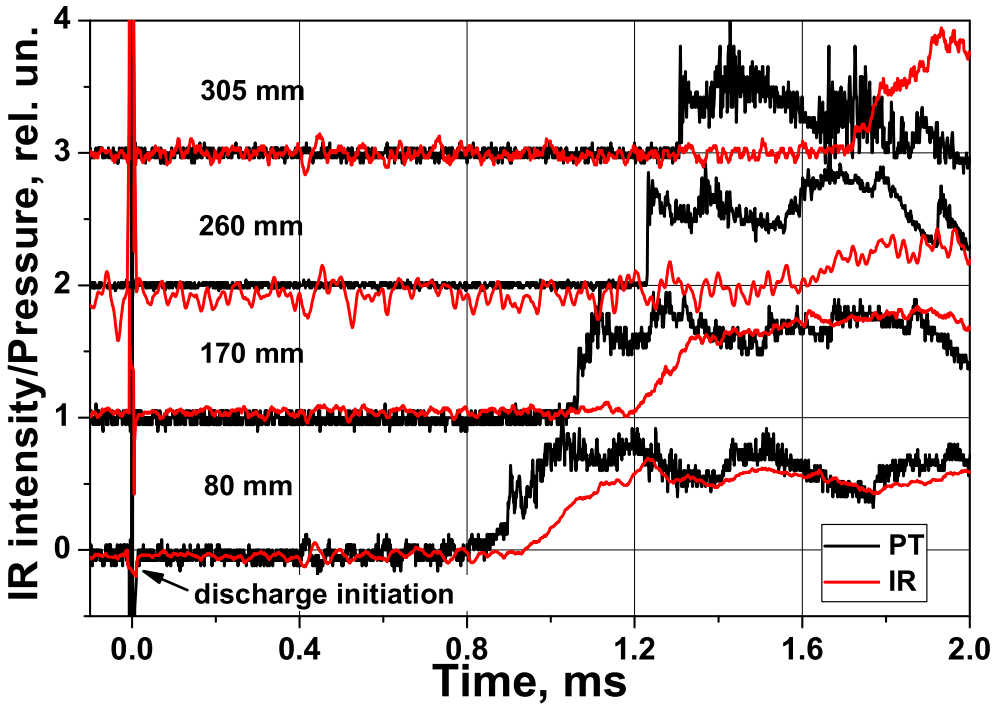


Fig. 3.31: Infra–red sensors (IR) and pressure transducers (PT) traces. DDT in acetylene–air at an initial pressure of 1 bar, streamer mode, energy input 0.25 J.

### 3.3.3 Acetylene–Air Mixture

A small series of experiments was carried out in acetylene–air mixture. All the experiments were performed at 1 bar under varying high–voltage pulse amplitudes and, therefore, initiation energies. The discharge still developed as a streamer under all pulse amplitudes. Under an amplitude of 55 kV, the energy input amounted to 0.25 J. As is seen from the IR and PT traces in Fig. 3.31, it resulted in the formation of a weak shock wave travelling at a velocity of ∼600 m/s and a rapidly decelerating flame wave travelling behind it with a delay exceeding 100 $\mu$s at the first sensor position. A threefold initiation energy increase under a pulse amplitude of 78 kV resulted in a very similar shock and flame wave propagation pattern (Fig. 3.32). The arrival time at the first sensor decreased noticeably, but the propagation velocities remained unchanged. The results are summarized in the x–t diagram in Fig. 3.33, where the x–t trajectories of the shock and the flame waves are shown separately. The decoupling of the shock–flame complex is clearly seen here.

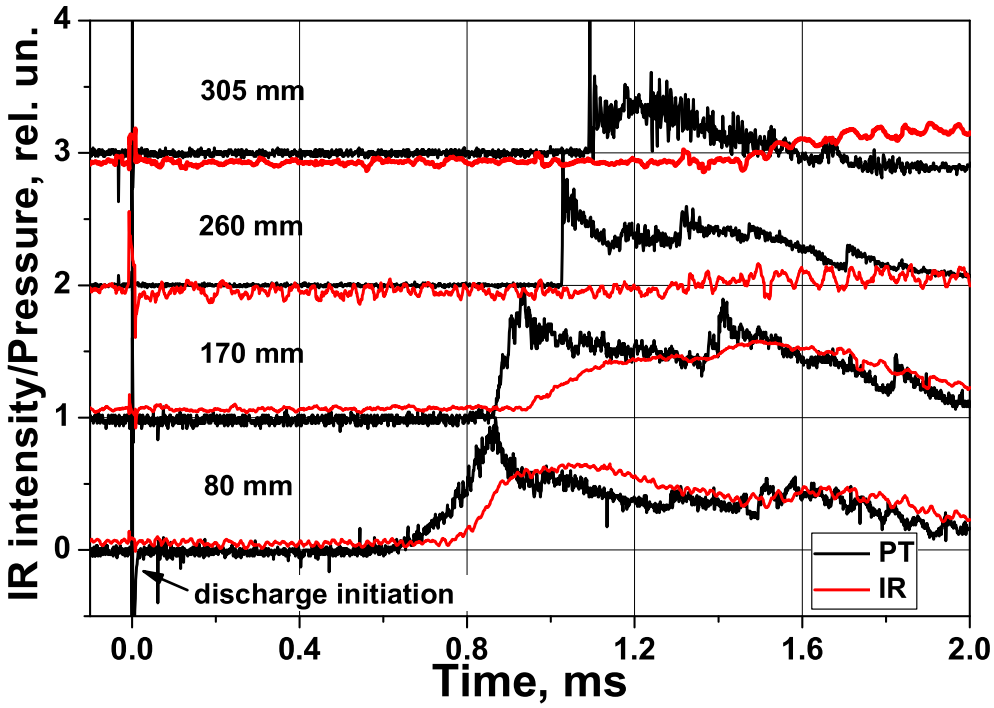


Fig. 3.32: Infra–red sensors (IR) and pressure transducers (PT) traces. DDT in acetylene–air at an initial pressure of 1 bar, streamer mode, energy input 0.7 J.

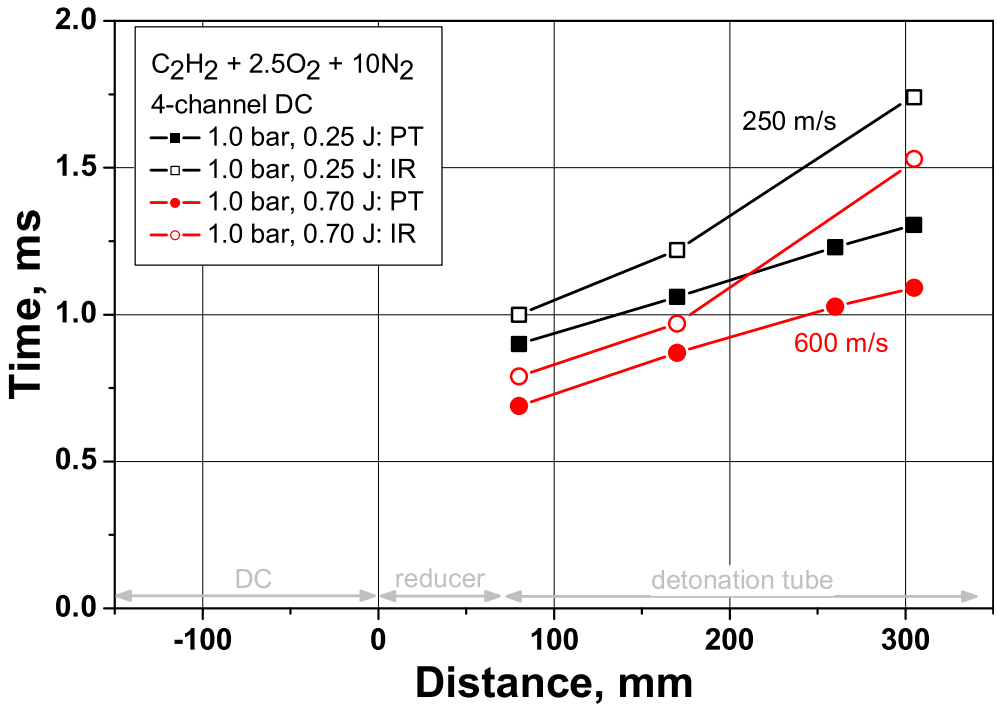


Fig. 3.33: X–t diagrams of DDT in acetylene–air at an initial pressure of 1 bar, streamer mode.

# Chapter 4

# Discussion and Conclusions

On the basis of our previous results, a technique for detonation initiation within short distances in smooth tubes under low energy inputs has been developed. The underlying mechanism, being a gradient mechanism, has been revealed and studied in more detail. The efficiency of the gradient mechanism has been demonstrated under various conditions.

A smooth square detonation tube with a transverse size of 20 mm has been assembled and used to study DDT mechanisms under initiation by high–voltage nanosecond discharges in all the experiments. Stoichiometric fuel–oxidizer mixtures were used at initial pressures from 0.09 to 1 bar. The diagnostics included pressure transducers, IR sensors, a back-current shunt, a high–speed streak camera, a single–frame ICCD camera, and an ultra–fast multi–frame ICCD camera. Discharge chambers of different geometries were attached to the input of the detonation tube for a broader study of different DDT modes.

In the single–cell discharge chamber, the discharge development has been studied in detail. Three modes of discharge development were realized under the experimental conditions: a spark mode with high–temperature channel formation, a streamer mode with non–uniform gas excitation, and a combined transient mode. Two general mechanisms of DDT initiation were observed and explained under these three modes. When initiated by a spark or a transient discharge, the mixture ignited simultaneously over the volume of the discharge channel, producing a shock wave with a Mach number over 2 and a flame wave. The delay between shock and flame wave formation was governed by the energy transferred into translational degrees of freedom. The waves then formed an accelerating complex, and, after it reached a certain velocity, an adiabatic explosion occurred, resulting in a DDT. At an initial pressure of 1 bar in propane–oxygen mixture, the DDT length and time did not exceed 50 mm and 50 $\mu$s, respectively.

A gradient mechanism of deflagration–to–detonation transition similar to that proposed by Zeldovich has been observed experimentally under streamer initiation. The mixture inside the discharge channel was excited non–uniformly by the streamer, thus forming an excited species concentration gradient. The gradient corresponded to that of ignition delay time. The hottest spot with the shortest ignition delay was at the high–voltage electrode tip. Originating at this point, the spontaneous combustion wave started propagating along the channel at a velocity over 1500 m/s and accelerated up to the CJ velocity value at the channel output. The initiation energy was, by an order of magnitude, lower for the streamer mode when compared to the spark initiation under the experimental conditions, whereas the DDT time was 3 times longer. However, the DDT length was still within 50 mm, which corresponded to 2 transverse tube sizes, and the DDT energy was, by two orders of magnitude, lower than the energy of direct planar detonation initiation.

For a detailed study of the gradient initiation mode, the four–cell discharge section has been designed and manufactured. The geometry allowed to obtain streamer discharge under low amplitudes of the high–voltage pulse in a wide pressure range. Typical pulse energy in the streamer mode was 0.2—0.3 bar, while amounting to 1.9 J in the transient mode under low pressures. In an undiluted propane–oxygen mixture, detonation inside the tube was observed at pressures from 0.1 bar and higher. The discharge propagated as a streamer or as a transient streamer in this pressure range. The simultaneous use of the multi–frame ICCD camera in the discharge channel and of the combined infra–red/pressure diagnostics inside the tube allowed to observe the whole DDT pattern. Detonation was initiated through the gradient mechanism in all these cases. That resulted in extremely short DDT distances of less then 4 tube sizes (80 mm, minimal measurable distance in the experiment). The DDT times varied from 0.2 and 0.5 ms depending on the initial pressure and the energy input.

The second series of experiments was carried out in a less sensitive and less energetic mixture of propane–oxygen diluted with 40% of nitrogen. A fast deflagration wave with a propagation velocity of over 1000 m/s was observed at pressures of 0.5 and 0.63 bar. The gradient mechanism has been shown to the governing one in these modes as well. However, the combustion wave could not accelerate to a high enough velocity to transit to a CJ detonation due to a lower value of chemical energy stored inside the excited mixture. At a higher initial pressure of 0.8 bar, the stored chemical energy was enough for a successful DDT to occur within 80 mm and after only 0.5 ms. A

very similar result was obtained at 1 bar of initial pressure under an even lower energy input of 0.2 J. Considering the volume of the four–cell discharge chamber, such energy input is formally equivalent to a uniform heating of the mixture inside the cells by 12 K. However, the mixture is actually rather excited than heated. Also, it is excited non–uniformly both radially and along the channels, which accounts for the presence of the areas with relatively low ignition delay times of 100—200 $\mu$s observed in the experiments. The comparison with the experiment in the same mixture, but in the single–cell discharge chamber, demonstrates that it is not the specific energy input which plays the key role in the gradient mechanism efficiency. The experiment in the single–cell chamber was carried out under an energy input four times higher than that for the four–cell experiment. Furthermore, the excited gas volume is yet four times smaller. Still, only a deflagration wave with a velocity of 600 m/s was observed instead of a CJ detonation. The crucial difference is most likely made by the overall amount of fuel mixture excited by the discharge, which is four times different for the cases. The lower specific energy input in the four–channel case may lead to a longer ignition delay time and a later emergence of the spontaneous combustion wave, but a detonation wave is still onset shortly after the discharge channels outlet.

Another comparison has been made with an acetylene–air mixture. The detonation cell size in this mixture at an initial pressure of 1 bar is the same as that for the propane–oxygen–nitrogen mixture discussed above and is equal to 4 mm. This implies similar detonability of the mixtures. However, the experimental results were totally different. Under a similar energy input, a deflagration wave with a velocity of 600 m/s was observed. An almost threefold energy input increase did not make a significant difference. The geometries and the discharge propagation conditions were the same in the experiments. The difference is again in the amount of the stored chemical energy inside the excited fuel mixture. Supposing that all the volume of the discharge chamber is excited by the discharge, the chemical energy in the acetylene–air mixture is 75 J, whereas for the propane–oxygen–nitrogen mixture this value amounted to 180 J under an initial mixture pressure of 1 bar. Though obviously not all the volume is excited by the discharge, the relationship is likely to remain justified, due to the intrinsic difference in the specific chemical energy stored in these mixtures.

The achieved understanding of the gradient mechanism of detonation initiation, together with the expertise in high–voltage pulsed discharges, may now be applied to the design of air–breathing PDEs.

# Bibliography


[1] Zhukov, V. P. and Starikovskii, A. Y., "Effect of a Nanosecond Gas Discharge on Deflagration to Detonation Transition," *Combustion, Explosion, and Shock Waves*, Vol. 42, No. 2, 2006, pp. 195–204.

[2] Zhukov, V. P., Rakitin, A. E., and Starikovskii, A. Y., "Initiation of Detonation by Nanosecond Gas Discharge," *44th AIAA Aerospace Sciences Meeting and Exhibit*, AIAA, Reno, USA, 2006, paper 2006-952.

[3] Zhukov, V. P., Rakitin, A. E., and Starikovskii, A. Y., "Effect of High–Voltage Pulsed Discharges on Deflagration to Detonation Transition," *Journal of Propulsion and Power*, Vol. 24, No. 1, 2008, pp. 88–93.

[4] Starikovskii, A. Y., "The Method of Initiation of Ignition, Intensification of Combustion or Reforming of Fuel-Air and Fuel-Oxygen Mixtures," patent PCT/IB 2006/003106, 2006.

[5] Kosarev, I., Kindusheva, S., Aleksandrov, N., Starikovskaia, S., and Starikovskii, A., "Kinetics in Gas Mixtures for Problem of Plasma Assisted Ignition," *45th AIAA Aerospace Sciences Meeting and Exhibit*, AIAA, Reno, USA, 2007, paper 2007-1386.

[6] Pancheshnyi, S. V., Starikovskaia, S. M., and Starikovskii, A. Y., "Measurements of Rate Constants of the N2(C3Pu) and N2+(B2S+u) Deactivation by N2, O2, H2, CO and H2O Molecules in Afterglow," *Chem. Phys. Lett.*, Vol. 294, 1998, pp. 523.

[7] Kaneshige, M. and Shepherd, J. E., "Detonation Database," Technical report fm97-8, GALCIT, California Institute of Technology, 1997.

[8] Ionin, A. A., Kochetov, I. V., Napartovich, A. P., and Yuryshev, N. N., "Physics and engineering of singlet delta oxygen production in low–temperature plasma," *J. Phys. D: Appl. Phys.*, Vol. 40, No. 2, 2007, pp. R25–R61.

[9] Hayashi, M., "Electron collision cross–sections for molecules determined from beam and swarm data," *Swarm studies and inelastic electron–molecule collisions*, edited by L. C. Pitchford, B. V. McCoy, A. Chutjian, and S. Trajmar, Springer Verlag, New York, 1987, pp. 167–187.

[10] Berdushev, A. V. et al., "Molecular Gas Heating in Pulsed MW Discharge," *High Temperature (Teplofizika Vysokikh Temperatur)*, Vol. 26, No. 4, 1988, pp. 661–666.

[11] Higgins, A. J., Pinard, P., Yoshinaka, A. C., and Lee, J. H. S., "Sensitization of Fuel-Air Mixtures for Deflagration to Detonation Transition," *High-Speed Deflagration and Detonation: Fundamentals and Control*, edited by G. Roy, S. Frolov, D. Netzer, and A. Borisov, Elex-KM Publ., Moscow, Russia, 2001, pp. 45–62.

[12] Zeldovich, Y. B., Librovich, V. B., Makhviladze, G. M., and Sivashinskii, G. I., "On the Onset of Detonation in a Nonuniformly Heated Gas," *J. Appl. Mech. Tech. Phys.*, Vol. 11, No. 2, 1970, pp. 264–270.

[13] Lee, J. H. S., "Initiation of Gaseous Detonation," *Annual Review of Physical Chemistry*, Vol. 28, 1977, pp. 75–104.

[14] Kapila, A. K., Schwendeman, D. W., Quirk, J. J., and Hawa, T., "Mechanisms of Detonation Formation due to a Temperature Gradient," *Combustion Theory and Modelling*, Vol. 6, No. 4, 2002, pp. 553–594.